Aero-Assisted Orbital Transfer Vehicles Utilizing Atmosphere Ingestion

by

THOMAS JOHN McGUIRE

B.S. Aerospace Engineering
Pennsylvania State University, 1999

Submitted to the Department of Aeronautics and Astronautics in partial fulfillment of the requirements for the degree of

MASTER OF SCIENCE
at the
MASSACHUSETTS INSTITUTE OF TECHNOLOGY

June 2001

Author .....
Department of Aeronautics and Astronautics
June 8, 2001

Certified by .....
Raymond Sedwick
Research Scientist in Department of Aeronautics and Astronautics
Thesis Supervisor

Certified by .....
David W. Miller
Associate Professor of Aeronautics and Astronautics
Director of the MIT Space Systems Laboratory

Accepted by .....
Wallace E. Vander Velde
Professor of Aeronautics and Astronautics
Chair, Committee on Graduate Students

Aero-Assisted Orbital Transfer Vehicles Utilizing Atmosphere Ingestion

by:
Thomas J. McGuire

Submitted to the Department of Aeronautics and Astronautics on
June 8, 2001 in Partial Fulfillment of the Requirements for the
Degree of Master of Science in Aeronautics and Astronautics.

Abstract

The atmosphere present in low Earth orbits can be used to provide working fluid to an electric propulsion system. As the craft plows through low Earth orbit (~175 – 225 km), incident gases are collected, ionized and routed through a high power electromagnetic thruster. A spacecraft utilizing this concept can generate thrust without expending on-board propellant. The performance of the system is explored in this thesis. An example mission of interest, orbital transfer of communications satellites from low Earth orbit (LEO) to geostationary Earth orbit (GEO) is presented and compared to the state-of-the-art techniques and a proposed solar thermal orbital transfer vehicle from the Boeing company. Performance increases possible with this system include lower cost per kilogram to the higher orbits, smaller and more cost effective launch vehicles for a given payload, and threefold increases in GEO capability of current launch vehicles.

In support of this concept, a large intake 'scoop' is required. Of the various options available, a solid hypersonic intake appears to be the simplest near-term option. The drag characteristics and low-density, high speed-ratio flow (speeds much greater than thermal speed) behavior around a solid-walled scoop is explored via a kinetic approach. A particle-in-cell method is used to model particle motion in a density and velocity field. The effects of surface interactions and collisions between neutral particles are treated with a Monte Carlo model. The general flowfield behavior is presented via density maps and velocity plots. The general scaling of the system drag, drag coefficient, and capture ratio are presented with variations in the cone angle of the scoop, intake radius, and assumed variables. The fine structure of the flow field is resolved within the limits of available computing power, showing a 'fuzzy' shock wave and weak bowshock effect. The last contributions of the model are drag and mass-capture values for a proposed reusable orbital vehicle.

Using the mission study and the scoop model, a high-level conceptual design of a reusable orbital transfer vehicle is presented. The proposed vehicle features a modestly-sized inflatable intake, 100 kW nuclear power source, and a spacecraft bus capable of years of operation. The mission consists of ferrying payloads from low Earth orbit to primarily geostationary orbits. The cycle time for conventional payloads is 4-5 months, allowing for many missions per year. The estimated revenue has the potential to be lucrative if development and operation costs are manageable.

Thesis Supervisor: Raymond Sedwick
Title: Research Scientist in Department of Aeronautics and Astronautics

Acknowledgments

I'd like to thank the American people for funding my graduate education.

To my advisor, for supporting my creativity.

To the DOD, for caring enough to believe in the future.

To MIT, for finally accepting me.

To my friends, for distracting me, thus making this go faster.

To Boston, for a change of scenery.

To our ancestors, for freedom.

To God, for choice.

Life, opportunity, happiness, discovery,

for all these reasons and more,

may we someday go to the stars and find ourselves.

Table of Contents

List of Figures

List of Tables

Chapter 1

Introduction

1.1 State-of-the-art spacecraft propulsion

The value of all the world's commercial satellites each year for the next four years will be greater than 10 billion dollars[2]. That value is spread over about 125 satellites each year, and half of these satellites are launched to Geostationary Earth Orbit (GEO). The launch cost of GEO satellites is a large percentage of the capital outlay of satellite programs. The launchers are expensive, and inefficient propulsion schemes have something to do with this. This thesis explores an improved method of propulsion that will allow smaller, less-expensive launch vehicles to do the job of the current behemoths. The motivation of this study is the huge market of about 60 satellites traveling to GEO each year for the conceivable future. A better system could potentially be very profitable and lower the costs associated with space launches in general.

Most GEO satellites are relatively massive and primarily used for communications (known as ComSats). The mass of these birds ranges from 1,000 to 4,500 kg, while the most common sizes are about 1,500 and 3,500 kg. Typically, these are high power systems (5-10 kW), due to the power needed to communicate over the large distance from the Earth's surface to GEO (35,786 km). These satellites are long-lived, with lifetimes from 8 to 15 years. Most of

these satellites are launched into an inclined geostationary transfer orbit (GTO) and use a solid rocket motor to achieve their final orbit. This is a high delta-V maneuver (about 1,600 meters per second) and the fuel needed is a large fraction of the total spacecraft mass (40%). Thus, an average satellite is worth 100's of millions of dollars, but almost half of its mass (all of which you pay for) is used just getting to orbit.

The launchers that are used for GEO ComSats are expensive. The most common way to get a satellite to GEO is to buy a flight to GTO on an Atlas, Ariane, Proton, Zenit or Delta rocket[1]. The least expensive of these is Boeing's Delta 3, which can launch 3,800 kg to GTO for about $53 million per launch. The Ariane series can launch multiple satellites, but cost per satellite is still on a par with other systems. There are other similar options, such as China's Long March line, which has seemed to recover from a string of failures, and Boeing's Sea Launch, which can launch 4500 kg to GTO from a converted ocean oil-drilling platform. But the costs for these launches are still high, $50 million for a Long March CZ-2E launching 3,370 kg to GTO and $90 million for a Sea Launch of 4,536 kg to GTO. The one relatively inexpensive option is the Russian Soyuz U, which can launch 7,000 kg to low earth orbit (LEO) for $20 million. If on-board chemical propulsion is used to achieve GEO, the Soyuz could compete for the smaller class of commercial satellite launches. An important fact to note is that a given launch system can launch quite a bit more mass to LEO as compared to GTO. GTO is a higher energy orbit and the launch vehicle has to give a GTO payload more 'kick', which means the payload has to be smaller compared to a payload headed for LEO.

There is a good reason to send payloads directly into GTO instead of first sending them to LEO. If we know that our final destination is GTO, and we are using chemical propulsion for the whole trip, then it can be shown that is more efficient to launch directly to GTO[4]. The key

assumption, however, is that chemical propulsion is used for all the delta-V. Chemical propulsion is pretty much required for the initial launch off Earth's surface, since it is the only option available today with a high enough power output (explosive nuclear launch was ruled out long ago and Iraq's supergun didn't make it through the gulf war). Once orbit is achieved, however, efficient electric propulsion engines can be used to conduct maneuvers. Keep in mind, the efficiency of space propulsion is classified by specific impulse, I_{sp}, which is the duration in seconds that 1 kilogram of propellant can generate 1 kilogram-force of thrust. The electric propulsion schemes range in I_{sp} from that of chemical propulsion (50-500 seconds) up to the tens of thousands of seconds for ion engines. The amount of fuel needed to perform an impulsive maneuver is given by the rocket equation:

$$m_p = m_o\left[1 - e^{-\frac{\Delta V}{I_{sp}g}}\right] \tag{1}$$

where m_o is the total mass of the spacecraft and g is the Earth's surface gravitational acceleration, about 9.8 m/s^2. While the benefit of electric propulsion is reduced propellant load, the main price of using electric propulsion is the mass of the power system, which can greatly offset the mass savings.

If we can ultimately trade chemical fuel for a power system, and come out ahead, we are one step closer to cheaper space access. So how do you answer the question, "did I come out ahead?" The answer, of course, depends on whom you ask and what their priorities are. For this study, the key metrics that are assumed to be important to users in general are final payload mass, total cost, reusability, and the time needed to field an asset. Gradually, advanced electric propulsion systems are being implemented in commercial satellite systems, but what are the system limitations in terms of the above mentioned metrics, and can we do better?

1.2 Advanced electric propulsion

In the interest of reducing propellant loads, many varieties of electric and/or magnetic thrusters have been developed. By looking at the systems that have progressed to the flight stage, I hope to show some of the limitations of these systems and provide motivation for eliminating fuel loads altogether. This introduction to electric thrusters will also serve to introduce some of the engine system issues for the proposed AAOTV.

Perhaps the first electric propulsion concept to jump off the drawing board and into space was the resistojet. The basic concept is to heat a gas flow by passing it over a hot filament, sort of like an electric stove burner. By attaching a heater to the exhaust of a standard monomethyl hydrazine (MMH) monopropellant engine, the I_{sp} can be increased from around 220 seconds to about 300 seconds. The MR-501B Electrothermal Hydrazine Thruster[5] from the Primex Aerospace Company is such a thruster and is used on the Iridium constellation of satellites. It has an I_{sp} between 294-303 seconds and operates on about 500 Watts. The improvement in propellant efficiency led to the adoption of this technology as the standard method to conduct North-South Stationkeeping (NSSK) on GEO Comsats for about 10-15 years, before being replaced by arcjets and ion engines about 5 years ago. The NSSK task demands about 50 meters per second of delta-V per year[3], which adds up for a satellite designed to last 15+ years. Aside from some workable problems with fuel lines clogging, the only reason resistojets aren't in favor is that there are systems with higher performance now (and correspondingly lower fuel loads)[4].

Arcjets are currently being used on numerous Lockheed satellites for GEO stationkeeping tasks[7]. An arcjet operates at higher I_{sp}'s by heating the exhaust gas with an electric arc. The Primex Aerospace Company has developed a series of hydrazine arcjets with an I_{sp} ranging from 500 to about 600 seconds[6]. In fact, the first commercial satellite to use arcjets was AT&T's

Telstar 401. The increase in I_{sp} allowed the spacecraft designers to cut fuel loads in half compared to resistojets and chemical monopropellants. The performance of arcjet systems could be increased further by reducing the molecular weight of the propellant, for example ammonia arcjets could attain an I_{sp} of 800-900 seconds. If long-term space storage of cryogenic propellants is achieved, hydrogen arcjets could push an arcjet's I_{sp} to 1000-1500 seconds. While this technology is still relatively simple to implement (it is compact and has a small power-processing system), the power requirements are much greater than resistojets. For example, the thrusters on Telstar 401 operate on 1.8 kW of power. For normal electric propulsion systems, the power scales directly with the I_{sp} for a given thrust.

One very nice thing about arcjets is that the power requirements are modest in comparison to the capability of modern satellites. The main reason that arcjets aren't the answer to all our propulsive needs are that their I_{sp} isn't high enough. If our goal is to reduce propellant loads to very small percentages of the spacecraft mass, we'll have to do better.

Hall Thrusters have been used extensively on Russian satellites for stationkeeping tasks. A Hall Thruster is a compact electrostatic ion accelerator. It has considerably better performance in terms of I_{sp} due to the acceleration mechanism. Instead of heat transfer, it relies on electromagnetic interactions to transfer kinetic energy directly to the exhaust beam. They can operate on a variety of power levels, from as low as 100 W to 20 kW[9]. For example, the BHT-HD-1000 nominally operates at 940 Watts at an I_{sp} of 1870 seconds with 53.5% efficiency. The I_{sp} capability of the Hall Thruster can go as high as 3,000 seconds, which means that the propellant loads can be a much, much smaller fraction of our spacecraft. With the stated I_{sp} and available power levels, one can easily calculate the thrust of an electric thruster.

$$F = \frac{2\eta P}{I_{sp} g} \tag{2}$$

So the thrust for the aforementioned BHT-HD-1000 is only 55 mN. While we have increased I_{sp}, we now find the dual-specters of low thrust and heavy power systems. The other very promising electric concept, ion engines, also suffer from these characteristics.

Hughes Electronics has developed kaufman-type gridded ion engines for station keeping on GEO satellites and primary propulsion for deep space missions. They can operate at very high I_{sp}, but cannot operate efficiently below a few thousand seconds. A Xenon ion engine on NASA's Deep Space One mission (DS-1) will log over 20 months of continuous thrusting over its lifetime and a delta-V increment of about 4.5 km/s. This is an excellent example of high-I_{sp} propulsion enabling a mission with stringent delta-V requirements. Assuming chemical propulsion with an I_{sp} of 450 seconds, the propellant mass would be 379 kg, or 64% of the total spacecraft mass (DS-1 full starting mass was 592 kg). Instead of this large propellant load that would be associated with chemical propulsion for this mission, only 81.5 kg of Xenon was used since the engine operates at an I_{sp} of 3,100 seconds[10]. This mass reduction lets you build much smaller spacecraft to hold the same amount of equipment.

The other main example is the XIPS engine, which was developed by Hughes Electronics Corporation, now a part of the Boeing Company. These engines are used for all station-keeping and spacecraft momentum control on their 702 bus. They operate on 4.5 kW at an I_{sp} of 3,800 seconds. With XIPS, Boeing has reduced its propellant load by a factor of ten for these missions. These maneuvers represent a modest delta-v requirement, but it adds up to about 750 m/s over a lifetime of 15+ years[3].

The XIPS on the 702 spacecraft can also be used to augment orbit-raising of the satellite. To do this, Boeing first launches the spacecraft into a supersynchronous elliptical orbit (24-hour

period) using traditional chemical propulsion. The XIPS engines then slowly change the eccentricity of the orbit, transforming into a circular geostationary orbit. This process takes about 6 months, and the reason is the low thrust nature of the propulsion system given the available power[13]. The benefit of waiting those 6 months is the increased payload mass. One nice property of this method is the spacecraft remains in view of one ground station through the whole process, which greatly reduces operating costs compared to the multiple stations required for a electric-only spiral transfer orbit.

While the XIPS have been shown to be very beneficial for the Hughes systems, they have an important drawback. The time required to perform the orbit-raising mission is an important consideration. The six months that are needed to raise a larger, more capable satellite to its final orbit must be weighed against six months of lost profits for a smaller system. The limiting factor in bringing the transfer time down is the power available for propulsion. It isn't necessarily straightforward to increase the power level and thrust of the electric thruster systems. The power system has a considerable weight associated with it, which may only be needed for the primary propulsion component of the mission. Does it make sense to have an extra 10 kW of power for the raising mission sitting idle over the 15+ year lifetime of the satellite?

This brings up the possibility of using electric propulsion to propel a 'space tug'. Consider a high power satellite with a very efficient electric propulsion system moving satellites around from orbit to orbit. Potentially, the space tug could take over the job of orbit raising for every GEO satellite. This would allow GEO satellites to only carry the power resources needed for its particular payload, while fuel loads would be minimized due to efficient ion propulsion. The GEO satellites would no longer need to be launched into a high energy, geotransfer orbit, and they wouldn't need to carry an inefficient chemical apogee kick engine.

So what are the problems with this picture? First of all, the biggest power system on any spacecraft will be the International Space Station, which will feature a football field sized set of solar arrays producing about 100 kW. Even a modest space tug would need about this level of power. If done with photovoltaics, a large array would be needed. Solar dynamic power is a more compact option, but still requires a large, deployable reflector. Space nuclear reactors have been developed that produce 100 kW, but their use has been stymied by funding and political backlash against all things nuclear.

Another key issue is not a surprise; that issue is propellant. While high specific impulse electric propulsion allows propellant loads to be greatly reduced, one still needs propellant. A 'standard' space tug task of LEO to GEO orbit transfer is a very high delta-V mission. Not only does the craft have to expend about 5 km/s on the way 'up' to GEO, it has to spend that amount on the way back down to LEO. Now multiply that total by the number of missions to be conducted over the lifetime of the tug, say 5-10 years. Suddenly, the only way this can be accomplished in a reasonable timeframe, say a year for each transfer, is to have ridiculously small payload fractions. One answer to this dilemma is for the space tug to refuel after each mission. The space tug could refuel at an orbiting 'gas station', or each payload could carry its share of propellant on-board and transfer it to the space tug. Propellant transfer has yet to be done in space. Although Progress spacecraft have routinely docked with space station Mir for orbit-raising, the mutual propulsion is done by the Progress, not by transferring propellant from one tank to another.

These are merely technically challenges, not deal breakers. Perhaps a refillable high-power orbital transfer vehicle is a future possibility, but what if we could do the job without worrying about propellant? Gone would be the problems associated with delta-V limiting our

mass fraction, and gone would be the nasty problem of propellant transfer. Numerous ideas have been forwarded to accomplish just this end, as we will see.

1.3 Propellantless propulsion

The quest for a dream of a massive human presence among the stars has motivated countless scientific and creative minds to dream up spacecraft that can use the interstellar medium for propellant among the stars. Indeed, one need not look all the way to the stars to realize the benefits of propellantless propulsion. The possibility of eliminating on-board propellant stores would lead to highly reusable near-earth and interplanetary transportation systems due to lower overall masses and practically unlimited operational life.

The Bussard Ramjet is the classic example of a spacecraft operating on only the 'stuff' in space. The idea is named for Dr. Robert Bussard who published a technical paper on the subject in 1960[14]. It has been analyzed, revised, tweaked and re-analyzed over the last forty years. The basic concept consists of a large scoop to collect ambient matter, a fusion reactor of some kind, an exit nozzle, and a payload. Two major problems that have been identified with the concept are the lack of a good intake and the lack of a feasible fusion reactor.

Given that most of the interstellar matter is atomic hydrogen, a fusion reactor would most likely need to operate using a proton-proton reaction. The problem is that its reaction cross-section is very small. This makes the reactor inherently large, and for useful missions we are talking about reactors kilometers wide[15]. There are possible solutions that entail more complex techniques, such as using a proton burning catalytic cycle. The Carbon Nitrogen Oxygen (CNO) Bi-cycle would use trace amounts of those heavy elements to drive the size of the reactor down to 10's of meters for a 1000-ton ship accelerating at one gravity[15]. These types of reactors are far

beyond our current capability, but they manage to keep the Interstellar Ramjet Concept alive and within the realm of possibilities.

The second big problem is the scoop. Several methods have been proposed to collect particles over an area several hundred kilometers in diameter. One way is to build a very powerful solenoid so that charged particles will follow the magnetic field lines into the center of the intake. A. Martin has shown that while this might be feasible at relativistic speeds, the size of a magnetic intake would be on the order of 10^7 km at low velocities and thus not very plausible[16].

There are, of course, other ideas such as a large array of electrostatic deflection rings, which was proposed by Bussard in his original paper, (Figure 1.1). This technique would use radial electric fields to electrostatically deflect incoming particles far ahead of the vehicle, redirecting them just enough so that are collected by the reactor. Some of the problems with this include the plasma effects of the converging ions and the question of how to maintain charge neutrality.

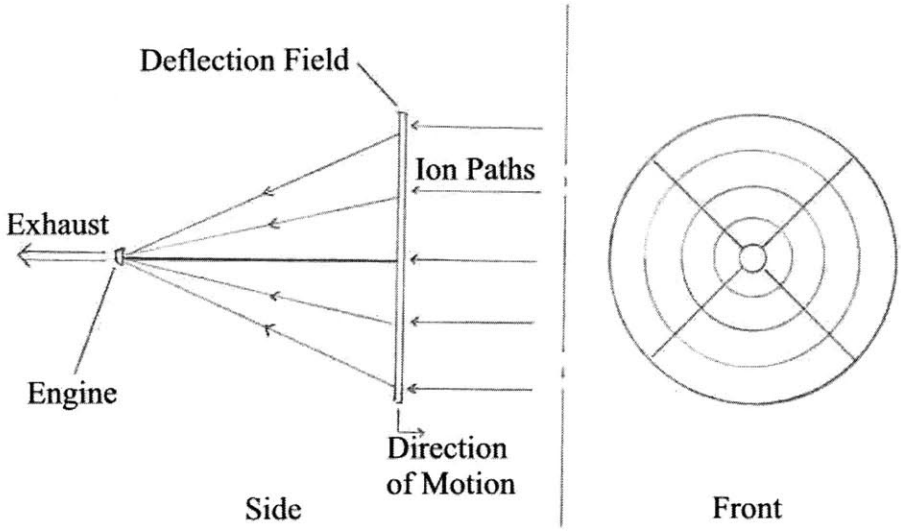

Fig. 1.1, Bussard's electrostatically deflected intake

Akin to the electrostatic concept are methods where large charged bodies are used to project electric fields far ahead of the spacecraft[17]. Other possibilities include using a very large gridded ion engine with separated grids that support a voltage gradient and laser ionization of incoming particles. While these concepts show promise in theory, we are still a long way off from performing a ramjet mission due to the complexity and size of the scoops and the lack of a workable fusion reactor.

Solar sailing is a concept that not only promises propellantless propulsion, but is feasible with modern technology and materials. The basic idea behind solar sailing is to use the momentum of light from the sun or ground based lasers to push on a large reflective sail. The force produced by the light is fairly small, so the sails must be large and lightweight. Likewise, the accelerations that result are on the order of electric propulsion systems, but could conceivably provide enough thrust to push vessels about the inner solar system with reasonable flight times (on the order of months, not years). They also present some unique options for the orbits. For instance, a solar sail could direct its force vector opposite to that of the local gravitational force vector, which would allow it to maintain a distance from the sun without orbiting. By similar thinking, it could perform other non-Keplarian orbits and could even provide enough delta-V to maneuver into a retrograde solar orbit.

Not only is this technology feasible, but a private company plans to launch the first solar sail mission using state-of-the-art materials[18]. The spacecraft would be a square sail with inflatable deployment booms and its payload would be the remains of deceased people. While this might be seen as a novelty mission, it will go far as a technology demonstrator. NASA has plans to eventually send a solar sail-based probe very far out of the solar system, a mission that would be very difficult and expensive to do with chemical propulsion.

The potential of solar sailing is limited by the capabilities of the material technology, difficulties in manufacturing and deployment of the gossamer structures, and the shear size of a sail needed to push payloads that would be useful for say, the colonization of Mars. Another limitation is that the effectiveness of a sail will drop as the spacecraft travels further from the sun, since the light diminishes in intensity. Eventually, solar sails may routinely be used to ferry goods between destinations in the inner solar system, but for now, the technology is not yet there.

An idea that operates similarly to the solar sail is a magnetic sail, or Magsail. Just as a solar sail reacts against light pressure, a large superconducting ring could develop a magnetic field that would react with the magnetic field carried by the ionic particle stream from the sun, better known as the 'solar wind'. The drag force can be used to generate a force in any direction except for towards the sun, much like a sailboat sailing into the wind.

Numerous papers have explored this, and it seems sensible if certain technological hurdles can be overcome[19]. The system is still very large, and a major concern would be the deployability of a superconducting ring with a diameter on the order of tens of kilometers. It would also require a reasonably large power supply to power up the magnetic field, not to mention the cryogenic cooling requirements of the ring. Still, superconducting cables are being developed for terrestrial power transmission[20], and deployable structures will surely develop in the coming years. Potentially, Magsails could perform the same mission as solar sails, probably moving cargo around the inner solar system.

Mini-Magnetospheric Plasma Propulsion, M2P2, is a technique that operates very similarly to the Magsail, except that there aren't any rings present to support the magnetic field. Rather, the researchers working on the M2P2 project at the University of Washington envision a

cloud of plasma that carries a magnetic field[21]. The magnetized plasma would interact with the solar wind or Earth's field in a similar way to Andrews' and Zubrin's Magsail concept. The plasma is coupled to the spacecraft and transmits thrust to the vehicle. The key improvement is the elimination of the huge superconducting ring, but plasma physics is not straightforward and the scaling laws may not allow very large devices to be built. At least here, the problems aren't of scale, but of complex and undiscovered physics. Stay tuned, it might actually work as advertised.

Electrodynamic tethers are another promising technology. By using long conductive wires, one can interact with a planet's ionosphere and magnetic field to generate forces or power. The concept was conceived by Grossi and Colombo circa 1980 and has reached the experimental phase in the US and Europe. Two shuttle missions and one free-flyer mission have been conducted and the results show promise. NASA is currently developing a mission (ProSEDS) in order to explore the technology further. This is basically how a thruster would work. A very long bare wire collects electrons from the surrounding ionosphere, a supplied potential drives them along the wire, forming a current, and that current produces a Lorentz force with the local magnetic field of Earth. The system can be reversed and the Lorentz force would then drive the electrons allowing the system to draw power from the wire. Prime missions for tethers include moving satellites around earth orbit and drag reduction of the space station.

Some of the major problems with tethers were highlighted by the flight experiments. These include deployability, instability and control issues, and unexplained physics. For instance, while one of the shuttle experiments was deploying, it arced and the wire broke due to a probable manufacturing flaw. Before it broke, the wire actually collected more current than was predicted by the models. The instabilities come into play when considering the vibration

characteristics of the system. Models predict that some of the modes are coupled to the secular disturbances of the earth, producing large, undesirable deflections of the wire, which itself can be kilometers long.

Tethers are still probably the best near-term way to get propellant-free propulsion around Earth and eventually the Sun and Jupiter, which both have large magnetic fields. While tethers show promise, they also face an uncertain future due to mostly their large size.

And that brings us to the central caveat with the methods of propellentless propulsion presented. While some of them might work, they are generally very large systems. The largest space structure we have yet built will be the International Space Station. Building something out of the ordinary is inherently risky, and there has to be a pay-off large enough to offset that risk. The AAOTV vehicle I propose here will be fairly compact, with a largest dimension of about 50 meters. The relatively small size of this concept gives it the potential to be a viable propellentless propulsion technology in the near term. The rest of the thesis discusses the system analysis and physics of the system in an effort to evaluate its merit, good or bad.

1.4 Aero-assisted Orbital Transfer Vehicle, AAOTV

The Concept

The main idea behind this study is the possibility that an orbiting spacecraft could operate a ramjet propulsion system in the thin upper atmosphere. The propulsion system is analogous to an atmospheric ramjet you would find on a hypersonic aircraft. An inlet would serve to compress the incoming gas flow and direct it into the 'combustion chamber'. However, instead of burning fuel in the combustion chamber of the spacecraft, the incoming gas is heated electrically or accelerated electromagnetically. The result is fast exhaust gases and the system

generates net thrust. The electrical energy is supplied by an on-board power supply, which could be solar or nuclear.

The spacecraft doesn't store the propellant it collects, but routes it directly into the thrusters. Since the engines can only fire when supplied with propellant, the engine can only operate when close enough to Earth (or other planetary body with an atmosphere). But what happens if and when the orbit isn't close enough, say with an altitude greater then about 225 km? The energy produced by the power sources can be stored when the engine isn't being fired, and that energy can be tapped when the engines are 'on'. The storage of electrical energy allows very high power to be delivered to the engine. So as long as the target missions spend at least some time at LEO altitudes, propellant is free for this system. That means refueling techniques are no longer needed and the spacecraft can operate indefinitely with respect to expendables.

A simple configuration is shown below in Figure 1.2:

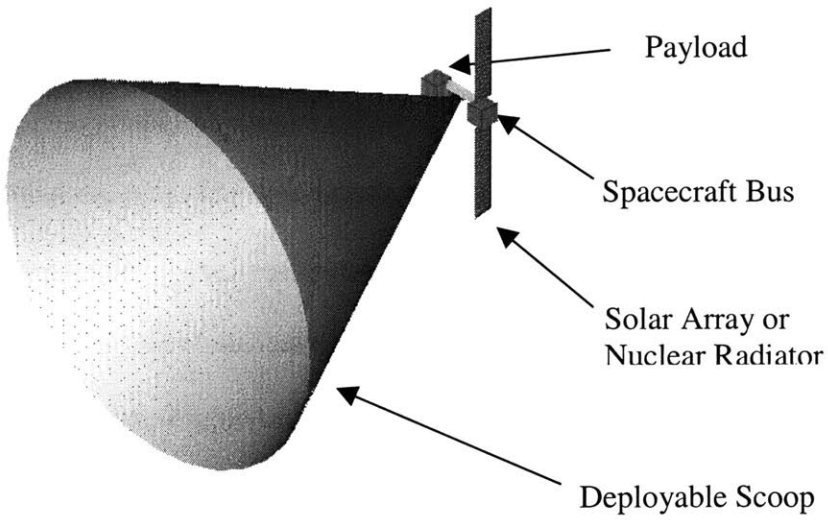

Fig. 1.2, AAOTV configuration

Sizing the scoop

The atmosphere is very thin at 200 km altitude, with a mean density of about 2.4e-10 kg/m^3. If this region does indeed have low density, won't the proposed intake have to be ridiculously large in order to get enough mass flow for an engine? Luckily the answer is no, since orbital velocity is at least 7,500 meters/second (Mach 21+ at sea level) and even a little gas counts. At these altitudes, the atmospheric drag force is appreciable enough to cause satellites to rapidly de-orbit, so the local atmosphere is still thick enough to be important. By calculating the area needed to supply the mass flow to an electric engine from:

$$F = \dot{m} v_{out} = \rho v_{in} A v_{out} \rightarrow A = \frac{F}{v_{out} \rho v_{in}} \tag{3}$$

where 'ρ' is the atmospheric density, 'v_{in}' is the orbital velocity of an intake, 'F' is the force produced by the engine, and 'v_{out}' is the exhaust velocity of the engine. For example, for v_{out} = 30,000 m/s, F = 50 Newtons, ρ = 2.4e-10 kg/m^3, and v_{in} = 8000 m/s, a square intake would only have to be 26 meters a side. This is simplified model, but it shows that the size of the needed scoop for this type of system can be relatively small.

Heat transfer concerns

Suppose for a moment that the scoop is a solid structure. What will keep this huge structure from burning up in the atmosphere? One can answer this question by performing an energy balance on the scoop. The energy added to the scoop from atmospheric heating would be at most the total kinetic energy of the gas that hits the scoop. The energy of the impacting gas is mostly due to the relative orbital motion, which we know. It can be calculated as follows:

$$Power_{in} = particle\ flux \cdot \frac{KE}{particle} = \frac{\rho A v_{in}}{MM} \cdot \frac{1}{2} MM v_{in}^2 = \frac{1}{2} \rho A v_{in}^3 \tag{4}$$

where MM is the molecular mass of the ambient gas. The greatest velocity at which this system can pass through the atmosphere is about 11,000 m/s, known as the escape velocity. It is the perigee velocity of a parabolic orbit that has a perigee in low earth orbit and an apogee at infinity, operationally, the edge of Earth's sphere of gravitational influence (SOI). As the distance from Earth increases, eventually the sun's gravity force becomes larger than Earth's; this is roughly the distance to the SOI. The power input for this worst-case scenario is then about 200 W/m^2. The energy radiated by the scoop surface can be equated to the incoming energy from atmospheric heating.

$$Power_{out} = A\varepsilon\sigma T^4 = Power_{in} \tag{5}$$

where σ is the Stefan-Boltzmann constant, 5.67e-8 $W/m^2/K^4$. Thus by assuming 'ε', the surface emissivity, the equilibrium temperature can be found. For aluminized Teflon, ε is given as 0.8, which yields an equilibrium temperature of 45.8 K, very low indeed! In fact, the energy input from direct sunlight is about 1,358 W/m^2 in space[3], which is much greater than the aerodynamic heating.

Comparison to electric propulsion

Since this system is electrically powered, it will share some of the disadvantages of purely electrical systems. For instance, if the system is used to do orbital transfer, it will still take at least a few months with near-term power sources (<300 kW). An important goal of the mission studies in this report is to find out how to keep the transfer times short. The prime difference and advantage of the AAOTV is the unlimited propellant supply. A purely electrical system would require frequent refueling in order to perform many missions, but the AAOTV can

operate its whole lifecycle without being refueled. The bus would have to be reliable enough to last the lifetime of the mission without suffering fatal failures of any critical systems or gradual degradation due to long-term space exposure. This isn't unrealistic given the lifetimes of some ComSats, 10+ years.

Mission applicability

More than a few missions could benefit from using the thin atmosphere for propulsion. Perhaps the first one that comes to mind is canceling the drag on satellites due to the atmosphere. The drag reduction mission is only important for satellites with a portion of their orbit below about 500 km due to the high atmospheric density there. LEO satellites carry a significant propellant load dedicated to boosting the orbit. The main problem is the complexity of the scoop system on a relatively small, cheap LEO satellite. Other problems include the interference of an intake scoop with communications and observation payloads. The major orbiting space station, ISS, requires a significant fuel load to maintain its orbit. If that propellant load was eliminated, so would be the cost of the re-supply missions that carry the propellant. However, these space stations are massive, so a scoop would have to be pretty big, with a sizable, dedicated power source in order to boost the orbit. First-order calculations don't say that these missions wouldn't work, but the pay-off is small in comparison to the orbital transfer missions.

An orbital transfer mission consists of picking up cargo and moving it to a different orbit. The three identified here consist of picking up cargo in LEO and moving it to GTO, a lunar transfer orbit and a Martian pre-transfer orbit. In each of these, the AAOTV and payload must complete many orbits, each one raising the apogee a little bit. The most radical of these is the Mars transfer, in which the payload is carried to a transfer orbit with an apogee close to the

Earth's sphere of influence. Once released, the payload would fire on-board engines at the orbit perigee in order to obtain a trajectory leading to Mars. The AAOTV could give the Martian payload that initial 'kick' of delta-V, which would increase the amount of payload that could be carried to Mars on a given launch system. The disheartening argument against this mission is principally with the massive siza of potential Martian cargo. A heavy payload would need a long time to achieve the pre-transfer orbit with today's power systems. Also, manned missions put a premium on travel time, and time spent lingering around Earth should be avoided. This mission might be feasible for unmanned cargo if high power nuclear reactors are developed.

Well what happens, if we want to go to the moon? Since the AAOTV wouldn't have to leave the Earth's gravity well, it could potentially ferry stuff to moon, drop it off and come back for more. It doesn't seem like such a good idea for material returning from the moon, since it would have to be accelerated to the AAOTV's speed to dock with it. That acceleration is almost the same needed to return to Earth in the first place. The same arguments against AAOTV manned Martian travel also apply to the Lunar manned missions. So, while heavy payloads will require long transfer times, the AAOTV could provide propellentless transportation to the moon for cargo.

Since the international community has shown little interest in supporting large scale Mars and Lunar missions, this thesis focuses on something the world does seem to be very interested in, launching geostationary communication satellites. As depicted in the following cartoon, the AAOTV picks up the payload in LEO, and through perigee burns, extends the apogee of the mutual orbit of the payload and AAOTV all the way to GEO altitude. The AAOTV then releases the payload where it would fire an apogee kick engine to achieve its final, circular orbit. The AAOTV would then lower its apogee until it returns to LEO, where it could pick up another

satellite.

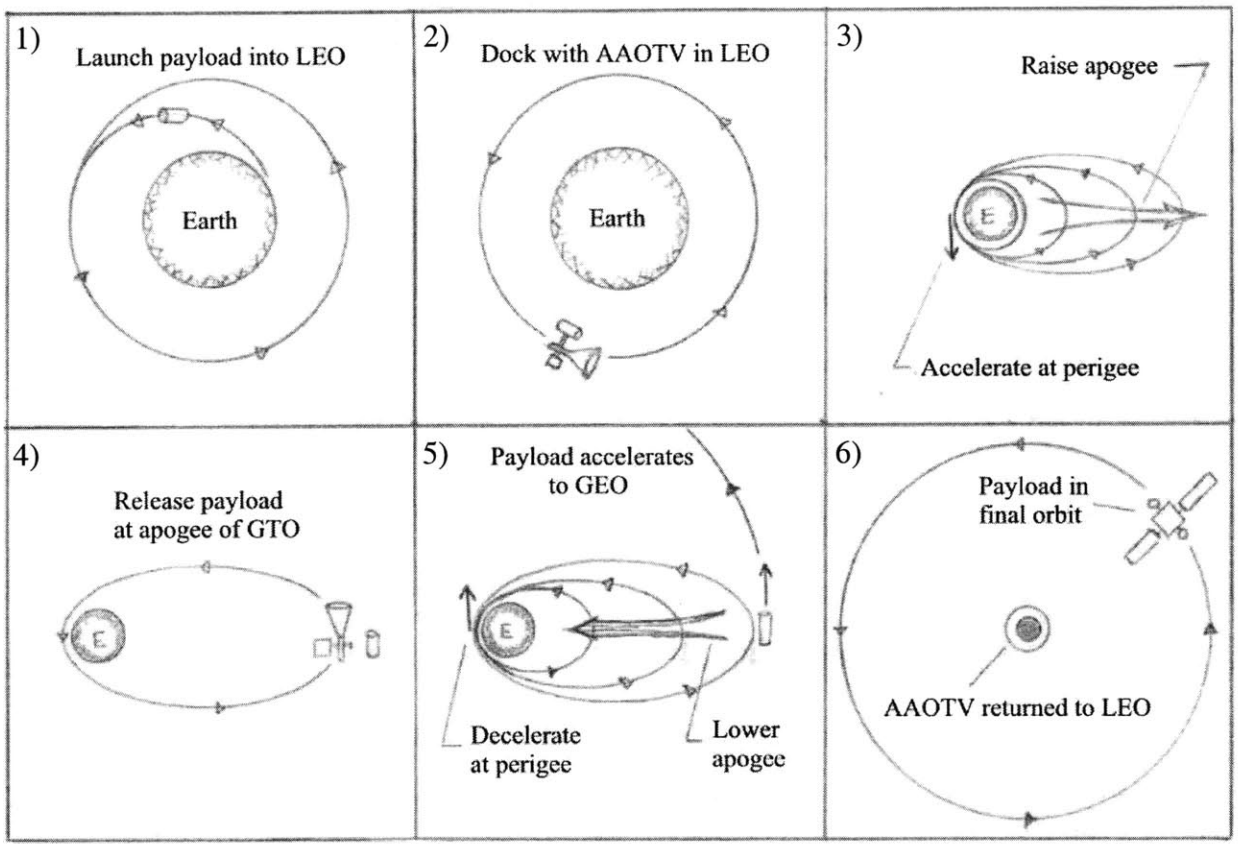

Fig. 1.3, Mission profile of a reusable Aero-assisted Orbital Transfer Vehicle, AAOTV

Overview

The remaining pages delve into the details of analyzing such a system. The success of the system will depend on how quickly it can move satellites from orbit to orbit and if it can do it at significant cost savings over conventional methods. The first third of the work characterizes the performance in terms of transfer times, comparative increase in payload capacity, and cost effectiveness for a generic 'scoop'. The second third explores the physics of a specific type of scoop via numerical analysis. In the last section, the solid-walled conical scoop knowledge is combined with the mission studies in order to present a workable concept and elucidate any challenges the system poses.

Chapter 2

Mission Studies

2.1 Method of analysis

Parametric analysis and optimization

The analysis of this concept consists of formulating expressions for the thrust created by the engines in terms of all the operating parameters and then propagating the spacecraft's position and velocity through a sufficient transfer time. In order to accommodate different drag models for the intake component of drag, the thrust equations are derived generally, with drag left in as an independent parameter.

The electrical energy stored over one orbit is given by multiplying the steady power supplied by the time spent charging. The charging time is the period of the orbit minus the engine burn time.

$$Electrical\ Energy_{stored} = (Period - \Delta t) * P \tag{6}$$

The power delivered during the burn is given by,

$$P = \frac{Electrical\ Energy_{stored}}{\Delta t} \tag{7}$$

The technique of storing electrical energy over a long time allows the thruster to operate

at high power (MW's) for short bursts (1-5 minutes), generating high accelerations with state-of-the-art spacecraft power levels (~20 kW). This effect becomes very pronounced in highly elliptical orbits where the time to store energy is large in comparison to the burn time, resulting in power multiplication factors as high as 300.

In order to develop expressions for the performance of the system, the intake and engine are separated as follows,

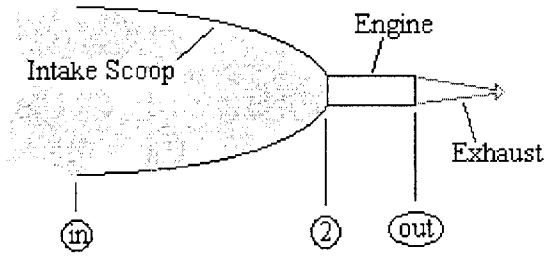

Fig. 2.1, System Diagram

From the above model, the drag on the scoop is defined by the gas momentum lost as it passes from station 'in' to '2':

$$D = \dot{m}(u_{in} - u_2) \tag{8}$$

The power added to the beam can be equated to the difference in kinetic energy between the gas entering the engine and the exhaust gas. The mass flow is assumed to be constant and an engine efficiency, η, is introduced.

$$P = \frac{\dot{m}}{2\eta}(u_{out}^2 - u_2^2) \tag{9}$$

Substituting (8) into (9), the expression for power becomes:

$$P = \frac{\dot{m}}{2\eta}(u_{out}^2 - u_{in}^2 + \frac{2D}{\dot{m}}u_{in} - \frac{D^2}{\dot{m}^2}) \tag{10}$$

The exhaust velocity produced by the system is given by rearranging terms.

$$u_{out} = \sqrt{\frac{2\eta P}{\dot{m}} + u_{in}^2 - \frac{2D}{\dot{m}} u_{in} + \frac{D^2}{\dot{m}^2}} \tag{11}$$

Note that the exhaust equation simplifies to the traditional rocket propulsion expression when intake velocity and drag are both set to zero.

A one-dimensional momentum equation gives a functional relationship between the net force on the system in terms of mass flow, drag, intake velocity, and exhaust velocity:

$$F = \dot{m}(u_{out} - u_{in}) - D \tag{12}$$

The force produced is given by,

$$F = \dot{m}\left[\sqrt{\frac{2\eta P}{\dot{m}} + u_{in}^2 - \frac{2D}{\dot{m}} u_{in} + \frac{D^2}{\dot{m}^2}} - u_{in}\right] - D \tag{13}$$

The most important measure of performance for the system is the velocity change produced by an engine firing.

$$\Delta v = \frac{F}{m} \cdot \Delta t \tag{14}$$

where 'm' is the total spacecraft mass and the net force, F, is assumed to be constant over the entire engine burn duration, Δt. In order to perform a mission in the least number of orbits possible, the delta-V per orbit (per firing) should be driven as high as possible. It is useful then to examine the relationship between delta-V and the parameters of the system. First, total mass should be low and thrust should be as large as possible. The thrust depends on three parameters that are variable: burn time, mass flow, and energy delivered.

Ultimately, Equation (14) suggests that burn time should be maximized for maximum delta-V. Now, power scales as the inverse of time (7), and force scales as the square root of

power or the inverse square root of time (13). Plugging (13) into (14), delta-V varies as the square root of burn time. For low-earth orbits, ones in which most of the orbit has the desired atmospheric density, the charging time is reduced by increasing burn time. Also, if a perigee burn is desired (required for a LEO-GEO transfer), the burn time should be limited. 'Perigee burn' simply means we are trying to approximate an impulsive maneuver at perigee, so as not to raise the perigee of the orbit out of the usable portion of the atmosphere. For elliptical orbits, the time spent at low altitude in each orbit falls to the range of minutes. The system only collects mass in real-time (no storage), so the engine should discharge its energy within this tight window. The maximum discharge rate of the energy storage system then constrains the burn time. So the end all is that you want to fire the engine as long as you have atmosphere to ingest.

Similarly, how does the power level affect the performance? Keeping all else equal, the thrust and delta-V roughly scale as the square root of the power supplied. It is not an exact scaling due to the inclusion of drag terms in (13).

The mass flow is the most intriguing parameter. To increase mass flow, the intake area of the scoop would have to be increased or the perigee lowered to an altitude where the atmosphere is more dense. Increasing the mass flow will tend to reduce the exhaust velocity and increase thrust for a given power level. But the increased mass flow rate will then increase the drag on the scoop. The dependence of drag on area and density depends on the physics of the scoop. Different approaches to 'scooping' a low-density, hypersonic, rarefied gas flow will undoubtedly have different drag characteristics and scaling. Since technology for compressing the upper atmosphere is not well developed, interesting trends can be found when using a conventional, velocity-squared relation for drag.

$$D = \frac{1}{2}\rho v^2 A C_d \tag{15}$$

In the previous equation, the drag coefficient, C_d, is assumed to be invariant with regards to scale for this first-order analysis.

For the simple ballistic drag model above, an expression for optimal intake area can be found by maximizing the thrust (and subsequently delta-V) as given in (16) and (17). This is accomplished by taking the partial derivative of thrust with respect to area, keeping power constant, and setting equal to zero.

$$\frac{\delta F}{\delta A} = \rho u_{in}\left[\sqrt{\frac{2\eta P}{\dot{m}} + u_{in}^2 - \frac{2D}{\dot{m}}u_{in} + \frac{D^2}{\dot{m}^2}} - u_{in}\right] + \rho A u_{in}\left[\frac{-\eta P}{\rho u_{in} A^2\sqrt{\frac{2\eta P}{\dot{m}} + u_{in}^2 - \frac{2D}{\dot{m}}u_{in} + \frac{D^2}{\dot{m}^2}}}\right] - \frac{1}{2}\rho v^2 C_d = 0 \qquad (16)$$

Solving for the optimal area,

$$A = \frac{\eta P}{\rho u_{in}^3\sqrt{2C_d}\left(1+\sqrt{\frac{C_d}{2}}\right)^2} \qquad (17)$$

Fig. 2.3 shows the square root relation between optimal scoop radius and power, taken at a representative orbital velocity of 8 km/s and a local atmospheric density of 2e-10 kg/m^3. One can see for a given power, the optimum radius is increased as the drag coefficient is reduced. The optimal area then scales linearly with power.

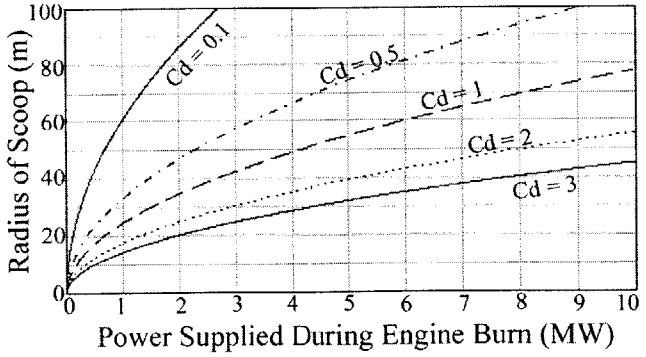

Fig. 2.2, Optimal radius vs. rower for different drag coefficients

The force corresponding to the optimal area at each power level is found by substituting

(17) into (13), the force equation. The result is shown below in Fig. 2.4. For a given drag characteristic, the optimal force varies linearly with respect to power.

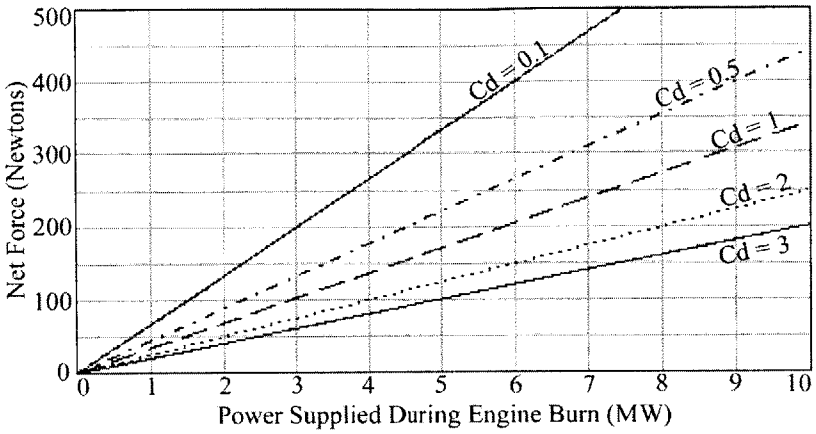

Fig. 2.3, Maximum force vs. power over different drag coefficients

This linear behavior shows that if the area is kept at the optimum, a system has a characteristic power specific force and area specific power for any drag characteristic, which is shown in Table 2.1. The power described here is the power the engine consumes. Also, the optimized force is positive for the whole range of powers and drag coefficients. The worst-case drag coefficient for any scoop should be around 4, which corresponds to total particle reflection. This analysis should be taken with the knowledge that the optimal area may change over a given mission, as orbital velocity, density, and available power vary.

Table 2.1, Performance metrics at optimum scoop area,
u_{in} = 8000 m/s, $\rho = 2 \times 10^{-10}$ kg/m^3, $\eta = 0.8$

	Drag Coefficients, C_d					
Metrics:	3	2	1.5	1	0.5	0.1
Power per unit Force (kW/N)	49.5	40	34.8	29.1	22.5	15.0
Power per unit Area (W/m^2)	1550	1024	772	528	288	85.7

From the above table, one can see that low drag scoops would optimize toward less force

produced for a given scoop area. Higher drag scoop schemes would be smaller and higher power devices.

An interesting parallel can be drawn to the modern electrical propulsion concept of optimum specific impulse for a given mission. By substituting the expression for optimum area, (17), into the exhaust velocity equation, (11), remembering mass flow is dependent on area, and simplifying, an expression for the optimum exhaust velocity is found.

$$\frac{u_{out}}{u_{in}} = \left(1 + \sqrt{\frac{C_d}{2}}\right)^2 \tag{18}$$

Since the optimal area scales linearly with power, the ratio of exhaust velocity to intake velocity is dependent only on the drag coefficient of the scoop.

The ratio of optimum exhaust velocity to the intake velocity is plotted against drag coefficient below.

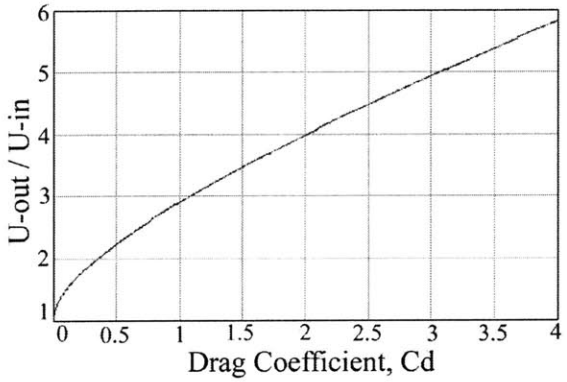

Fig. 2.4, Optimal exhaust velocity for different drag coefficients

At very low drag coefficients, the value is slightly greater than one, since there isn't much drag to counter-act. At higher drag coefficients, the optimal exhaust velocity is higher, in order to make-up for drag. A practical limitation is that if the power is low enough, the exhaust velocity would be lower than existing ion or MPD engine capabilities. For example, at LEO orbital velocity of 7,500 m/s, and C_d = 0.5, the optimum exhaust velocity is 15,000 m/s. This issue could be resolved through engine development and/or having the system operate at sub-

optimal areas and/or exhaust velocities.

In order to take into account the variations in power, burn time, and density that would occur in a real mission, an orbit-raising model was constructed. The purpose of the model is to define the transfer time for a given mission and observe how the individual parameters affect performance.

2.2 Orbit raising model

The model uses an orbit-by-orbit approach. From an initial orbit, the orbital elements are used to calculate the orbital period. The amount of time used to store energy in a given orbit is found by subtracting from the orbital period the time in which a full orbit is under a certain cut-off altitude. This altitude represents the edge of the atmosphere in which the spacecraft engine operates. The density is taken as a constant for the burn, so this altitude should be limited to a corresponding density that is within some percentage of the design atmospheric density and altitude. For this case, +50% density was chosen, corresponding to 230-km cut-off altitude. For those orbits within the atmosphere, a maximum burn time is specified which would estimate an impulsive burn instead of the reality of a thrust arc. A more accurate model would be to vary the density and hence the mass-flow at the different altitudes and corresponding velocities. The adverse effects produced by this sub-optimal burning could possibly be compensated for by adjusting the power level supplied to the engine. So then, to first order, the burn time is the time spent under the cut-off altitude. This time is calculated for each orbit as follows.

First, the semi-major axis of the orbit is calculated,

$$a = -\frac{\mu}{2\left[\frac{v_p^2}{2} - \frac{\mu}{R_p}\right]} \tag{19}$$

Second, the radius of apogee is found,

$$R_a = 2a - R_p \tag{20}$$

where v_p is the orbit velocity at perigee and R_p is the orbit radius at perigee. Third, the eccentricity is calculated,

$$e = \frac{R_a - R_p}{R_a + R_p} \tag{21}$$

Fourth, the true anomaly at the cut-off altitude, R_c, is found,

$$v_c = \cos^{-1}\left(\frac{a(1-e^2)}{eR_c} - \frac{1}{e}\right) \tag{22}$$

Fifth, the eccentric anomaly for the cut-off point on the orbit can be found,

$$E_c = \cos^{-1}\left(\frac{e + \cos v_c}{1 + e \cdot \cos v_c}\right) \tag{23}$$

The mean anomaly at the cut-off point is then given by,

$$M_c = E_c - e \cdot \sin E_c \tag{24}$$

Lastly, the time spent on each orbit below the cut-off altitude is given by,

$$t_c = 2M_c\sqrt{\frac{a^3}{\mu}} \tag{25}$$

For each orbit, the delta-V for a given vehicle is then calculated and used to increment the perigee velocity for the next orbit. The process thus steps up the apogee of consecutive orbits with time.

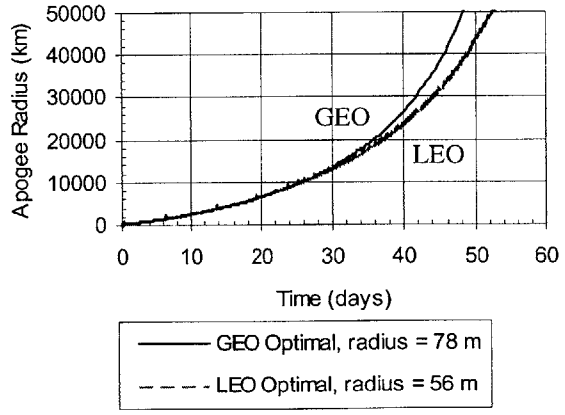

Fig. 2.5, Apogee progress for 100 kW systems with thrust optimized at different altitudes

The altitude time history is the primary indicator of performance. For example, if one is interested in the amount of time that the system will spend in the Van Allen belts, the time history will you tell you that a significant portion of the mission is spent passing through these zones. If solar cells are chosen as the power system, the repeated exposure necessitates the use of radiation-resistant systems. One could also plot engine power, orbital period, energy stored, exhaust velocity, and other useful quantities versus time. The model allows the specification of different configurations, power levels, energy storage capacities, and drag characteristics. For instance, a velocity or area-dependent drag coefficient could be included. The speed and flexibility of the model allow for quick analysis and exploration of the parameter space.

The general approach to defining a particular mission starts with the specification of an initial orbit, atmospheric density, steady-state power level and the spacecraft mass. The optimal area for the system is then found by trial and error and looking at the effect on total transfer time.

The plots of apogee radius vs. time show interesting behavior with respect to what altitude the scoop area is optimized. Fig. 2.5 shows the apogee progress vs. time of two systems. The first approach optimizes thrust for the initial LEO orbit climb-out by setting the scoop size at this altitude. These initial orbits are the slowest phase of the raising process in terms of apogee progress. By increasing the scoop size a faster climb to GEO can be accomplished. The scoop size will then be optimized for the power levels somewhere in the middle of the raising process. The second approach takes longer to climb out of LEO but reaches GEO quicker. It shows that using a larger scoop on a 100kW system can reduce the transfer time from about 47 days to 44 days. The obvious suggestion is then to devise a scoop that can vary its size based on the power available, which may or may not be reasonable. In any case, this is not a major issue since the transfer time is only mildly sensitive to deviations from the optimum. The orbit model shows

that the system can be off by as much as 25% in area and only suffer less than a 10% increase in transfer time. However, large deviations from the optimal area still produce large increases in transfer times.

Another parameter that can be varied in the model is the starting orbit. The mission might not want to start in a LEO circular orbit for drag and docking considerations. While the AAOTV is waiting for its next payload, it must contend with atmospheric drag like any other satellite. It has a few options, such as continuously firing its engines in order to counter-act drag or only firing periodically. Also, the AAOTV will need to conduct docking maneuvers in LEO with its payloads, which will be difficult if it must also concurrently fire its engines to counteract drag. Another option then is to maintain an elliptical LEO, say 300 by 200 km and dock at the apogee, where the main engines would be idle. Prospective payloads would then be launched into similar elliptical orbits. The effect of the different possible starting orbits is fairly negligible on the transfer time of the payload to GTO and GEO. The perigee velocity is given by:

$$v_p = \sqrt{\mu \frac{2R_a}{R_p(R_p + R_a)}} \tag{26}$$

One can then calculate the change in velocity needed to go from a 200 by 200 km orbit to a 200 by 300 km orbit, and the delta-V is 29 m/s. This increment corresponds to just a few orbits of the AAOTV, and thus doesn't greatly affect the overall mission time.

The model shows that the drag coefficient of the scoop greatly affects the transfer time, as one might expect. As the drag coefficient goes up into the high 3's and even 4's, the mission time increases, and the optimal scoop area drops. A C_d of 4 is equivalent to a flow being turned 180 degrees back on itself. Most surprising is that the mission will still work; it just has to drive the exhaust gases out at a higher velocity to make up for the drag. Those higher velocities

require more energy, which is fixed. Thus, it takes longer to build up the needed delta-V.

Variation of design atmospheric density and altitude

The orbit model assumes that the engine firings are done at a particular altitude and its corresponding atmospheric density. This makes it easy to simply change the atmospheric density input and see the effect on the transfer time of the orbit. The first test is to vary the density and see how the performance changes if both systems have optimum radius scoops.

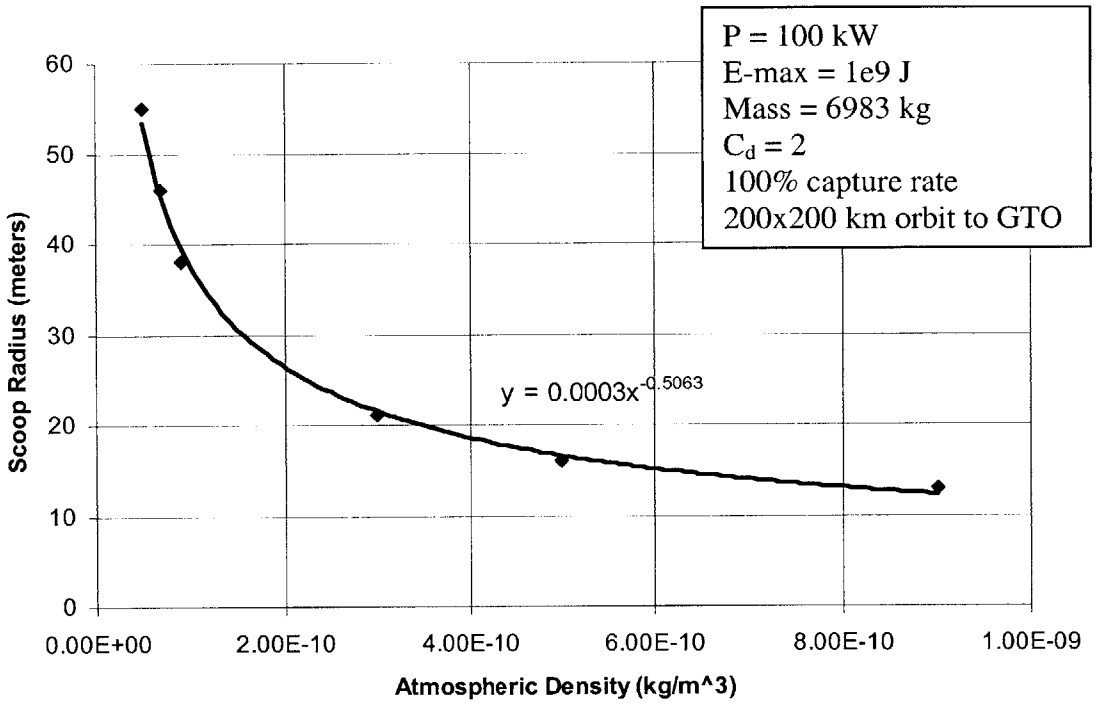

Fig. 2.6, Scoop radius and transfer time vs. density with optimally sized scoops at each density.

The interesting thing to note is that there is almost no performance, trip time, gain to be had by scooping the atmosphere at different density, provided that the size of the scoop is optimized to that density. For the test case above, the performance difference over a wide range of atmospheric densities is only one day. This is because there is a set amount of energy available to add to the incoming mass flow, and incoming gas density doesn't affect the optimal

exhaust velocity. Note also that the optimized scoop radius follows an inverse square root trend, as predicted by Equation 17 (Area~Radius^2). The slight deviation of the curve fit from an inverse square law is due to the error introduced by optimizing the scoop size by hand. This relation also tells you that although you won't get better performance, scooping gas with a greater density reduces the scoop size. I will revisit this in Chapter 4 as we will find the scoop size is a key factor in its physics and performance. Also, there is a limit to the density increases since eventually the heating will become an issue and/or the scoop size will be smaller than the significant spacecraft dimensions.

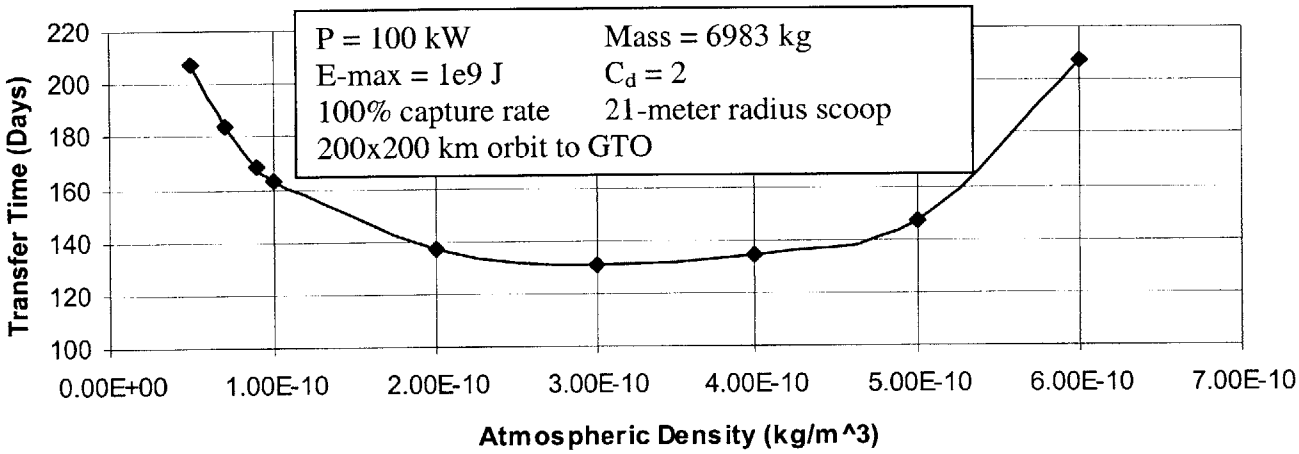

Fig. 2.7, Transfer Time vs. Density with fixed dimension scoop

The second test is to take a scoop optimized at a given density and then see how changes in the density affect the performance without changing the size of the scoop. The results for this test are shown above in Figure 2.7. Note the shape of the trend line, which forms a shallow bucket around the minimum value of 131 days. This means that a scoop optimized at a density of 3e-10 kg/m^3 wouldn't lose much performance even for density changes as high as ±50%. Once out of the bucket, however, the story changes. As the density increases, eventually the scoop cannot overcome the drag in LEO and cannot complete its mission. As the density is

lowered far from the design point, the transfer time becomes very large and exhaust velocities skyrocket as a lot of energy is being put into less and less gas. The shape and 'width' of this 'bucket' does vary over different optimization densities. As Fig. 2.8 shows, scoops optimized at lower densities have tighter 'buckets', and scoops optimized at higher densities have much wider ranges of operating densities. The 5e-10 kg/m^3 is much more tolerant to density variation as one optimized for 1e-10 kg/m^3. This provides further reason to operate the system a little lower in the atmosphere, since the scoop size will be smaller and the sensitivity to atmospheric density is more lenient.

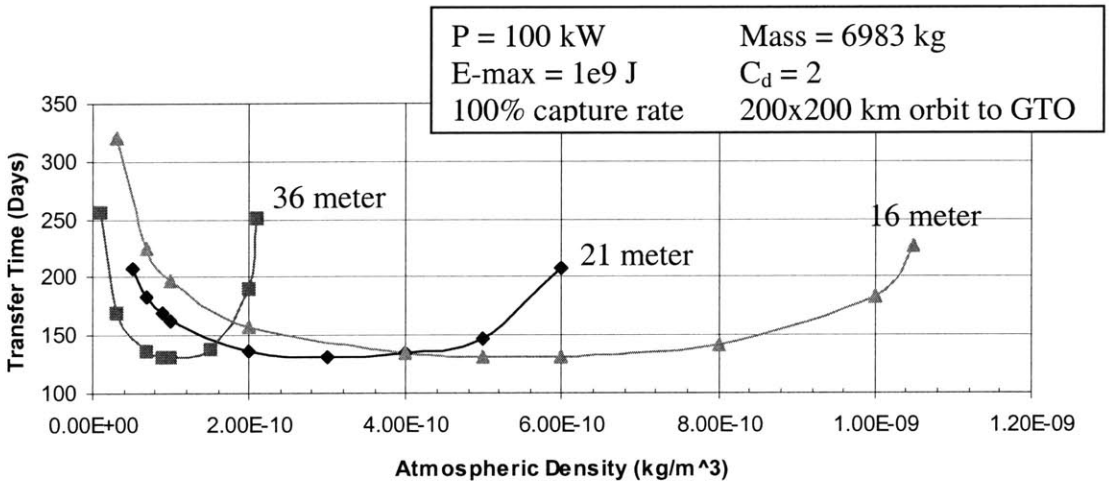

Fig. 2.8, Transfer time vs. density with various fixed dimension scoops

Variation of battery capacity

How much battery capacity does the AAOTV need? The maximum capacity is dictated by the longest period orbit, which occurs at the end of the orbit raising mission (GTO, ~200x35,786 km). In this orbit, there is about 10.5 hours of energy storage, compared to about 200 seconds of engine burn time. If you assume a 100 kW power supply, this translates into 3.8e9 Joules of energy. The simplified model assumes that the batteries that store this energy are

very lightweight, but if we look at current energy storage densities, it begins to look grim. As you can see in Table 2.2, current battery technology is fairly heavy and there are other options. The energy storage system also must be capable of high discharge rates (MW's), which batteries are not known for.

Table 2.2, Energy storage systems and considerations

Energy Storage System	Specific Energy Density (W hr/kg)	Discharge Rate (W/kg)	Maturity
Nickel cadmium[3]	25-35	low	standard
Nickel hydrogen (common pressure vessel)[3,22]	45-60	low	flight test
Sodium Sulphur[3,24]	140-210	low	development
Li Ion[3,23]	110-250	200-600	development
NEC Proton Polymer[3,25] battery	10-20	1000	development
Okamura Laboratory Inc. Capacitors[25]	15	2,000	development
Flywheels	44-66	high	development
Superconducting Magnetic Energy Storage[29]	?	high	ground installations

For the above example, for a maximum battery capacity of 3.8e9 J, with 60 W·hr/kg Nickel Hydrogen batteries, the battery mass is ~18,000 kg. This is a very large mass in comparison to the payload mass. It is essential to reduce this. The trade then, is to look at how sensitive the performance is to reduction in the energy storage capacity of the spacecraft. To see the general trend, we can use the example put forward in the previous section. The payload mass is held constant at 2,594 kg and advanced 200 kW·h/kg batteries are assumed. The target density is 3e-10 kg/m^3. The scoop radius is allowed to change in order to optimize the transfer time for each case. One can see in Figure 2.9 how the transfer time increases as the storage capacity is decreased. The trend shown is a strong function of the specific energy density of the batteries.

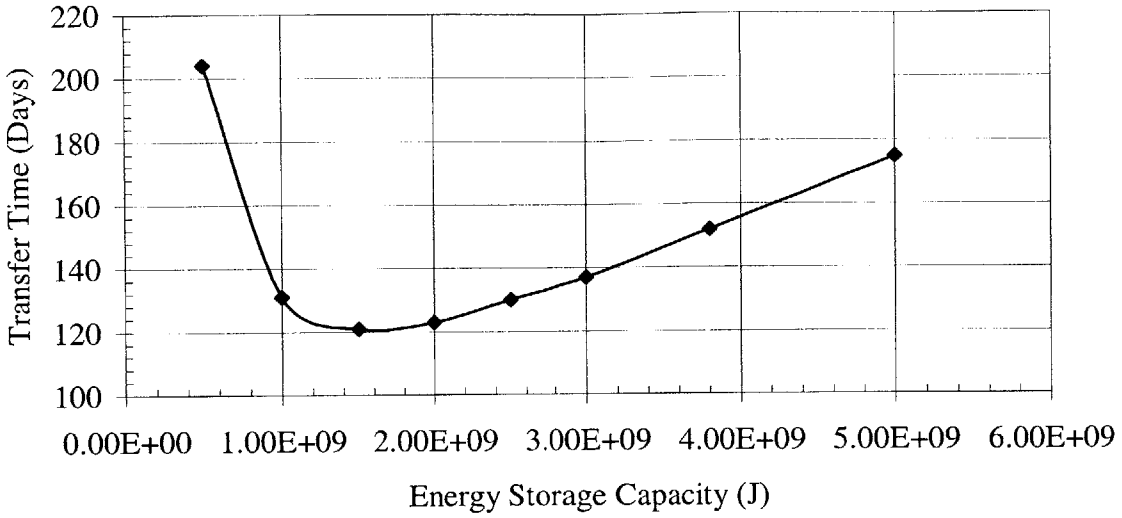

Fig. 2.9, Transfer time versus energy storage capacity

You can see that the performance is greatest at some intermediate value of capacity. The performance drops near maximum capacity because the high battery mass tends to retard the acceleration of the system during the initial climb out of LEO. The performance at low capacities suffers due to the limited amount of available power the system can expend in driving the thrusters.

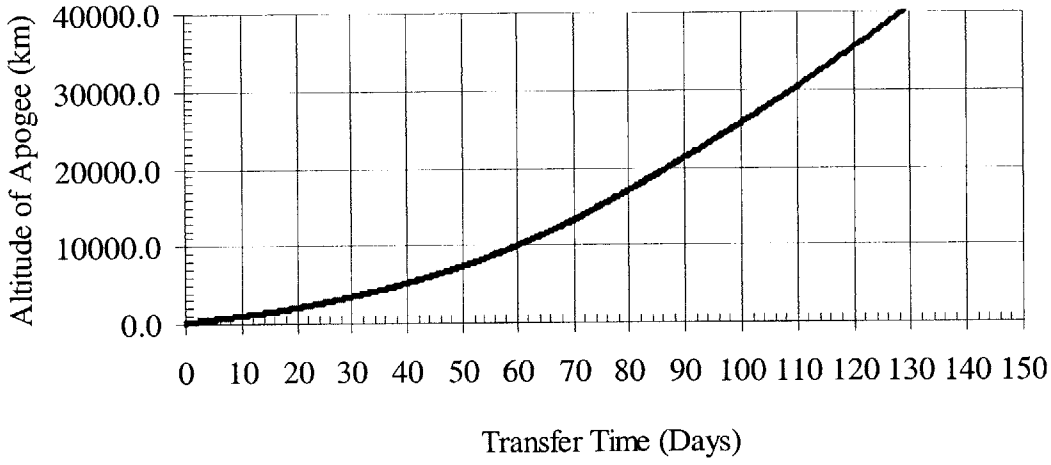

Fig. 2.10, Apogee radius vs. time for limited capacity energy storage, 1.5e9 J

As Figure 2.10 shows, the optimum results in an increasing rate of climb out of LEO and once capacity is reached, a steady rate of climb to GTO. These trends are important for defining the proper energy storage capacity for the baseline system concepts.

Variance of burn duration

The orbit-raising model can be used to find how the performance changes as the allowable burn time varies. Once again, the example of a 6983 kg, 100 kW system with a 21 meter radius scoop and 1e9 J of energy storage is used.

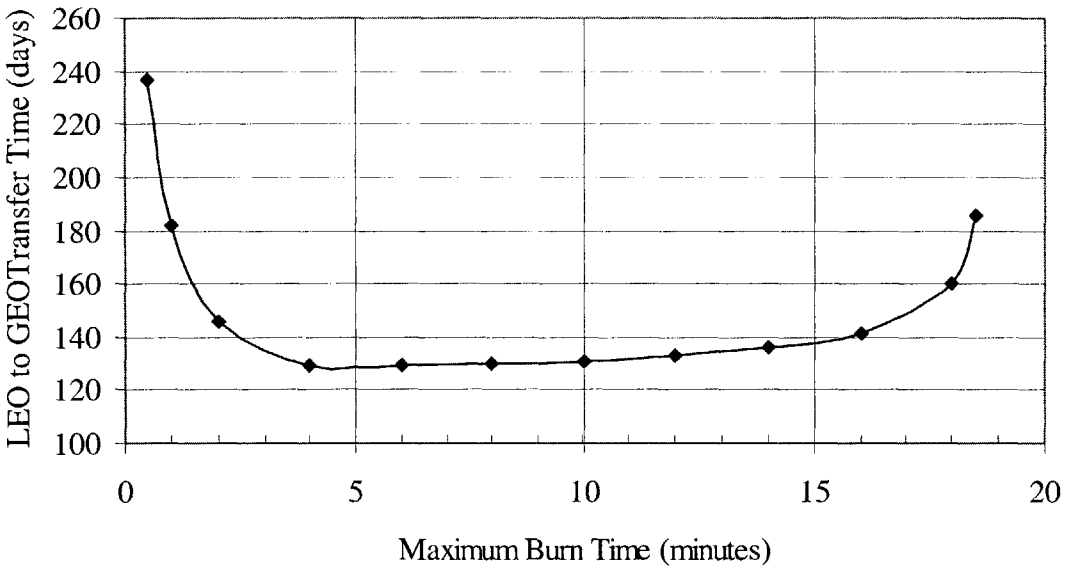

Fig. 2.11, LEO to GTO transfer time versus maximum engine burn time

On the above figure, as the burn time is allowed to go beyond 18.5 minutes, the AAOTV can no longer make enough delta-V to climb out of LEO and cannot complete its mission. At very short burn times, the thrust becomes very small and the transfer time becomes very large. Also, at short burn times, the engine must supply very high power levels that are probably not reasonable. As the AAOTV climbs to more eccentric orbits, the burn time becomes limited by

the time spent in the atmosphere, not by an arbitrarily chosen burn time.

Other system concerns will come into play here, such as the ability to approximate an impulsive perigee burn from what is actually a short continuous thrust arc. Also, the engine may have a lower limit on the exhaust velocity, which might force the stored power to be expended over a shorter time. The maximum discharge capability of the energy storage system will also limit how short the burn time can be, due to the associated increase in power delivered to the engines. From Figure 2.11, it seems that the system will be very close to optimal as long as the burn time is chosen somewhere between 4 and 15 minutes, and this shouldn't change much as the other parameters such as power level, scoop radius, mass, and energy storage change.

2.3 Idealized orbital transfer vehicle study

Ideal single-use mission

The first mission of interest is the one-time launch of a modern communications satellite to GEO orbit. An Atlas 2AS launch vehicle is used in order to see the difference between using state-of-the-art (SOA) chemical insertion into GTO, a proposed solar thermal system, and the AAOTV. The term 'ideal' means that no particular scoop technology is specified, just a certain collection area and a low drag coefficient of 0.5. The system bus mass is simply assumed, and the payload mass is maximized for the Atlas 2AS launch vehicle.

In the SOA case, the booster inserts the satellite into GTO with 28.5-degree inclination. A solid fuel kick motor circularizes and takes out the inclination with one burn at apogee. The mass of the apogee kick motor was taken from current Star-class motors.[3]

The solar thermal system uses solar concentrators to heat hydrogen propellant producing an I_{sp} of about 800 seconds. The system is under development by Boeing for the Air Force and NASA[26]. The proposed power levels range from 5 kW to 50 kW, and the solar stage produces

power for the payload after the orbit transfer. The cited transfer times are about one month for LEO to GEO, including the required plane change of 28.5 degrees. In order to estimate the mass of the stage, mass estimates corresponding to solar dynamic power systems were used.

The AAOTV is launched in tandem with the payload into LEO. There, the scoop and power system is deployed. The AAOTV then raises the orbit to GEO and sheds excess inclination. This raising segment takes 147 days. The scoop could then be retracted or discarded. The spacecraft would then execute circularization burns at apogee using propellant stored on-board. Once GEO is achieved the stage would supply power to the payload. For this mission, the steady power level would be 30kW at beginning of life. A specific power of 25 W/kg for solar panels was used[3]. The circularization burns would operate at an I_{sp} of 2000 seconds. The I_{sp} chosen should be large enough to gain the advantage of low-mass fractions, but not so high as to extend the mission unnecessarily.

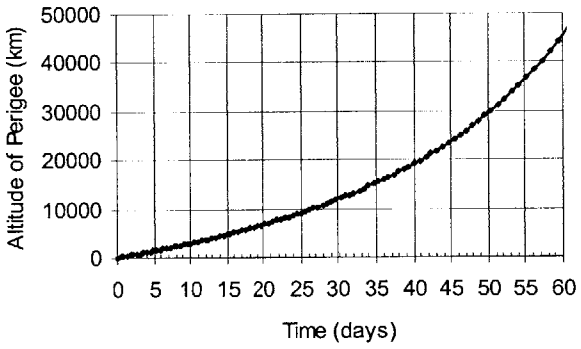

Fig. 2.12, Altitude of perigee versus time during orbit circularization to GEO, 35,870 km

As shown above in Figure 2.12, an I_{sp} of 2000 seconds results in a 54-day circularization. The over-all mass budget results are shown below in Table 2.3. Please note the assumptions made. Battery mass was sized by using the capacity required and figures for future battery systems given in Ref. 3. Likewise, the specific power for the AAOTV was taken as state-of-the-art solar panels, as given in Ref. 3. Delta-V was calculated for the given orbital maneuver. The I_{sp} and tankage mass for the SOA system was taken from flight system data[3]. The tankage mass

for the SOTV and AAOTV was assumed to be 10% of the fuel mass. As this is a high level study, there is considerable play in values regarding battery and power technology.

Table 2.3, Ideal single-use mission mass budget

	SOA	SOTV	AAOTV	
start mass	3490	8000	8000	kg
delta-V	1830	5700	1598	m/s
Isp	290	800	2000	sec
fuel needed	1657	4133	626	kg
tankage	83	413	63	kg
battery mass	N/A	N/A	1132	kg
power	N/A	5000	30000	W
specific power	N/A	15	25	W/kg
power mass	N/A	333	1200	kg
Payload w/ power	1750	3120	4979	kg
Transfer Time	<1	30	201	days

Most of today's communications satellites are under 2500 kg and are typically launched from Ariane-class rockets. Due to the use of chemical propulsion, only about ¼ of the mass capability to LEO makes it to GEO. As shown above, advanced transfer vehicles enable the use of smaller, cheaper launch vehicles. The proposed SOTV provides about double the mass capability of current technology, but takes about a month to reach orbit. The moderately powered AAOTV lifts three times the current standard in less than 7 months. The recently launched Hughes 701 satellite took several months to attain its final GEO orbit using ion thrusters to reduce the eccentricity of a super-synchronous transfer orbit. Also, most satellites take several months to conduct checkout procedures, so a transfer of several months should be acceptable if these tasks could be done concurrently. Reducing the size of the payload to SOA sizes reduces the stated transfer times. Aside from reducing launch vehicle costs, the AAOTV also expands the capabilities of a given launch system.

The extension of this single mission system is the transfer of relatively large masses to

high orbits, limited only by the LEO capability of available launch systems. This technique would enable the Ariane-class systems to launch heavy modules for GEO space stations.

Ideal reusable missions

The concept can then be expanded into a reusable space tug.

The first scheme would consist of a high power vehicle picking up satellites in LEO, and carrying them to GTO (zero inclination), where it would release them. The satellite would then fire on-board propulsion to circularize, and the AAOTV would return to LEO by reversing thrust at perigee. Reverse thrust is discussed further in Chapter 5.

The second scheme would transfer propellant from the satellite to the AAOTV. This fuel would be used to circularize the satellite's orbit, after which it would be released and the AAOTV would use the remaining propellant to lower its perigee back into the atmosphere. The main advantage of propellant transfer is the high I_{sp} capability of the AAOTV's engine and the associated reduction in fuel mass launched with the satellite.

The basic trade to consider is the reduction of payload launch costs compared to the price of the initial system and its operation. A 100 kW nuclear-powered system is used to bring down transfer times into the range of many missions per year. The power specific mass is assumed to be 20 kg/kW, as given in Ref.3. An average payload is assumed to be 4000 kg, allowing for growth of current designs. The assumed drag coefficient is 0.5, corresponding to hypersonic drag coefficients for oblique shocks. This study also assumes that all incident gas particles are 'captured' by the intake. The AAOTV bus mass is the same in both cases for sake of comparison and includes the mass of lightweight, high capacity battery systems. One way to keep the battery mass lower is to size the systems with a capacity lower than optimal. It should be noted

that reducing the mass of payloads to the standards of today's satellites could also help alleviate inadequacies in future battery technology.

Table 2.4, Time budget for two reusable missions			
	On-Board Chemical	Propellant Transfer	
Power	100	100	kW
Specific Power	20	20	kg/kW
Power mass	2000	2000	kg
AAOTV bus mass	1000	1000	kg
Payload final mass	4000	4000	kg
Delta-V	1600	3200	m/s
Isp	298	2000	sec
Payload fuel mass	2918	872	kg
Launched mass	**6918**	**4872**	kg
Apogee Raising			
start mass	9918	7872	kg
time	70	55	days
Circularizing			
start mass		7872	kg
time		17	days
final mass		7255	kg
De-circularizing			
start mass		3255	kg
time		7	days
final mass		3000	kg
Apogee Lowering			
time	22	22	days
Payload Time to GEO	**71**	**72**	**days**
AAOTV cycle time:	**93**	**101**	**days**

The time to perform each cycle is shown in Table 2.4. The time the payload spends in transit is about the same in each case. The cycle time of the transfer vehicle only varies by 8 days. The cycle time is used to find that this ideal system is capable of about 3.5 missions per year. If a lifecycle of ten years was assumed, the total launch and operating cost would be amortized over 35 missions. More detailed considerations of scoop technology will reduce the number of missions per year, as will be discussed in Chapter 5. For this system to be economically advantageous this 'per mission' cost should be less than the 'per mission' cost of launching satellites normally. The savings would come in the form of smaller, less expensive

launch vehicles, as much as $50-100M per launch[4]. This condition is highly dependent upon the future economics of operating spacecraft like the AAOTV and the specific cost of launching satellites. The economics of the system could be improved by increasing the on-board power of the transfer vehicle, which would reduce the cycle time.

A given reusable system could also serve other roles, such as satellite retrieval from GEO and return to LEO. There is also no reason it couldn't service a wide range of payload sizes. It could also regularly give interplanetary missions about 3.2 km/s of delta-V (the difference between orbital and escape velocity in LEO) in support of Lunar or Martian exploration and settlements. As long as propellant transfer from a payload isn't required, the system could be designed with very little interaction with the payload except for a basic hard dock. This versatility would allow the system to perform the most pressing mission at the time, sort of like an orbital 'Jeep'.

2.4 Remarks and motivation for scoop work

The above mission studies show that an ideal AAOTV craft has potential. As a single-use integrated power and propulsion system, the AAOTV can as much as triple the payload capacity to high orbits for a given launch system. The easing of propellant mass fractions allows smaller launch vehicles to be used for satellites with non-LEO final orbits. A reusable system could significantly reduce the cost and time (in comparison to current electric propulsion schemes) needed to reach GEO. The success of this concept relies on the reduction of operating costs and the development of key supporting technologies. High power, variable I_{sp} electric thrusters are required. Also needed are lightweight, high capacity energy storage devices that would be capable of the high rates of electrical discharge, such as terrestrial magnetic energy

storage systems[29]. Lightweight solar and nuclear power systems in the tens to hundreds of kWs are needed. The least developed technology is the scoop. A working system would have to be light, deployable, and not power-hungry. Possible ideas include inflatable structures operating on electromagnetic principles or low-density molecular flow principles. Work on magnetic nozzles for advanced propulsion systems may provide insight into this area. Another concern is the cost of operating the system continuously over many years, such as oversight, tracking, and troubleshooting. If these technical and managerial issues can be satisfactorily answered, the AAOTV could help to meet the world's orbital maneuvering needs in the near future.

The accuracy of the above analysis depends on the accuracy of the assumptions used. The scoop element is a vital component of the mission analysis, and its physics should strongly affect the operation and optimization of an AAOTV. The above analysis merely assumes that some 'scooping mechanism' is used, but doesn't go into particulars. In order to better characterize the performance of an AAOTV, the physics of scooping technology is explored in the following chapter.

Chapter 3

Scoop Options

3.1 Introduction

So what type of scoop should the system use? There two main sources of inspiration, interstellar ramjets and supersonic aircraft. The interstellar ramjets tend to employ electromagnetic fields in order to draw in thin ambient gas. Supersonic aircraft use shock structures to compress and slow incoming flows. Of the electromagnetic concepts, a few seem like they could be used for the AAOTV.

3.2 Electromagnetic Scoops

The solenoid concepts aim to create strong fields in which ionized particles become entrained, spiraling around the magnetic field lines. Sources such as Reference 15 claim that this will not work and that instead a magnetic bow shock will be set up, similar to the Earth's magnetosphere, as shown in Figure 3.1.

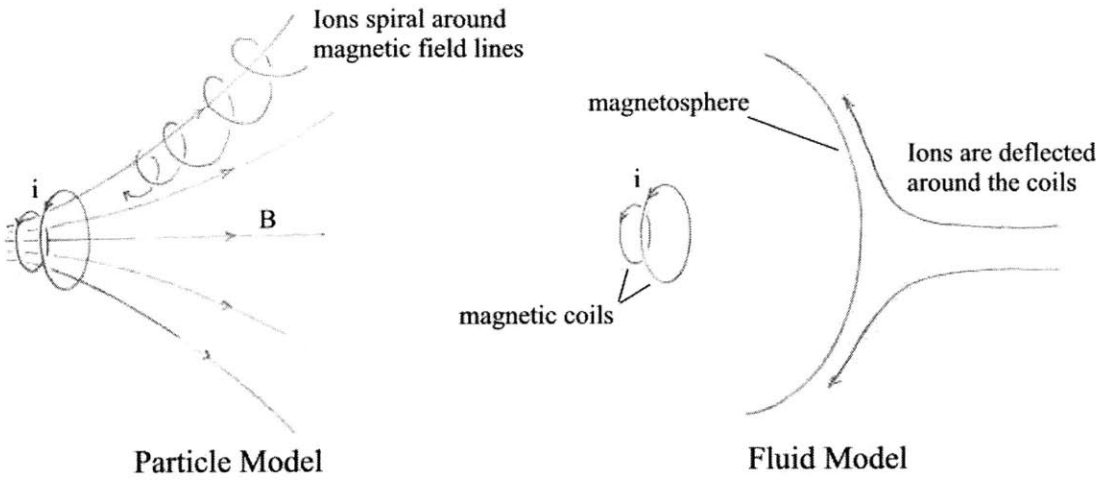

Fig. 3.1, Particle vs. fluid models describing flow around solenoids

The main reason for this difference is that initial models looked at single particles moving in a field, where the reality is a dilute flow field. An initial particle model was constructed to test this idea and these initial investigations showed very poor collection properties for various magnetic ring configurations. Another complication to this idea is that the incoming gas must be ionized before or as it gets to the intake. This idea is still alive in some form, however, as NASA is investigating the use of magnetic nozzles for the exhaust flows of fusion propulsion concepts.

The electrostatic deflection concept described in the introduction and shown in Figure 1.1 is another valid option. The problems with this for the AAOTV are that the ions still must be ionized before they get to the deflection grid and the space charge effect of ions and electrons streaming between the deflection grid and the engine.

Other electrostatic concepts include very large gridded ion engines such as Reference 15 and 28. These would combine the intake and engine in one unit. Another problem with for the AAOTV is the thrust density of an ion engine system. The area of the grid would have to be very large, and since the mass flow still has to be modest, the AAOTV would have to operate

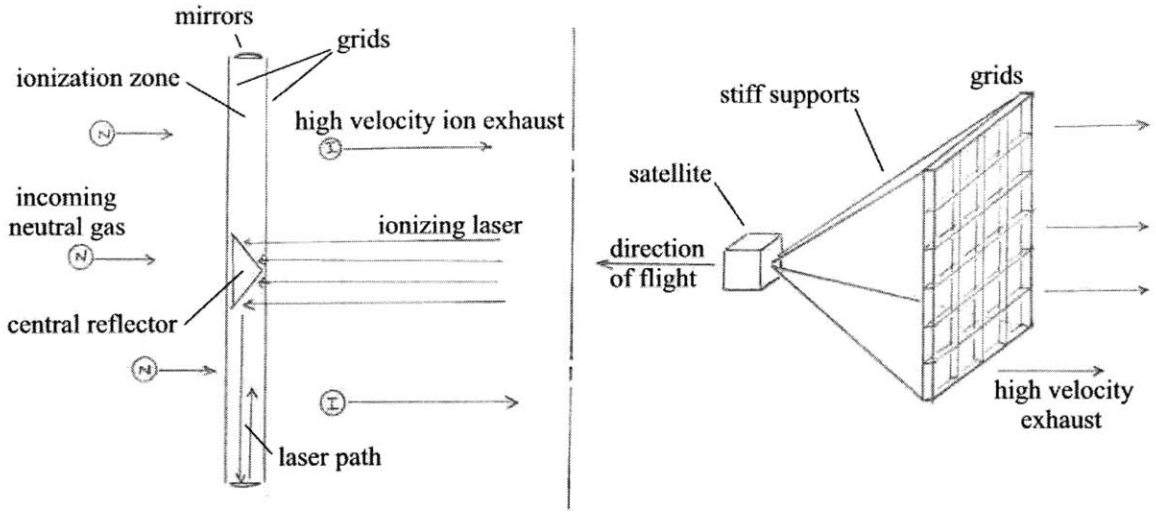

Fig. 3.2, Gridded ion engine concept, laser ionization shown in left box

at much lower atmospheric densities. The high power output (MWs) that the orbit raising model predicts would be very difficult to implement in a gridded ion engine. Ionization of the incoming gas is also a substantial hurdle, laser ionization is depicted below in Figure 3.2. The general concept is shown to the right.

3.3 Shock structure based scoops

Supersonic flight relies on shock structures to compress incoming flows. There are two important properties for these systems. First, the shocks are phenomena resulting from the acoustic properties of continuum flow gas. If the collisionality of the gas is absent, so are the shocks. In the upper atmosphere, one cannot assume that the continuum assumption for the flowfield is valid. So one cannot assume shocks will work. It doesn't mean that they won't, but the behavior will be different from a hypersonic flowfield. The downside to a solid-walled intake is the size of such a system. The surface area of the intake would be very large and the mass of the scoop would probably scale with the surface area. In order to keep the mass down,

the areal density of the scoop material would have to be low. Another difficulty would be the deployment of such a scoop.

Inflatable space structures offer an intriguing possibility that answers the issues of low areal density and deployability. An inflatable scoop would basically look like a cone with inflatable struts in the walls that would inflate to deploy the scoop. It would benefit from proven deployment techniques of large space structures[30] and the lightweight properties of thin films. The possible problems with this include micrometeoroid damage, atomic oxygen erosion, and durability over many years of operation.

Due to its simplicity and potential, this is the method focused on by this study. The detailed flow physics of an inflatable scoop are explored in the next chapter via numerical modeling.

The size, shape, and mass of an inflatable scoop are estimated in Chapter 5, during a detailed conceptual design study of a reusable system.

Chapter 4

Scoop Modeling

4.1 Introduction

The main question to answer by modeling the scoop is, "Will it work?" It would also be nice to know how much drag an inflatable cone-type scoop would have. From the engineering perspective, it would be nice to know how the scale and shape of the system affected the drag. Knowing these scaling laws is necessary in order to optimize the AAOTV. Depending on how sensitive the drag is to the size and shape, it may render the AAOTV unrealistic for certain missions and/or make it even more attractive.

This analysis starts by considering the flow regime in which the AAOTV operates, and then continues by identifying an appropriate method to model it.

4.2 Flow regime

The scoop will conceivably operate in the region of the atmosphere between 150-300 km (allowing for a wider range than stated previously). These altitudes are normally considered 'space' and the atmosphere there is very diffuse. As you can see in the following figure, the density is between 5e-12 and 1e-15 gm/ cm^3 or between 5e-9 and 1e-12 kg/m^3.

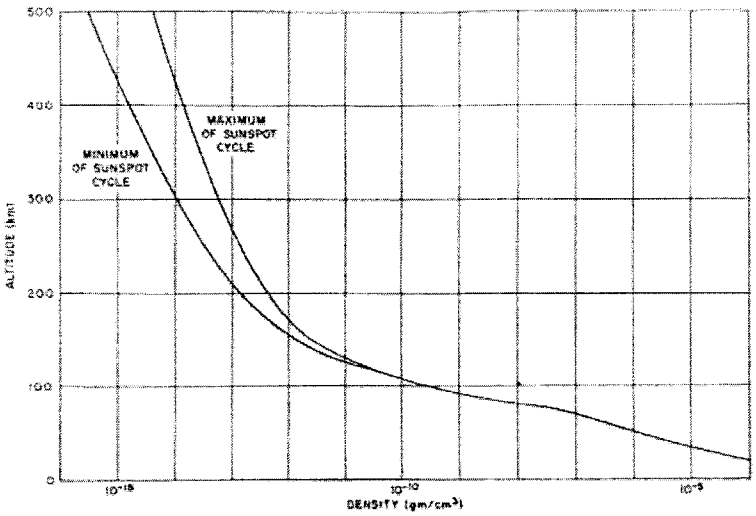

Fig. 4.1, Average daytime atmospheric densities at the extremes of the sunspot cycle[31]

The molecular make-up of the atmosphere at these altitudes is primarily oxygen and nitrogen molecules and atomic oxygen and atomic nitrogen. The composition is shown in Figure 4.2. The degree of dissociation of N_2 and O_2 increases as altitude increases past 100 km. At 200 km, which is in the middle of our range of interest, the composition is ~5% O_2, ~45% O, ~5% N, and ~45% N_2. This means that the AAOTV's scoop and engine would operate using these molecules. As the altitude increases further, the atmosphere becomes dominated by atomic oxygen. The sunspot cycle mostly affects the degree of dissociation in addition to the effect on overall density.

Figure 4.3 shows the mean molecular mass versus altitude. The sudden drop at 100 km from the constant number of 29 g/mol from sea level to 100 km is largely due to the dissociation of oxygen. The molecular mass starts to level off, but then falls sharply again at 800 km for solar min and 1300 km at solar max due to the importance of atomic hydrogen at these altitudes. For the AAOTV models, the molecular mass will fall somewhere between 16 and 29 g/mol, and the value will not be a strong function of sun cycle.

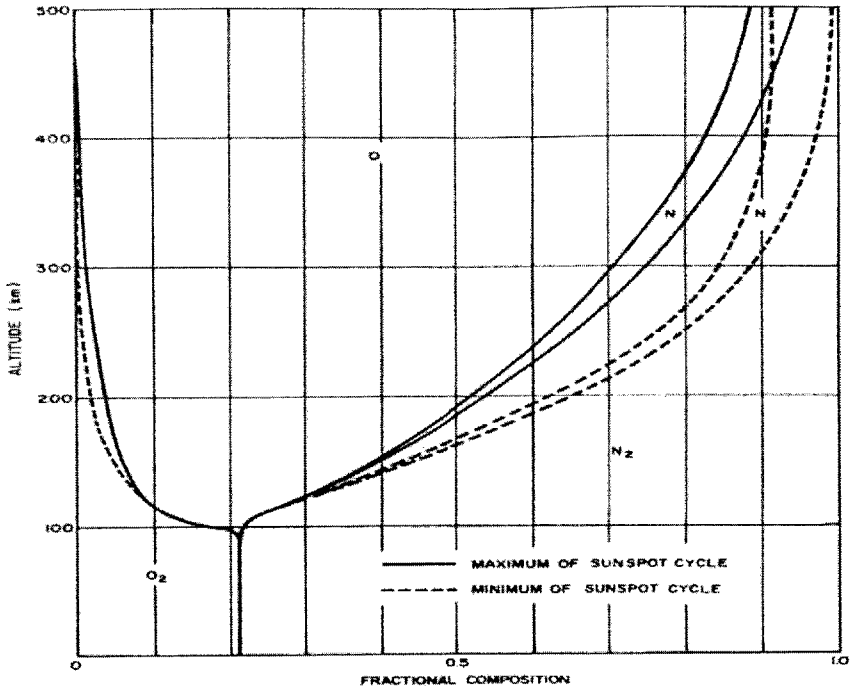

Fig. 4.2, Fractional composition of the atmosphere (O, N, O_2, and N_2) as a function of altitude at the extremes of the sunspot cycle[31]

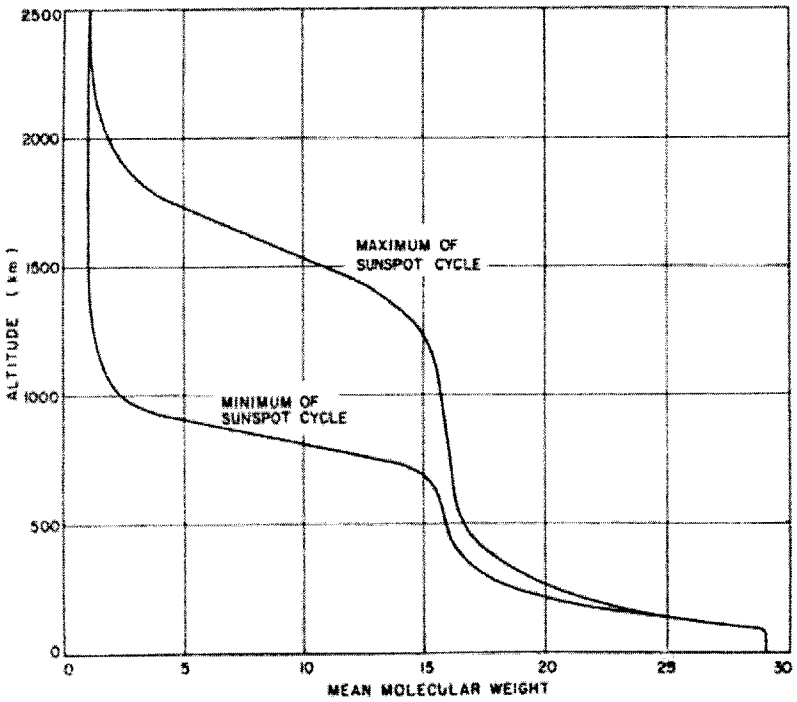

Fig. 4.3, Mean molecular mass as a function of altitude at he extremes of the sunspot cycle[31]

The temperature of the atmosphere in LEO is between ~500 K and ~1,000 K. This corresponds to a thermal velocity of between 500 and 1000 m/s, which is small in comparison to the perigee orbital speed of Earth-orbiting satellites (7.5 to 11 km/s). This means that the flow relative to the spacecraft will be supersonic and mostly anti-parallel to the spacecraft velocity vector[32].

The phenomenon of diffuse reflection is important for understanding the flow in LEO. High speed, hypersonic flow can be approximated by Newtonian flow. Newtonian flow on a flat plate at an angle of attack assumes two things about momentum transfer. First, the normal velocity to the surface is reduced to zero. Second, the tangential momentum with respect to the surface is conserved. Thus, the flow hits the surface and the resultant velocity lies along the surface. This flow model assumes acoustic behavior, and at low-densities the particles will tend not to be affected by their neighboring particles.

The situation now becomes a stream of discrete particles impacting the surface. How do they reflect? The familiar kinetic behavior of a body elastically impacting a plane is known as specular reflection, as shown in Figure 4.4.

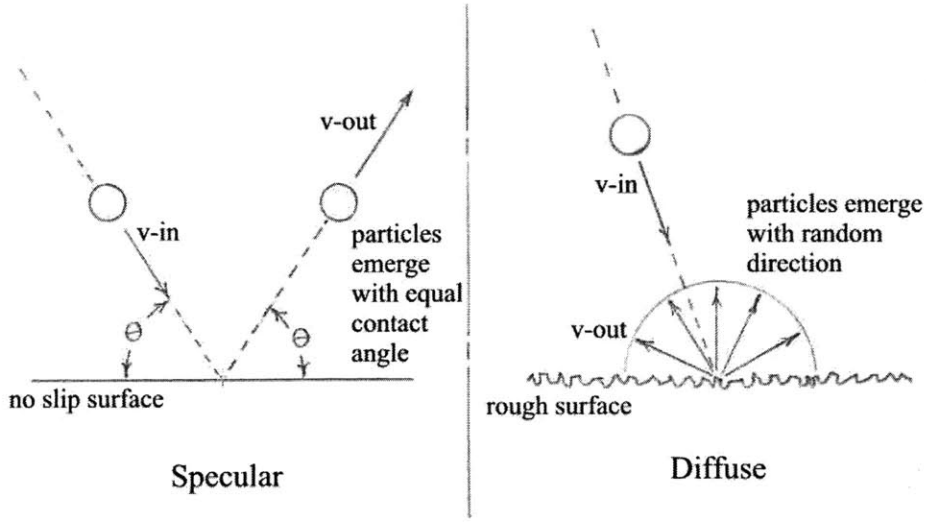

Fig. 4.4, Difference between diffuse and specular reflection

Specular reflection governs everyday things like billiard balls bouncing off rails and racquetballs careening off walls. But what happens if the surface is not smooth? If the roughness of the wall is on the same scale of the 'ball' impacting, we know that it won't necessarily bounce off the wall in a predictable manner. That is the idea behind diffuse reflection. For low-density particle flows, the 'balls' are molecules and the surface is generally not smooth on the molecular level, so the particles emerge from the surface with random directions. If the surface is somewhat smooth, there can also be a mix of specular reflection and diffuse reflection.

There are two main metrics that describe the behavior of collisions, one for momentum transfer and one for energy transfer. The first is the fraction (g) of tangential momentum transferred to the wall. The second is the coefficient of accommodation (α); it describes the difference between the energy of incident and reflected particles.

$$\alpha = \frac{E_i - E_r}{E_i - E_w} \tag{27}$$

where E_i is the particle's incident mean kinetic energy, E_r is the kinetic energy of the reflected particles, and E_w is the mean energy corresponding the wall temperature[33].

Experimental investigations have found that for high altitude flight, 'g' can be assumed to be 1. The coefficient of accommodation can be assumed to be in the range $0.9 \leq \alpha \leq 1.0$. This means that incoming particles lose all their tangential momentum, and emerge from the surface at a random direction with a velocity somewhat less than would be consistent with the wall temperature. Under similar conditions, experiments show that 'g' is greater than 'α'. This means that more collisions are required to equalize temperatures than to produce random emission[33].

The main chemical reaction that must be dealt with in the flow is surface sputtering due to atomic oxygen. There is both experimental and analytic evidence regarding the effects of atomic oxygen interactions on LEO space structures[34]. Certain materials such as Kapton and other plastics suffer from high surface regression rates (several hundred μm/yr for Kapton). The degree of reactivity depends on the orientation to the spacecraft velocity vector and the solar cycle. From the same study, we know that oxides will tend to form on metals and metal-coated surfaces. These oxides can protect the surface from further damage, but in some cases like silver, significant spalling of oxidized material occurred.

In general, the impacting gas doesn't have enough kinetic energy (~5 eV) to mechanically remove material from the spacecraft[32]. Thus as long as materials which are resistant to atomic oxygen are chosen, the flowfield around the AAOTV can be assumed to contain only particles carried by the incoming ambient gas.

4.3 Hypersonic continuum model

The hypersonic shock relations offer a convenient starting point for estimating flow behavior for the intake[35]. These equations are a result of taking the full Navier-Stokes equations to the limit of Mach number much greater than 1. If these were applied, it would be relatively straightforward to calculate the flowfield around a scoop. The problem is that the mean free path for particles is much too large in comparison to the size of the scoop to assume that pressure forces will be present in the flow. Pressure forces are necessary in the development of discrete shock structures, effectively communicating downfield flow information upstream. Even so, the relations should apply as a limiting case. If you look at pictures of flow phenomena as the density of incoming flow is reduced, oblique shocks do not abruptly disappear. Shocks first

grow wider and can no longer be represented accurately by discrete jumps in pressure, velocity, density, and temperature. If you think of the shock being related to the mean free path of the gas, you can begin to see how shocks will 'grow' as more distance is needed to achieve the collisions necessary to build up the shock. These 'fuzzy' shocks still serve to turn the flow and communicate downfield flow information, as shown in Figure 4.5. Similar 'fuzzy' behavior can also be expected to occur with bow shocks.

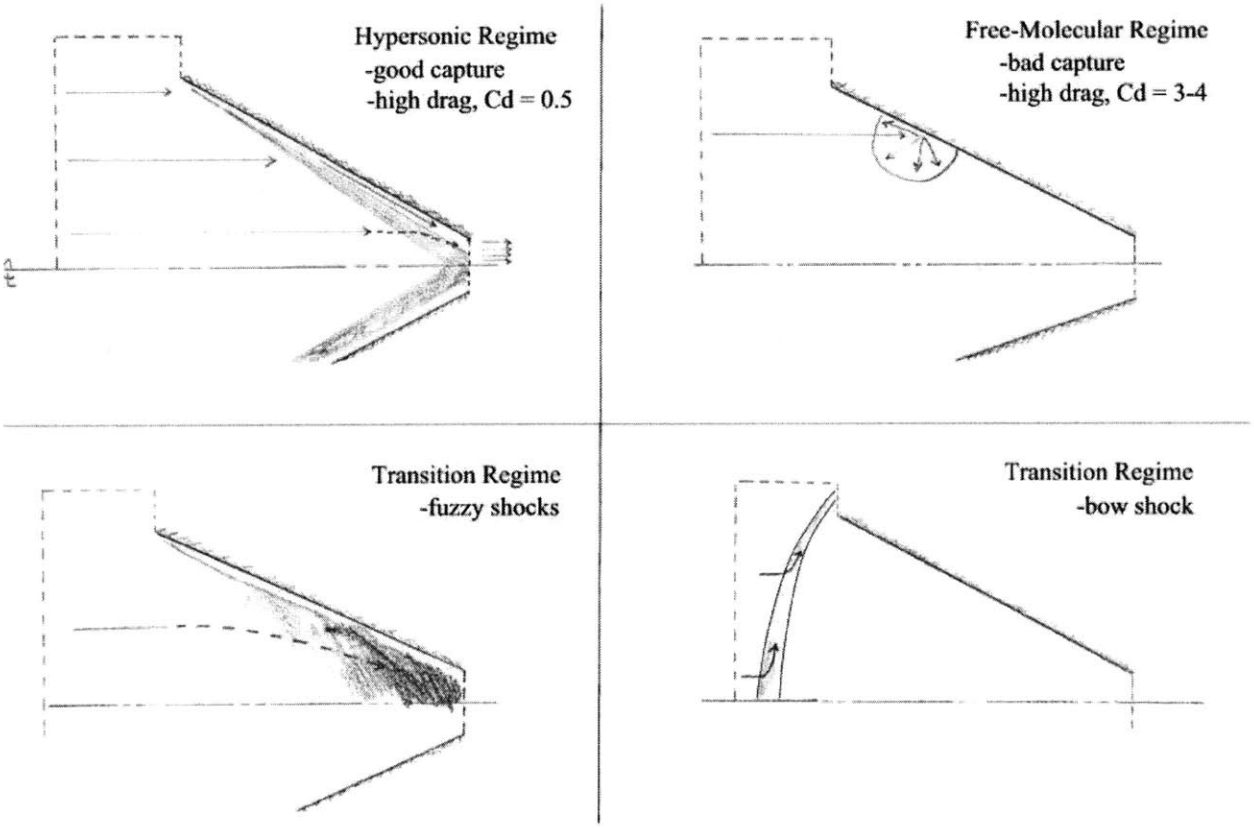

Fig. 4.5, Shock wave structure for low-density flows

So, to estimate drag under the hypersonic equations, the drag coefficient for a flat plate with Newtonian flow is given by the following relation (for small angles):

$$c_d = 2\sin^3\alpha \tag{28}$$

where α is the inclination of the plane. If we look at a cone-shaped scoop, we can

approximate this by a 2-dimensional wedge with the wedge angle equal to the cone angle. Thus, to the first-order we can estimate the 3-dimensional drag coefficient by the 2-dimensional drag coefficient. If the scoop is very large in comparison to the mean free path, this might be a very good approximation, since locally, the curvature would be small. If the flowfield is not governed by merely local phenomena, this assumption will not be as good. Also inherent to this formulation is that the ratio of specific heats, $\gamma \rightarrow 1$. The drag coefficient depends on the cone angle. Also, the cone angle dictates the surface area for a given intake area.

$$SA = \pi r^2 \sqrt{1 + \frac{1}{\tan^2 \alpha}} = \pi r^2 \sqrt{\frac{\tan^2 \alpha + 1}{\tan^2 \alpha}} = \pi r^2 \sqrt{\frac{\sec^2 \alpha}{\tan^2 \alpha}} = \frac{\pi r^2}{\sin \alpha} \tag{29}$$

where r is the intake radius. If the drag on the scoop is given by a simple velocity squared drag relation (Eqn. 15), the drag can be rewritten as a function of the intake area and the cone angle. Substitution of (28) and (29) into (15) yields:

$$D = \rho v^2 A \sin^2 \alpha \tag{30}$$

where A refers to the intake area, not the surface area. This relation gives a maximum drag coefficient of 2 for $\alpha = 90°$. This is consistent with known drag coefficients of orbiting satellites, which go upwards of 2. Most conventional satellites would be better modeled by a bow shock, which would exhibit very high drag coefficients. Also, this drag relation would suggest that the best scoop would have a very small α. However, the surface area of the intake would scale directly with the system mass. But if surface area and mass are optimized, more drag is created which would be countered by a more powerful, heavier power system. As you can begin to appreciate, even in the simple hypersonic case, there is no clear-cut design from which we can estimate system performance, which doesn't require knowledge of other system parameters. Still, this model would suggest that a fairly tall cone might be a good design.

Also important is the shock angle as a function of the cone angle. If we suppose that shocks are discrete and not fuzzy, a long, narrow cone could produce shocks and flow that sit right on the body surface. Ideally, then the engine could just ingest these shocks without worrying about the shocks reflecting of the opposite wall. Remember that the size and aspect ratio (ratio of cone height to base diameter) of the cone affect the drag. Add in that shocks will not be discrete and the model deteriorates further.

In any case, representative values of drag coefficient can be evaluated to give an idea drag behavior. For a 30 degree scoop of the size stated in the mission studies, with an intake radius of 50 meters, a length of 100 meters has a 2-D drag coefficient of about 0.5. This models the flow with discrete shocks with no secondary reflections (off the opposite side of the cone). If a characteristic density of 3e-10 kg/m^3 and orbital speed of 8 km/s are used, the drag on the scoop is 30.2 Newtons. The previous mission studies show that this is a feasible situation, but let's look further.

Free-molecular flow

The other limiting flow condition is a free-molecular flow. It is characterized by the absence of particle-particle collisions and is therefore called 'collisionless'. In a free-molecular flow there is no pressure communication between particles, so the molecules interact only with surfaces and electromagnetic fields. For this study we can ignore electromagnetic forces as small in their effect on the bulk motion of the gas. This is justified by the neutral state of incoming gas and ability to control surface charging of a metallic surface. Plasma contactors can be used to counter-act any build-up of charge due to impingement of ionized particles and electrons. For the free-molecular model, the lack of pressure forces and other body forces then

eliminates the possibility of shock structures in the flow. We are left with a flow that only depends on the surface interactions.

For free-molecular flows, it is common practice to assume diffuse reflection for surface interactions. The importance of assuming diffuse reflections in a low-density flow becomes important if you consider a particle entering the cone. If that particle were only specularly reflected, it would bounce from wall to wall and eventually be thrown back out ahead of the craft. This can be visualized by a ping pong ball bouncing around in a cone in zero-g, depicted in Figure 4.6.

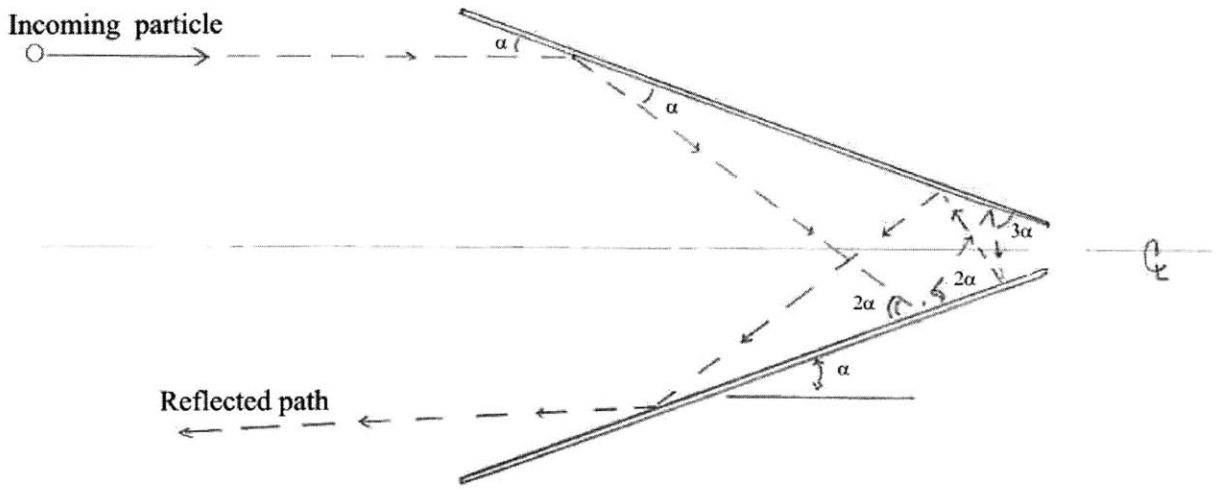

Fig. 4.6, Collisionless specular reflection in a cone-shaped intake

This ray-tracing model means a parabolic bowl shape would be required to have incoming particles be captured to a spot (the engine).

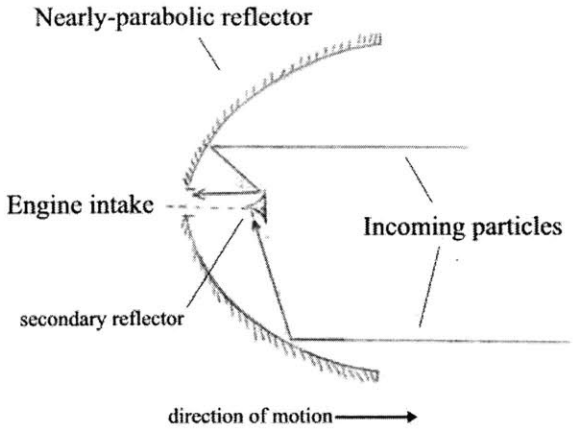

Fig. 4.7, Parabolic intake for free-molecular flows

But since diffuse reflection dominates behavior, particles hitting the wall can emerge in a direction 1) out of the scoop, 2) into the engine, or 3) towards the opposite wall of the scoop as shown in Figure 4.8. Since the new emergent velocity direction is random, the probability of each action is governed by the geometry of the scoop. If it hits the opposite wall, the same choices apply, but with different geometry. A Monte-Carlo model can be used to test a particular geometry. Many different particles are introduced and followed through the system, complete with random introductory positions.

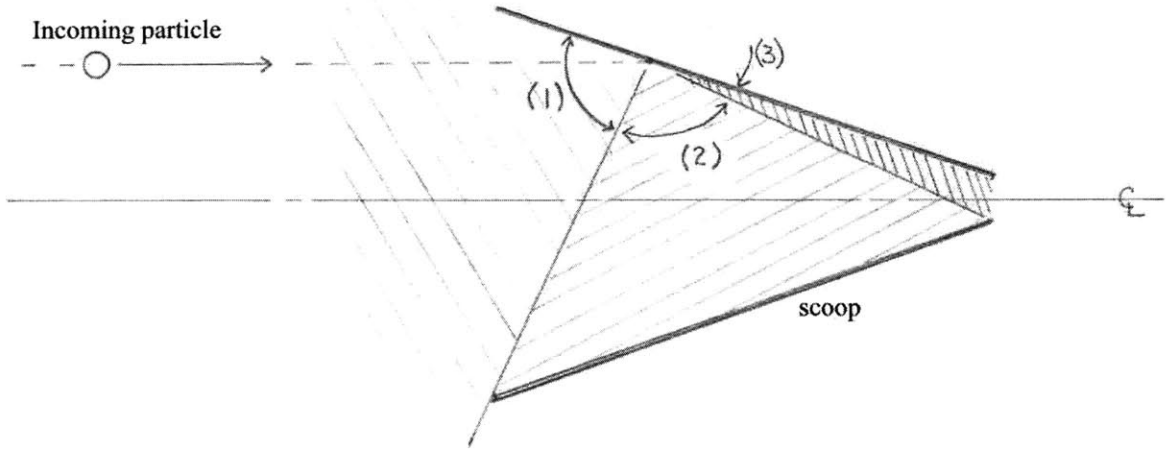

Fig. 4.8, Possible collisionless particle paths for a cone-shaped intake

The basic result apparent from studies using a simplified version of the code later

described shows that the capture ratio is limited by 50% and that the drag corresponds to half of the particles being totally reflected, a drag coefficient of 2. It comes down to flipping a coin, the particles in the end either make it through or are rejected. The size of the entrance, size of the exit, and length of the cone govern just how close to 50% you get. The key is that since there are no collisions, particles can bounce around forever until they are lucky enough to bounce in the direction of a hole.

An interesting element of the free-molecular assumption is that particles that are emitted from the scoop don't interact with the incoming cloud of ambient gas. In reality, a collision would very likely, given the high relative velocity between the two flows. This absence of collisions prohibits collisions that would otherwise result in a bow shock behavior, which limits the effective area to just the physical intake area.

Transition regime

The middle ground is called the transition regime. It could very likely exhibit different behavior than merely a shading of the two capstone regimes. A small degree of collisionality in the gas can greatly affect the results. For instance, the drag might be much higher than either hypersonic or free-molecular models due to bow shock spreading. Since the two impinging molecular streams interact over a much larger distance, a diffused bowshock could extend much farther in front of the spacecraft.

A successful transition flow model needs to take into account the local conditions in a collision model. For instance, on an idealized spherical satellite, the particles in the ram-compression region in front of the satellite will undergo more collisions than those in the wake of the satellite. The effect of some degree of diffuse reflection in the surface interaction is also key.

Except for analytical models for simple geometries, this is not a particularly well-developed flow regime. This is mostly due to lack of a 'need to know'. The first order models for simple geometries along with experimental data are good enough to generate ballpark figures for atmospheric drag. Add to the mix the high degree of variability in the make-up of the upper atmosphere due to atmospheric tides and solar activity[32], and it is not necessary to generate higher order models. Other examples: the National Aerospace Plane (NASP) program would have operated in this region of the atmosphere, but the drag was deemed negligible at this altitude and very little analysis was done. Fusion and electric propulsion studies involve low-density flows, but they also tend to use collisionless, electromagnetically dominated behavior.

The main element we want from this numerical study is an idea of what the flow field looks like, and an appropriate way to characterize the drag. There should be some elements of pressure related structure, such as diffuse oblique shocks. There should also be some upstream communication of pressure due to diffuse reflection. That communication should be in the form of collisions that deflect some the incoming gas around the body, like a weak, spread-out bow shock. This presents an effectively larger frontal area to the impinging flow and may result in higher drag than predicted by either the hypersonic or free-molecular theories. Capture percentage is another key result. What percentage of the incoming particles will actually travel into the engine and how many will be rejected?

Assumptions

The intake condition is an incident beam of neutral atoms with a relative speed of 8,000 m/s. The beam has no tangential component, essentially assuming negligible thermal motion in the gas. This assumption is made in order to simplify the introduction of particles into the

system and speed up the computation.

The atmospheric density for the following numerical studies is assumed to be 3e-10 kg/m^3 unless stated otherwise. This value corresponds to about a mean density at 200 km altitude.

The molecular mass of incoming particles is assumed to be uniform and equal to 14 g/mol or 2.326e-26 kg per atom. This corresponds to having a gas composed fully of Nitrogen atoms. In reality, this will vary slightly due to the presence of O, O_2, N_2 at the altitudes of interest. The Nitrogen value was chosen as a characteristic average number. Remember that these numerical studies aim to merely characterize the flow behavior and to generate rough drag numbers. More accurate numbers, say better than within 20%, are simply not necessary for this stage of the concept's development.

A hard-sphere collision model is implemented with a particle size of 0.9 Angstroms, the size of a Nitrogen atom[38].

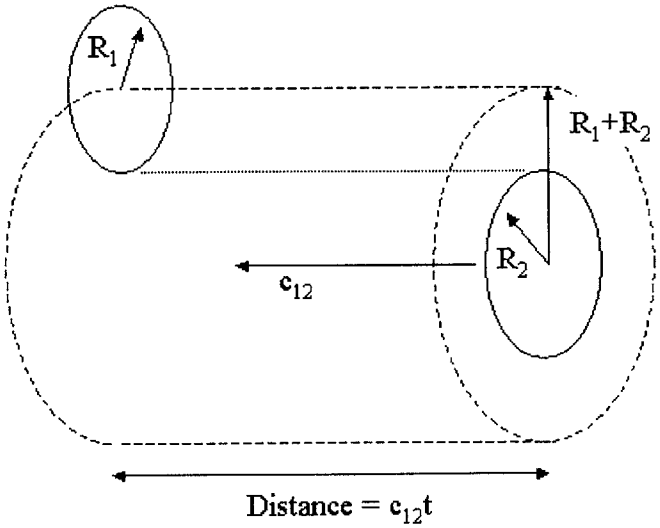

Fig. 4.9, Diagram of hard-sphere collision model

In the above figure, 'c_{12}' is the average relative velocity between the particle and the targets it will collide with. The collision frequency is found by defining the amount of particles that would fall within a particle's path in a given time. For the hard sphere case, as shown in the above figure, the volume of space that a moving particle sweeps out is given by:

$$Volume = \pi \left(R_1 + R_2 \right)^2 c_{12} t \tag{31}$$

The number of particles that would be present in this volume of space can be found by multiplying by the density of the target population.

$$\#\ of\ collisions = n_1 \cdot Volume \tag{32}$$

The collision frequency is the number of collisions per unit time. With the simplifying assumption that there is only one type of particle, the collision frequency is given by:

$$\nu = c_{12} 4\pi R^2 n \tag{33}$$

The time between collisions is given by the inverse of the collision frequency and the mean free path is defined using the relative speed between the particle and the gas in which it is moving.

$$time\ between\ collisions = \frac{1}{\nu} \qquad mean\ free\ path, \lambda = \frac{c_{12}}{\nu_{12}} = \frac{1}{\sigma_{12} n} = \frac{1}{4\pi R^2 n} \tag{34}$$

The collision frequency is used to calculate a probability that the particle will collide with another in a given time step. The Monte Carlo aspect of the code comes from the technique of using probabilities to define the behavior of individual particles during collisions. A random number is generated and compared against the probability to collide in this case. The scheme works thusly: For a given time step, *dt*, if a random number between 0 and 1 is less than (*dt / time between collisions*) then there is a collision. In the code, a particle's collision frequency depends on the local density of the gas and its local velocity, which necessitates the computation

of this information for a field of cells in the flow.

The surface interaction of the scoop is an important boundary condition. These models assume the wall to be at the same temperature as the incoming flow. This means that only momentum is exchanged, and no energy is exchanged. Speed is then conserved during reflection as a conservative approximation allowing for the most energetic flow. In reality, the temperature of the scoop would affect the speed at which particles emerge from the wall after striking it. A cool wall would slow an incoming flow, but the wall would also get hotter. A more accurate analysis would take into account the amount of energy transferred to the surface from particles and solar heating and balance that energy to the power lost to blackbody radiation. First order calculations show that the heating from particles is much less than solar heating, but this changes near the throat of a scoop, where the density has increased considerably over the background. An accurate model would then take all this into account, but for this first pass, it is not necessary. In practice, coatings could be applied to the scoop to control the temperature at various locations if that were deemed necessary or beneficial. Later, for completeness, the code is modified to allow the modeler to set the wall temperature. The results differ greatly in densities and flow structure, but not in drag and capture percentage, the two main metrics of interest.

Algorithm

A Direct Simulation Monte Carlo / Particle-in-a-Cell method is used to simulate the flow through a 2-D wedge-shaped scoop. The code has a simple architecture, as shown below in flowchart form.

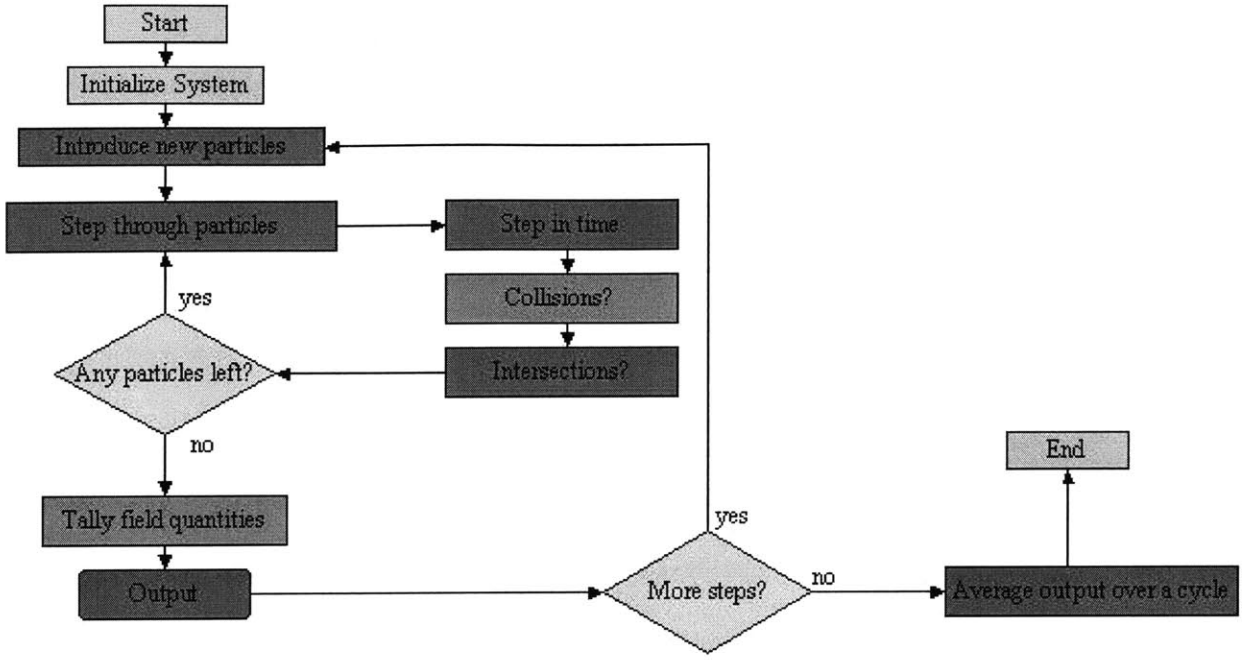

Fig 4.10, Flowchart of DSMC-PIC algorithm

The location and velocity of a large number of particles is retained in memory. These are called superparticles, each representing many real-world molecules. These particles are allowed to move through a computational space at discrete time steps. If the particles encounter a boundary during the step, appropriate action is taken on that particle. For example, if a particle hits a wall, its new position and velocity is calculated with the wall knowledge. Each time step more particles are introduced on the 'front' boundary, these particles number in proportion to the mass flow that would be introduced into the control volume, the computational space, during the time step. Collisions between particles are accomplished by using a Monte Carlo process to determine the probability of a collision with the gas in the vicinity of the particle. The properties of the flow field used in this process are determined by constructing a 'field' of cells, each of which has a determined number density and average velocity vector. This tallying process is also useful for determining the flow patterns and structure.

Monte Carlo processes are used to model any process that is not deterministic, including collisions with the gas cloud, emergence from a diffuse reflection, and the spatial distribution of incoming particles. Deterministic processes are used to model behavior that is well defined, such as specular reflection about the centerline and force-free particle motion. The method is inherently stable, but has the drawback that a steady solution can take a long computational time to form. 'Convergence' versus computation time for a solution, in this case, a particular flowfield, depends on the initial conditions, the behavior of the code, and the amount of noise in the model. For example, if an empty initial condition is used, the flowfield structures like shocks must be built entirely by incoming particles, and may take a long time to reach equilibrium. Depending on the boundary conditions chosen for energy exchange on the wall, the amount of particles needed to build these structures changes considerably. Luckily, the hot wall (i.e. no energy transfer) results in shocks that are only 3-4 times the density of the incoming flow. The hot wall assumption allows steady-state flows to be realized after only a few cycles. If the wall is allowed to absorb energy and slow the incoming molecules, the shocks become very dense (similar to a hypersonic oblique shock) and the computation time increases rapidly.

The other important factor is noise. In order to better resolve the properties of a cell, more particles should be present per cell. For example, if a cell has only ten particles on average, then a single particle represent a change in mass of 10%. If the cells average, say, 50 particles, the percentage falls to 2%. The more particles present, the smoother the output will be. Bird puts a 'good' value at 30 particles per cell, but states that reliable results can be obtained with less than ten particles per cell[36]. This noise can be tolerated somewhat by integrating any results of interest over many time steps. This is verified by comparing the same model run at different average particles per cell and comparing the result as more particles are added. These

codes were implemented with anywhere between 7 and 50 particles per cell. More computational troubles arise from the desire to gain higher resolution pictures of the flowfield, which requires more cells and many more particles.

These details become important when considering the computational power needed to tackle the problem. These codes are memory intensive, having to keep track of as many as 250,000 particles. Most of the computations are floating point operations, with graphics only as a final display (except for debugging). Also, these codes would lend themselves to parallel computation readily, since the particles don't interact with each other directly but rather with a field of cells. PentiumIII desktop PC's where used to run all the codes with run times on the order of days. One can begin to appreciate the need to keep the model as simple as possible if any exploration of a parameter space is to be explored within the timeframe and resources available to a Master's student (months, $0.00, and 5 PC's).

Implementation

The code was written in Matlab, making use of built-in graphics functions for data display. The code was then compiled into a stand-alone C program that could be run on any PC running windows. Compiling results in halving the runtime of a given code.

The computation space is shown in Figure 4.11. The space is a 2-D wedge with unit thickness. The bottom boundary is the centerline of the scoop, a line of symmetry. Particles enter the space from the left boundary and move to the right. The sloping line represents the scoop wall. The right boundary is the intake to the engine and the top boundaries are simply free boundaries to space.

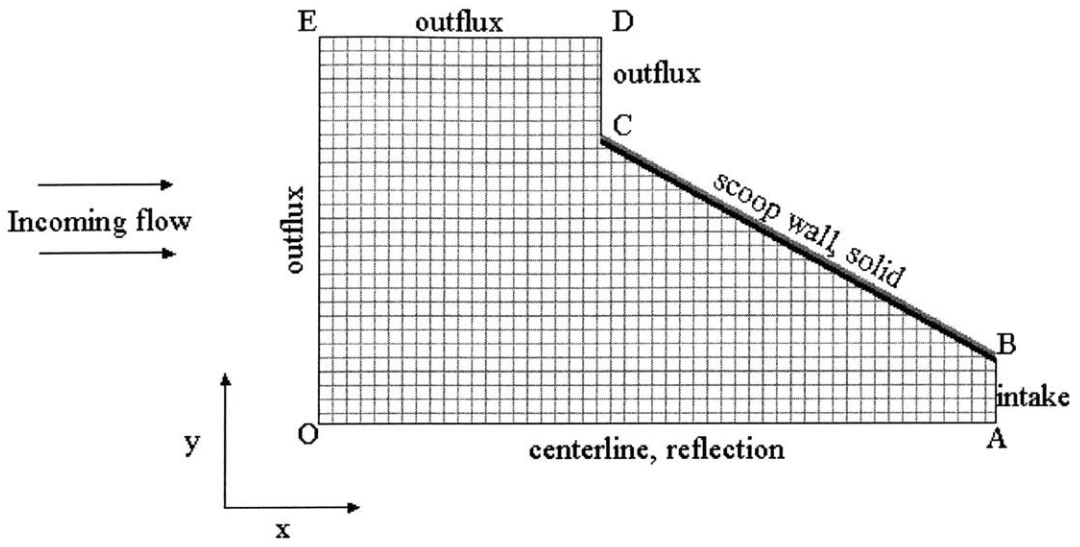

Fig. 4.11, Computational space (control volume)

The space is divided into equal area and dimension rectangular cells. This includes the cells in which the sloping scoop boundary passes. This approximation produces somewhat jagged data near the scoop wall, but greatly simplifies the scheme. With this scheme, the grid can be easily adapted to changing scoop dimensions, computational space size, and grid spacing. A more complex scheme would allow for a mapping of conformal cells to a rectangular computation grid. This complexity would not add considerably to the accuracy, just the aesthetic appeal, and would greatly increase the coding and computational workload. Increased resolution of the near wall flow is obtained by decreasing the overall cell size. This approximation will only come into play when considering the effect of collisions in these cells very close to the wall, which will be examined later in this discussion.

Each cell has a defined average number of particles. The speed of the incoming of particles is also defined. The cell dimensions along the direction of the incoming speed is also known. Since there are no mechanisms by which a particles speed or kinetic energy can increase over its initial value, the incoming speed is an upper limit on the particle's speed. The time step

is chosen such that a particle moving at maximum velocity will travel less than the full dimension of a cell. If this limit were not imposed, a particle would have the opportunity to 'jump' over a cell and not interacting with that cell. This can be thought of as tunneling through a cell, which could contain a region of high density, like a shock. This doesn't make physical sense and must be avoided. A faster, but more complex scheme would allow cell sizes to differ, and the associated time steps through that particular cell to vary in accordance with its spatial dimension. Once again, this complexity was deemed unnecessary since acceptable runtimes are possible using the simpler uniform cells and uniform time steps.

The factor relating density of a cell to the number of superparticles in a cell is needed to reconstruct the flow from the simulation. The number of molecules in a cell is found by taking the volume of the cell and multiplying by the number density of incoming gas. This value divided by the average number of superparticles per cell gives the factor.

The particle factor is then used to determine the amount of superparticles to introduce into the system via the left boundary every time step. The number of particles entering is determined by finding the volume swept out by the left boundary over a time step and multiplying by the number density. The number of superparticles is found by dividing this influx by the particle factor found above. These particles are then distributed randomly within a box of dimensions of the whole left boundary in y and $v_{in}dt$ in x.

Initially, the computation space is empty of particles, equivalent to a vacuum. The simulation then introduces particles, much like a scoop would experience as it hits the atmosphere. An alternative would be to start the simulation with a proposed distribution of density and velocities, but is not advantageous for the hot wall assumption. Even with dense shocks, variations on the initial solution would still take a long time to manifest due to a small

influx of particles.

Particle data is stored in a two-dimensional array (a matrix). Each row represents a particle slot, in which seven pieces of information are stored. First, the status of each slot is determined by a '1' or '0'. If the particle is still in the control volume, a '1' is stored. A '0' tells the program that the slot is empty, and a new particle can be stored there. For particles then, the current x and y positions, previous x and y position, and x and y velocities are stored.

From the algorithm flowchart, the first step in a cycle is to introduce new particles. These are plugged into the first empty slots available. These particles are distributed in space randomly and are given initial velocities.

The next step is to move all the particles along force-free trajectories over a time step, '*dt*'. Absence of forces means acceleration on any particle is zero. The particles' old positions are just incremented by products of their old velocities and the time step.

Each particle is then examined to see if it will collide according to the Monte-Carlo collision model. The rectangular grid is an important simplification here, in that it allows for simple schemes to find out which cell the particle is in. Collisions are treated by finding a new, random velocity direction vector, and then incrementing the particle's old position by the product of the new velocity and the time step. The magnitude of the velocity vector is conserved for collisions. The momentum of the particle is not conserved during a collision. Since there are many particles and collisions, and there is a random emergent velocity, the total average momentum change due to collisions is zero. Thusly, non-elastic collisions can be used to approximate elastic collision processes.

Then each boundary is checked in turn just once. For each boundary the line segment made by the initial and final particle position is written as a linear equation. The intersection

point of this line and the boundary is then calculated. If the intersection is on the line segment, then the boundary is considered 'crossed'. Each boundary calls for different action to be taken on the particle.

If the particle crosses boundaries O-E, E-D, or D-C, the particle is counted as a 'lost' particle. Its momentum is tallied and the status of the particle is changed to a '0' to create more space in memory for new particles. The momentum tally is then reset after each time step is completed after all the particles are examined. The other contributor to the momentum tally is the intake, A-B. The only difference for A-B is that the particle is counted as 'captured' by the scoop. The ratio of particles captured to total particles coming into the system is an important measure of the mass flow actually making it to an engine. The ratio of incoming particles to the sum of particles lost or captured is a measure of transience of the system. At steady-state that ratio will average to unity.

If a particle's trajectory should intersect the centerline, the particle undergoes specular reflection, its normal velocity is reversed, i.e. y-direction velocity is made negative. The tangential direction is conserved. Since the model represents the scoop as perfectly symmetric, particles leaving the centerline boundary are balanced by a replica coming out of the boundary from the symmetric region. The total path length of the particle is kept track of and conserved.

A particle colliding with the B-C boundary undergoes a totally diffuse reflection. A new random velocity direction is found and applied to the remainder of the particle's time step. The magnitude of the velocity vector could be modified if some energy transfer to the wall were desired. The momentum change due to the collision is tallied in order to find the drag on the scoop.

The rectangular grid poses some concerns near the B-C boundary. The sloping line

affects the area of some of the cells near the wall. In these cells, on average, there won't be as many particles present. When the cell's density is calculated in order to do collision modeling, the cell density will be underestimated. This will reduce the chance of a particle collision in the cell. This isn't so bad, however, since the error is on the conservative side (fewer collisions) and occurs very close to the wall. The effect can be thought of increasing the stand-off distance of any pressure-related structure from the wall. This shouldn't be a problem if the grid is relatively fine in comparison to the wall length. Also, the error introduced by this effect will be reduced as the grid is made finer.

The process of checking each boundary 'only once' presents a problem of order. The boundaries must be checked in a particular order. For example, a particle very close to the scoop wall could be found to interact with the wall, collide with another particle, and then end up hitting the wall again. In order to avoid these problems, collisions are done first, then the scoop wall and centerline, and finally the exit surfaces and intake. The distance between the scoop wall and the centerline defines another limitation on the time step. The time step should be smaller than would allow a particle to bounce off either of these more than once in a given time step. This supercedes the previous limitation on time step only if the cell size is larger than the throat dimension. This limitation could be lifted by looping through the boundaries repeatedly until the particle has stopped moving. In general, though, the throat size is larger than the cell size and this measure adds unnecessary computation.

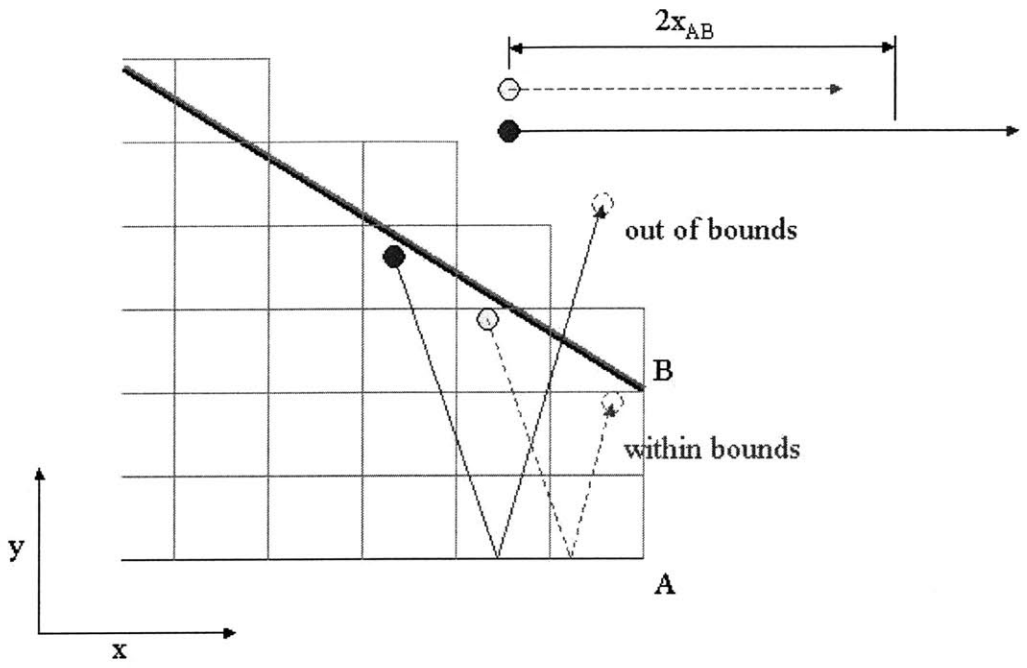

Fig. 4.12, Throat-imposed time step limitation

After all the particles have been advanced, the field quantities are calculated by stepping through the particle array and tallying each location and velocity. The bulk velocity for each cell is then found by dividing the magnitude of the sum of the velocity vectors by the number of particles present in that cell.

The field data can then be output as a density map and velocity vector plot. The field data can also be analyzed to find density cross-sections in the flow.

The main outputs, however, come from the tallying of particle interactions. Momentum transfers to the walls are used as one measure of drag. Another measure of drag is found by performing a momentum balance on all particles passing through the control volume of the computational space. In the steady state, these two values of drag should average to be equal. During transients, the wall drag tends to differ greatly from the flux drag since the mass flux through the control volume isn't zero. In order to account for noise, the time history of drag and capture percentage is recorded to help determine the relative amount of noise in the solution and

to determine when it has reached steady state. Also, the 'final' values of drag, drag coefficient and capture percentage are averaged over a cycle. A cycle's period is defined by the amount of time a particle moving at the incoming speed would take to traverse the control volume unimpeded.

A further improvement to the code would be the introduction of 3-D effects by weighting cells far from the centerline in order to model the axi-symmetry of a cone. Since this is not a first order effect, it was not done, but would certainly be required if more detailed design studies are required.

In the end, a code emerges that is just fast enough to run with sufficient accuracy over the course of a day. This allows for numerous parameters to be varied in order to bring drag and capture dependencies to light. Before a parametric study could be done, however, several tests were made to ensure the code was indeed accurate over the range desired.

Validation of number of particles per cell

For the parametric study, a small average number of particles per cell is desired for short runtimes. Trial and error showed that 7 particles per cell produced good results with reasonable runtimes. In order to quantify the effect of this number on the results, a simple study was performed. For a scoop configuration of 30 degrees and 15 meters radius, 4 different values of the average number of particles per cell were used, [3 7 11 15]. The computational space is set up in the same manner as described in Figure 4.23 under the section on the parametric study. In order to define how 'good' the results are, two metrics are looked at. The first is simply the average steady-state drag coefficient result. The second is the average percentage error normalized to the average drag coefficient over one 'cycle'. It is given by the following formula:

$$Percent\ error = 100 \cdot \frac{1}{Avg.C_d} \sqrt{\sum_{time\ step, i=1}^{\#of\ samples} \frac{(C_{d_i} - Avg.C_d)^2}{\#of\ samples}} \tag{35}$$

The percent error is a measure of the noise in the system. It measures how much the global performance values (i.e. drag coefficient and capture percentage) fluctuate around an average solution. The results are shown below in Table 4.1:

Table 4.1, Variation of particles per cell tests

Particles per cell	# of particles (runtime)	Drag Coefficient	RMS error	RMS % error
3	18815	2.731	0.381	38.1
7	44079	2.757	0.238	23.75
11	69273	2.741	0.189	18.9
15	94749	2.776	0.177	17.7

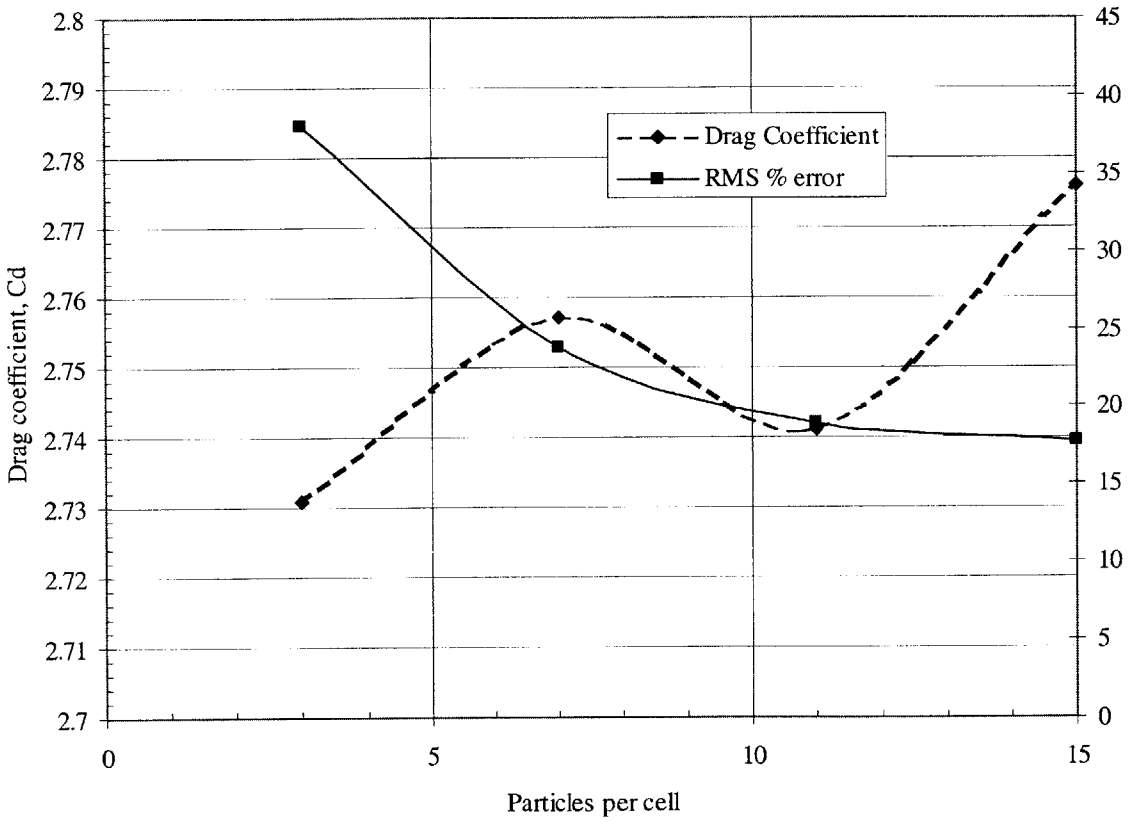

Fig. 4.13, Drag coefficient and percentage error versus average number of particles per cell

As shown in Figure 4.13, the values of drag coefficient agree very well over the whole range of particles per cell. The difference between the extremes is only 1.7% of the smaller value. The percent error is shown to decay with increasing numbers of particles per cell. The ability of the code to 'average out' these fluctuations is important. This shows that a code can be have large fluctuations about the average (almost 40% in the 3 particles per cell case), yet still produce good averaged global data. The computational runtime is a linear function of the number of particles in each simulation (holding all else constant). The advantage of using fewer particles is then for example, the factor of two decrease in runtime going from 15 particles per cell to 7.

Validation of grid size

In order to make a fast code, an appropriately sized grid is desired. A grid should be coarse enough to allow reasonable runtime, yet provide data of sufficient accuracy and resolution. Since this code is primarily used for a parametric study on the performance dependence on geometry, resolution of fine flow structure is not necessarily important. A study was then conducted to see how coarse a grid could be made and still produce good data. This wasn't exactly predictable since the study looks at cells that are within an order of magnitude of the scoop structure in size. A major goal was to find if shock structures had to be resolved finely in order to produce accurate data. The desired baseline for a parametric study was deemed to be 2 meters square as shown in Figure. 4.23. Each simulation used 7 particles per cell, a scoop 15 meters in radius, with a 30 degree angle and a 1.5 meter mouth. The results for running the simulation at 1 meter square and 3 meter square grids are shown in Table 4.2.

Table 4.2, Results for the variation of grid size tests

Grid Size (length of one side, m)	# of particles (runtime)	Drag Coefficient	RMS error	RMS % error
1	176484	2.754	0.123	12.3
2	44079	2.757	0.238	23.8
3	19871	2.742	0.363	36.3

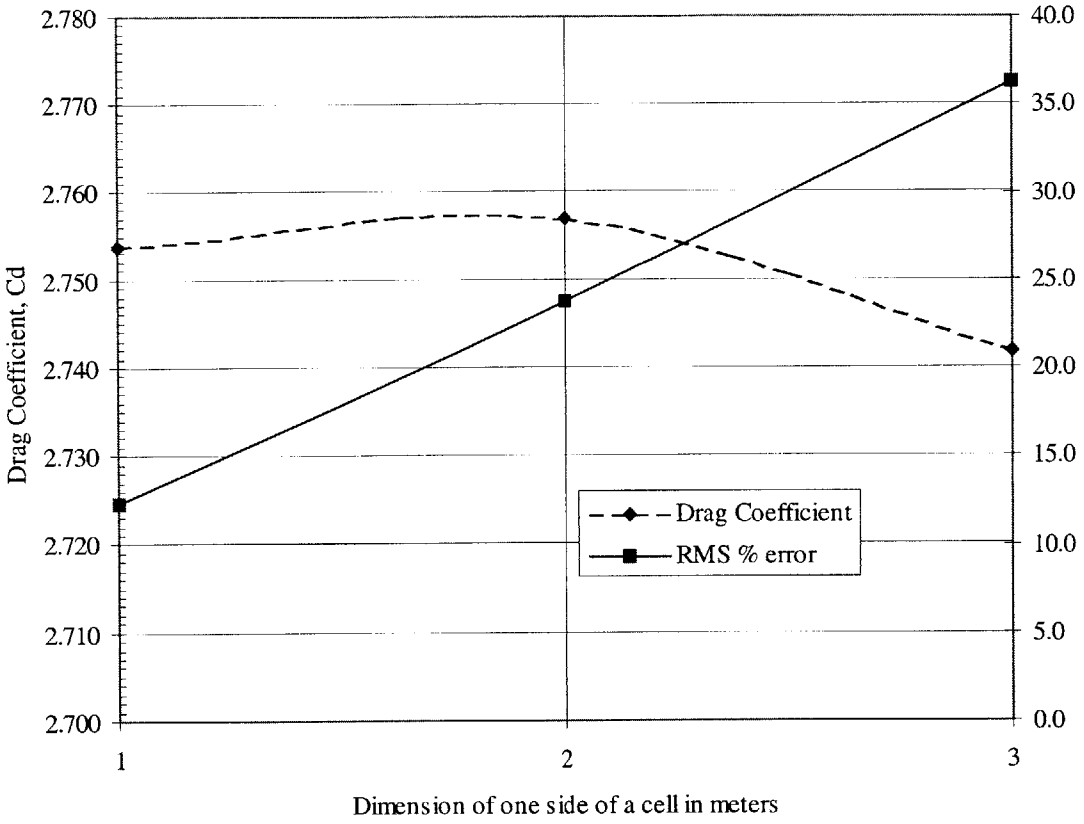

Fig. 4.14, Drag Coefficient and percentage error versus grid size in meters

The drag coefficient agrees very well (less than 1% difference) between all the chosen grid sizes. The variation of grid size shows a linear relationship with the instantaneous percent error, which tells us that the finer grid has less noise. The number of particles, which corresponds to runtime, scales as the grid size squared, which means coarse grids are desired if possible. In order to see the loss of resolution between these cases, the density and collision

density maps are shown in Figure 4.15.

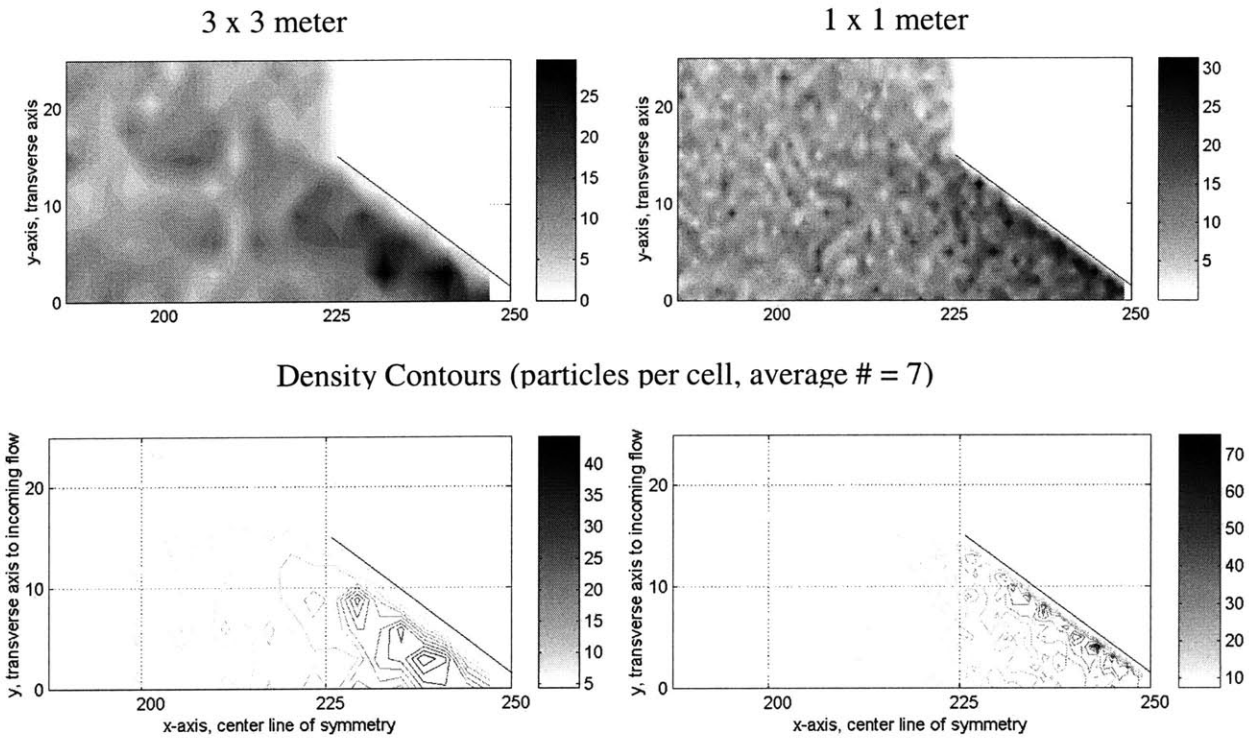

Fig. 4.15, Density contour and collision density contours for a coarse and fine grid, 3 meters and 1 meter square.

One can see that even in the coarse grid the dense shocks are not very well defined, but apparently model the behavior shock well enough for this level of collisionality in the flow. This study would have to be repeated for a model with more collisionality or different wall effects, since both of these cases would rely on more detailed flow structure to get the physics right. This study shows us that a noisy, coarse grid can accurately predict average drag coefficients with fast runtimes (hours). This speed allows us to conduct parametric studies with many sample points, and hopefully, will allow us to find the major scaling relationships in that large space.

Flat plate flow validation test case

The flow around a flat plate is used to validate the results of this code. An analytical treatment of a similar problem from Al'pert allows for a comparison with numerical results[37]. The analytical solution of density contours around a spherical spacecraft is shown in Figure 4.16.

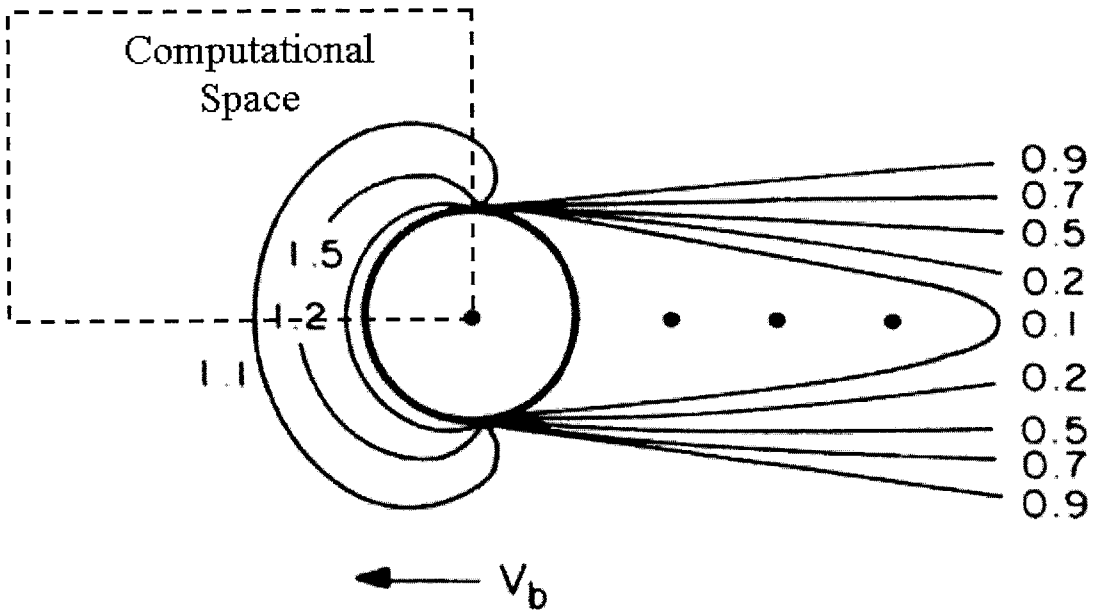

Fig. 4.16, Density contours around a spherical spacecraft normalized to incoming gas density. Modified from Al'pert[37]

The dashed region shows the computational region considered in the simulation. The key differences are 1) the analytical solution is collisionless and 2) the analytical solution is for flow around a sphere, not a flat plate. The numerical study can be run without collisions in order to compare drag coefficients, which should be similar to the sphere with complete accommodation. We know the analytical drag coefficient should be less than 4, which would correspond to specular reflection of a flat plate at 90-degree angle of attack. An exact answer can be found as follows. Write the force on a general flat plate from a collision with a particle[32].

$$f_d = m_p v_i + m_p v_r \cos(\theta_i + \theta_r) \tag{36}$$

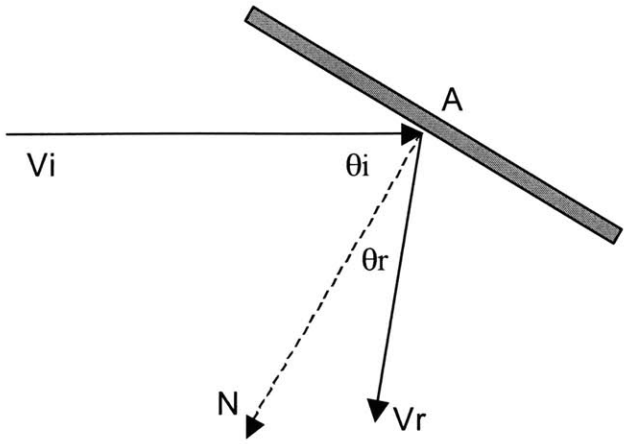

Fig. 4.17, Particles impacting a flat plate at an angle of attack[32]

The incident velocity for the flat plate is normal to the surface, $\theta_i = 0$. The incident and reflected velocities can be related via the accommodation coefficient, α. In the hyperthermal regime (incident velocity >> thermal velocity), it is given by:

$$\alpha = \frac{v_i^2 - v_r^2}{v_i^2} \tag{37}$$

For our case of a 'hot' wall without energy transfer, $\alpha = 0$, which gives $v_i = v_r$. Thus, (37) simplifies to:

$$f_d = m_p v_i \left[1 + \cos(\theta_r)\right] \tag{38}$$

Now since we assume diffuse reflection, θ_r has an equal probability of being anywhere between $-\pi$ and π. While the average θ_r is zero, the average of $\cos(\theta_r)$ over the applicable range is non-zero. The average drag for similar particles is then given by:

$$f_d = m_p v_i \int_{-\pi}^{\pi} \left[1 + \cos(\theta_r)\right] d\theta_r = m_p v_i \left(1 + \frac{2}{\pi}\right) = 1.63662 m_p v_i \tag{39}$$

The drag force from a total particle flowrate of $\dot{m} = nv_i A$ impacts per second is

$$Drag = 1.63662\rho v_i^2 A \qquad \therefore C_d = 3.273 \tag{40}$$

The numerical drag was calculated with a low-resolution model. The model used a grid size of 20 cells by 20 cells and 20 particles per cell. In one case, collisions are off, the second, on. Both cases are shown below in Figure 4.18.

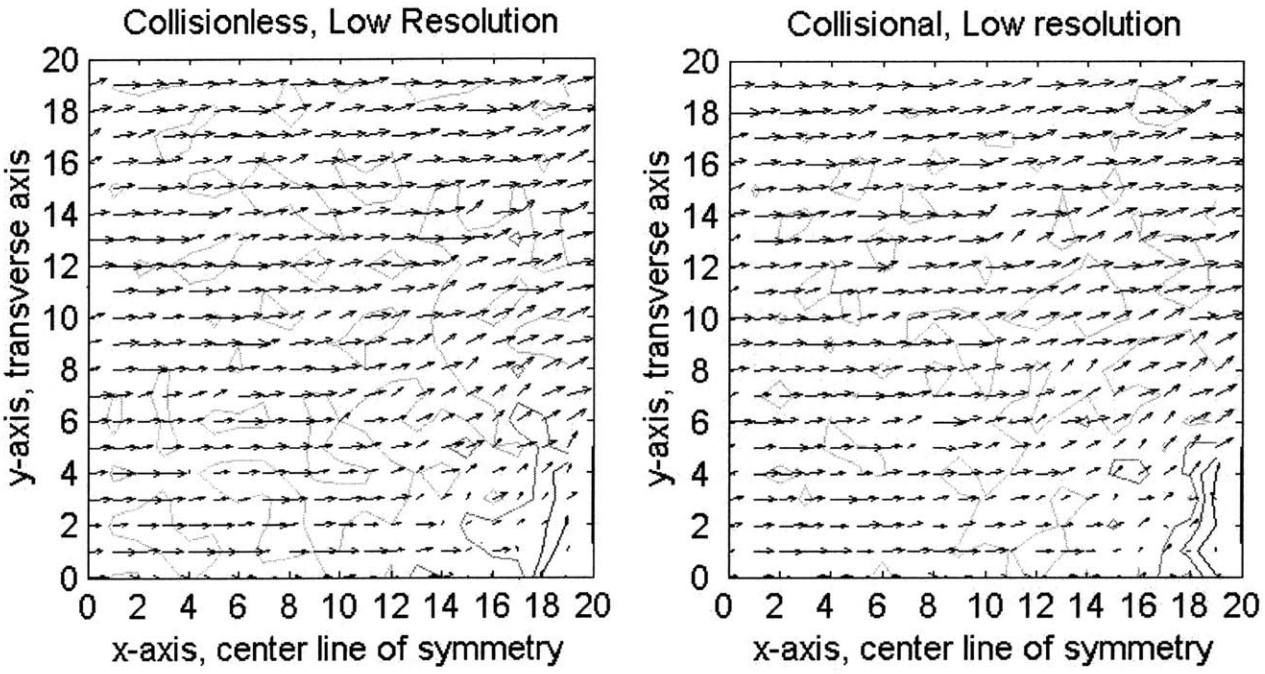

Fig. 4.18, Numerical results for a flat plate with and without collisions.

When collisions are considered, the density forward of the disk is found to increase and the drag goes up (although only slightly for this case). Qualitatively the effect of collisions is small and difficult to see from the flowfield plots above. The difference in drag for this case is small, less than 1% difference (Table 4.4). The streamlines are seen to bend around the plate, but this is mostly due to the averaging of incoming and reflected particle velocities. Since collisions are infrequent in this flow regime, their effect should be only to perturb this collisionless flowfield. Most noticeable is the slight increase in drag coefficient. The collisions change the

shape of the distribution of reflected particles from evenly distributed in angle to a distribution with angles biased perpendicular to the incoming flow. This alone should reduce the drag coefficient, but this also makes the body appear larger to the incoming flow, allowing body-referenced drag coefficients to be higher. As the density and collisionality of the flow is increased, the drag coefficient is found to decrease gradually (see Table 4.3), but this model only applies to low-density flows and care must be taken when increasing the collisionality. It cannot be arbitrarily increased without regard to the accurate modeling of the mean free path of a particle. These results show that for a flat plate, collisions aren't so important at the baseline density of the AAOTV, ρ = 3e-10 kg/m^3, but they can be important as the flow becomes more dense. The noticeable effect is reason enough to include collisions in the model for parametric studies.

Table 4.3, 2-D drag coefficients for a flat plate at different densities (collisionality)

	$\rho/10$	$\rho/4$	ρ = 3e-10 kg/m^3	$4\cdot\rho$	$8\cdot\rho$
Drag Coefficient	3.35	3.38	3.33	3.13	3.06

In addition to the low-resolution models shown in Figure 4.18, a higher resolution flat plate flow model was run for comparison. The following figures are the numerical results of a collisional flat plate flow for two different grid refinements.

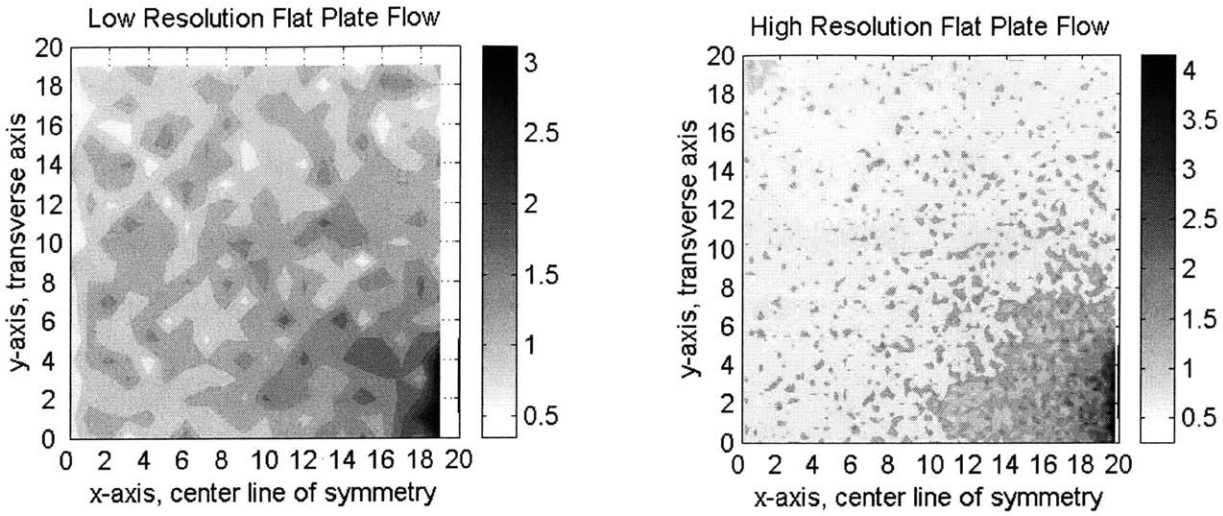

Fig. 4.19, Density contour maps for flat plate validation case

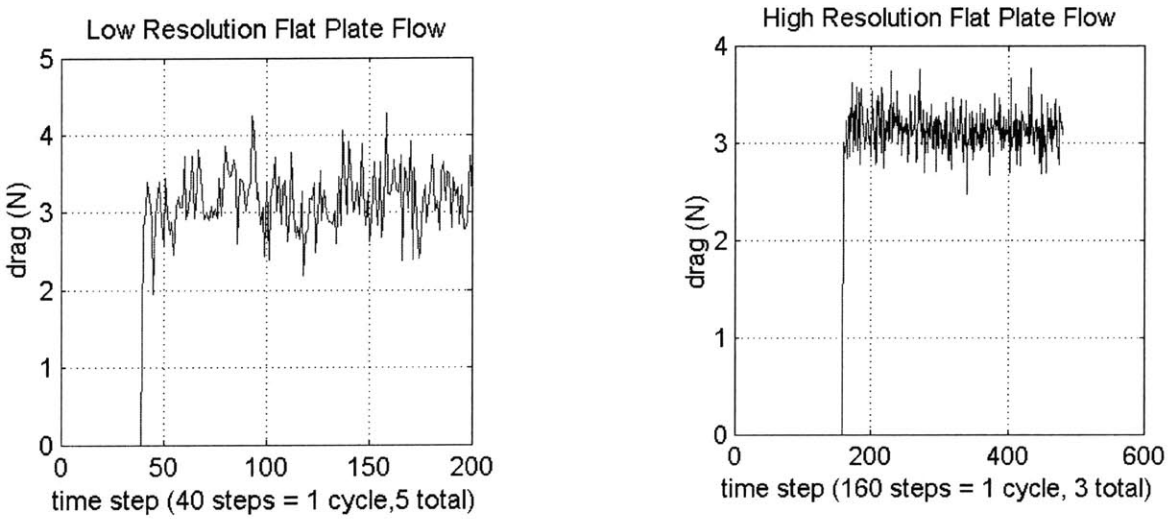

Fig. 4.20, Drag time history for flat plate validation case

The high-resolution plots include 160,000 particles and the low-resolution simulation includes 10,000 particles. The low-res plot used a grid size of 20 by 20 and 20 particles per cell. The high-res plot uses an 80 by 80 grid over the same physical space with 20 particles per cell. The plots have been interpolated to smooth the data somewhat. Notice that the difference in the drag with time. The low-res version has much more noise, but is centered about the same value as the high-res value.

Table 4.4, 2-D drag coefficients for a flat plate

	Collisionless Analytical Result	Collisionless Numerical Result Low Resolution	Low Resolution Model	High Resolution Model
Drag Coefficient	3.273	3.31	3.33	3.24

This is a good example of the ability of a noisy code to get the macroscopic properties correct, but miss the fine structure. This will allow us to conduct our trade studies with confidence in noisy models.

Performance

The speed of the code varies linearly with the number of particles in the system. For a Matlab program converted to C and compiled as a stand-alone program, the code steps through about 2,500 particles per second. This corresponds to 216 million steps per day. The total runtime of the code depends on the number of cells, the number of particles per cell, the size of the opening A-B, and the number of 'cycles' required to establish steady-state flow. The largest computation consisted of 250,000 particles and took over a day to run on a PentiumIII PC.

General behavior results

The scoops in general exhibited similar behavior for the range of sizes (1's to 10's of meters radius) and shapes examined (angles from 0 to 90 degrees). This behavior included large amounts of particle backstreaming, a fuzzy oblique 'shock' attached to the rim of the scoop, a diffuse bow 'shock' forward of the scoop, an oblique shock extending forward in space from the scoop rim, and capture percentages lower than 50%.

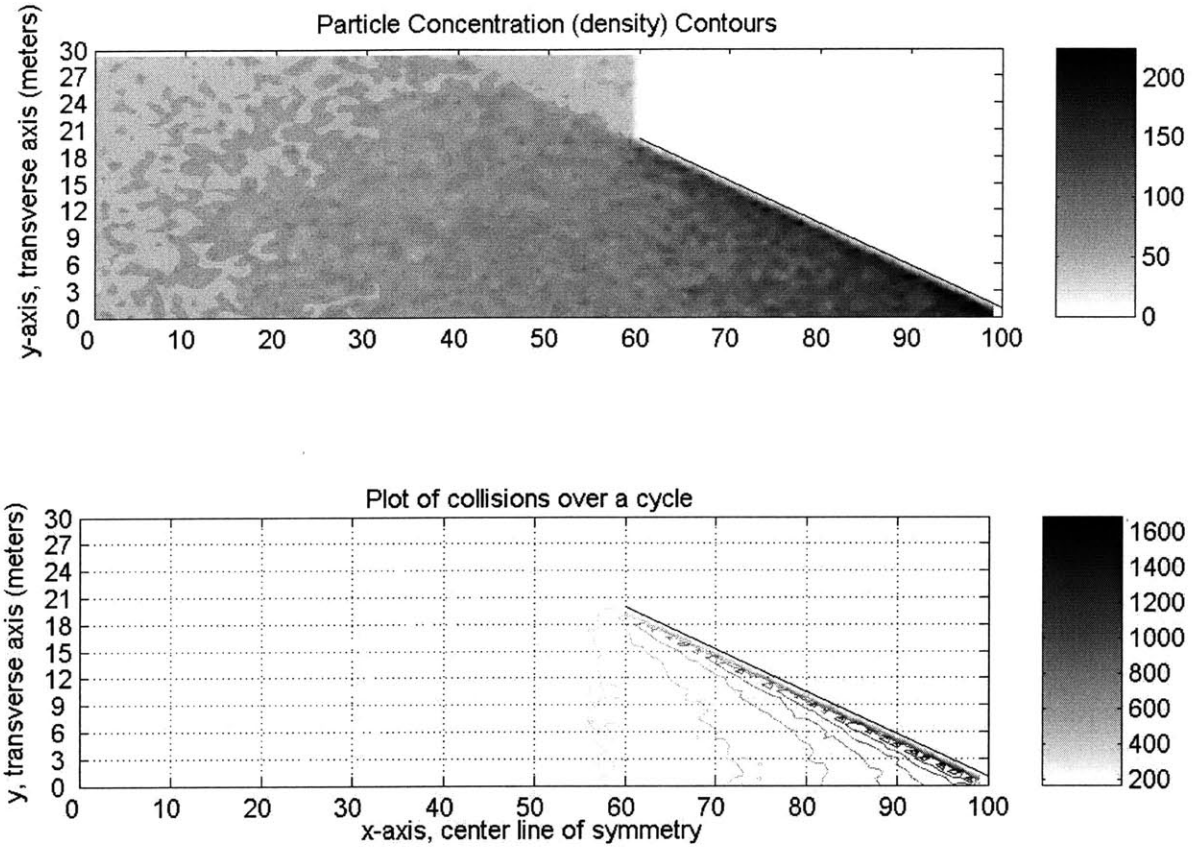

Fig. 4.21, General scoop behavior

The particle backstreaming is due to the mean free path of the reflected particles, which is still fairly large due to the low density. These back-streaming particles collide far ahead of the scoop and create disruptions in the flow that effectively routes the gas around the scoop. This is the cause of the diffuse bowshock that causes the incoming gas to see an effectively larger body. The fuzzy oblique shock is a structure predicted from hypersonic theory, but its extension into the flow field (Fig. 4.22) is new. This structure is due to particles flowing out along the scoop wall, past the rim, and into the passing flow. The low-density allows these particles to flow upstream a good distance before colliding with the bulk flow. The total flow then, sees a jump in bulk flow velocity direction and magnitude along a line coinciding with a the scoop line B-C extended into space forward of the scoop.

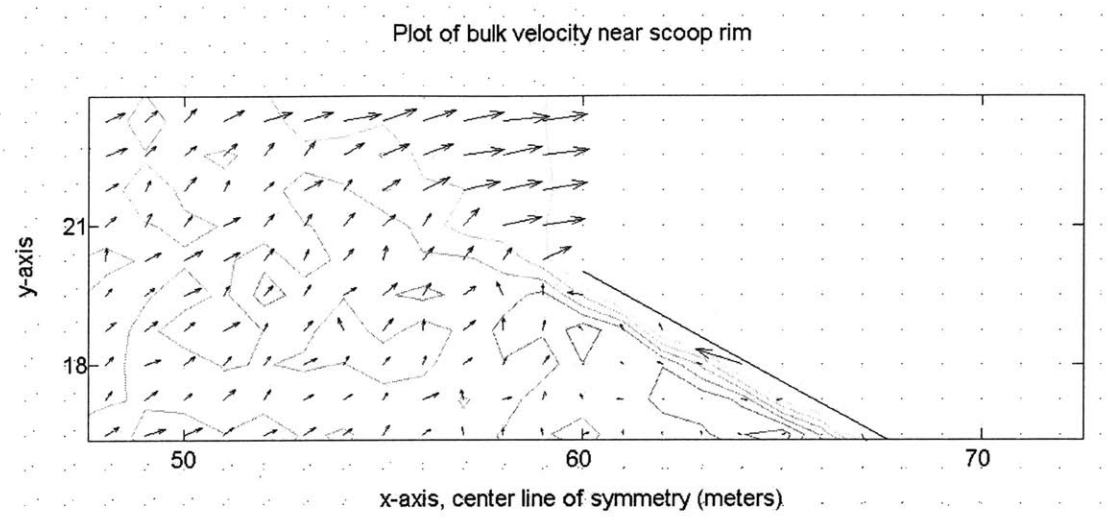

Fig. 4.22, Oblique shocks extending into flow

Parametric relations

A parametric study was constructed in order to find the relations between scoop angle and intake radius on the drag and capture percentage. 25 cases were performed, which include all the combinations of a set of angles, [10 20 30 40 50 degrees] and a set of radii, [5 10 15 20 25 meters]. The computational space was kept constant with parameters as shown in Figure 4.23:

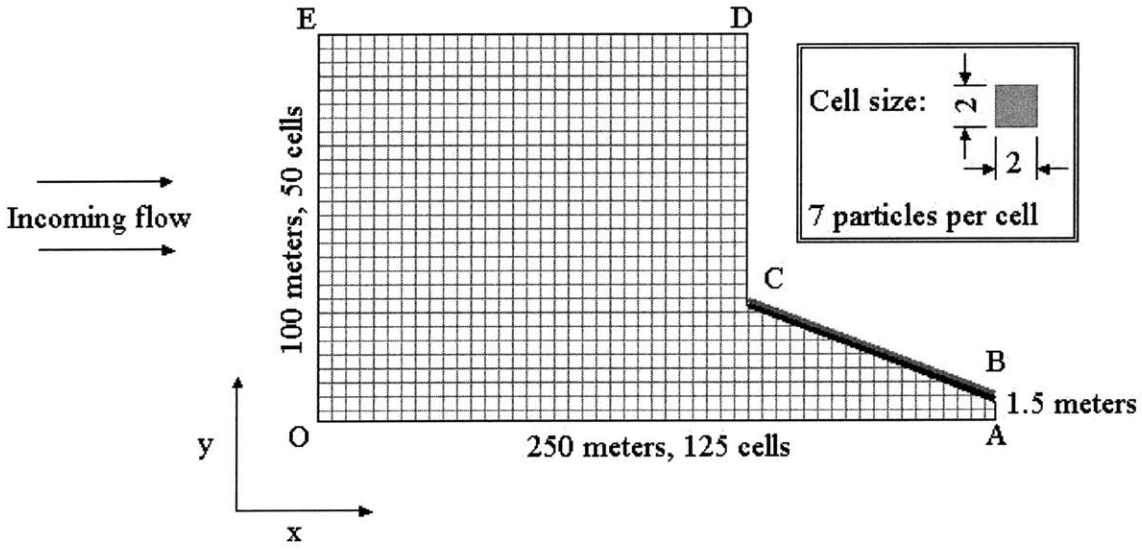

Fig. 4.23, Computational space for the parametric study

In each case, the model completed 3 cycles, and the flow field had reached steady state. The number of particles per cell was chosen on the small side in order to speed up the code. While these parameters produce very 'noisy' behavior, the data was compared to finer resolution models with good agreement, as discussed earlier. The computational space needs to be large in the x-dimension since the mean free path for rejected particles is very long. The proper length for this dimension was determined by plotting the locations of collision events and finding where the collisions effectively stopped being important. This can be seen in Figure 4.15. The majority of the collision events occur within one scoop length upstream of the scoop. This happens because collectively, the rebounding particles are spreading out in space as they move upstream, like light propagating from a point source. By trial and error, it was found that 2 to 3 scoop lengths (x projection of line B-C) are necessary to capture the collision behavior. However, due to computational performance constraints, dimension O-A was limited to ~ 2 times the longest scoop, 25 meters by 10 degrees. The raw results are shown below:

Table 4.5, Parametric study raw results

Cd

	Angle (degrees)				
Radius	10	20	30	40	50
5	1.88	1.88	2.01	2.13	2.08
10	2.35	2.43	2.52	2.55	2.64
15	2.62	2.65	2.74	2.85	2.89
20	2.78	2.76	2.86	2.91	2.94
25	2.88	2.9	2.89	2.98	2.95

%

	Angle (degrees)				
Radius	10	20	30	40	50
5	48.23	50.43	47.41	43.19	42.46
10	32.6	33.24	29.98	28.06	25.81
15	25.34	22.93	22.79	20.72	19.58
20	21.32	20.99	18.64	17.05	15.46
25	18.45	17.35	16.88	14.35	12.61

If one plots drag coefficient and capture percentage versus angle, the results show a large dependence on the radius,

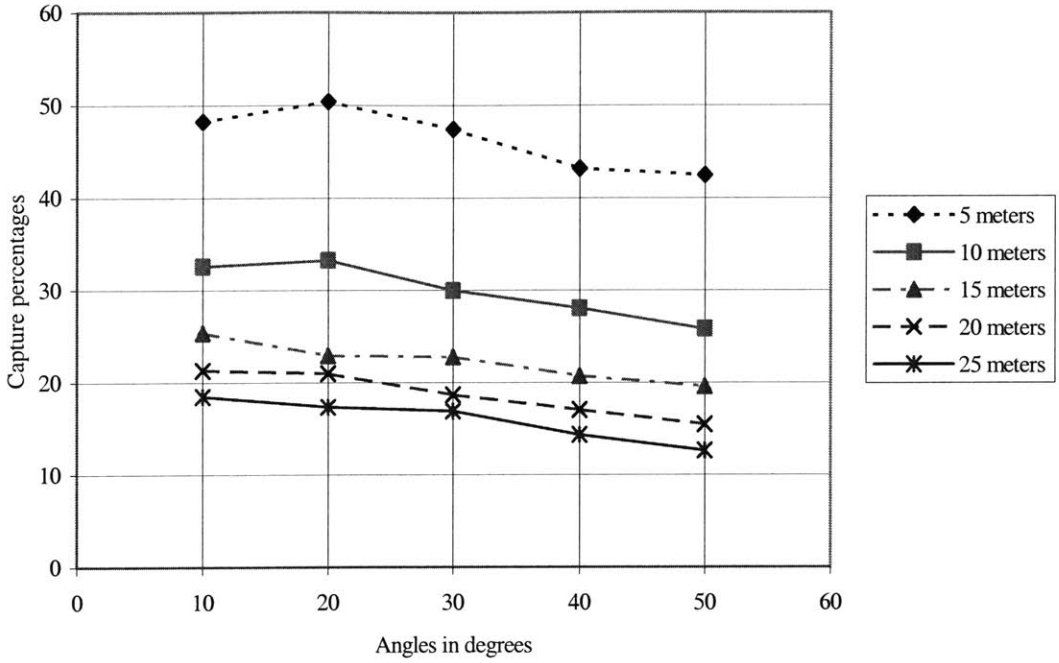

Fig. 4.24, Capture percentage versus angle

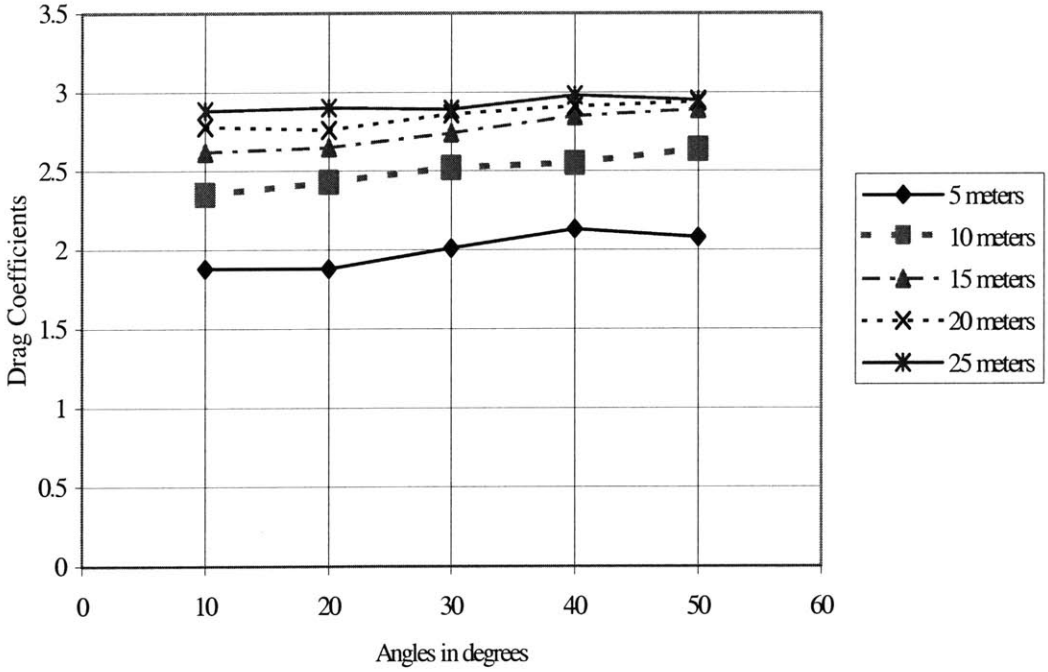

Fig. 4.25, Drag coefficients versus angles

One would rather have the results expressed as a function of only one parameter. The way to do this is to introduce the 'compression ratio', which is defined as the intake radius divided by the mouth radius. It is a measure of how much mass flow is being stuffed down into the mouth of the scoop.

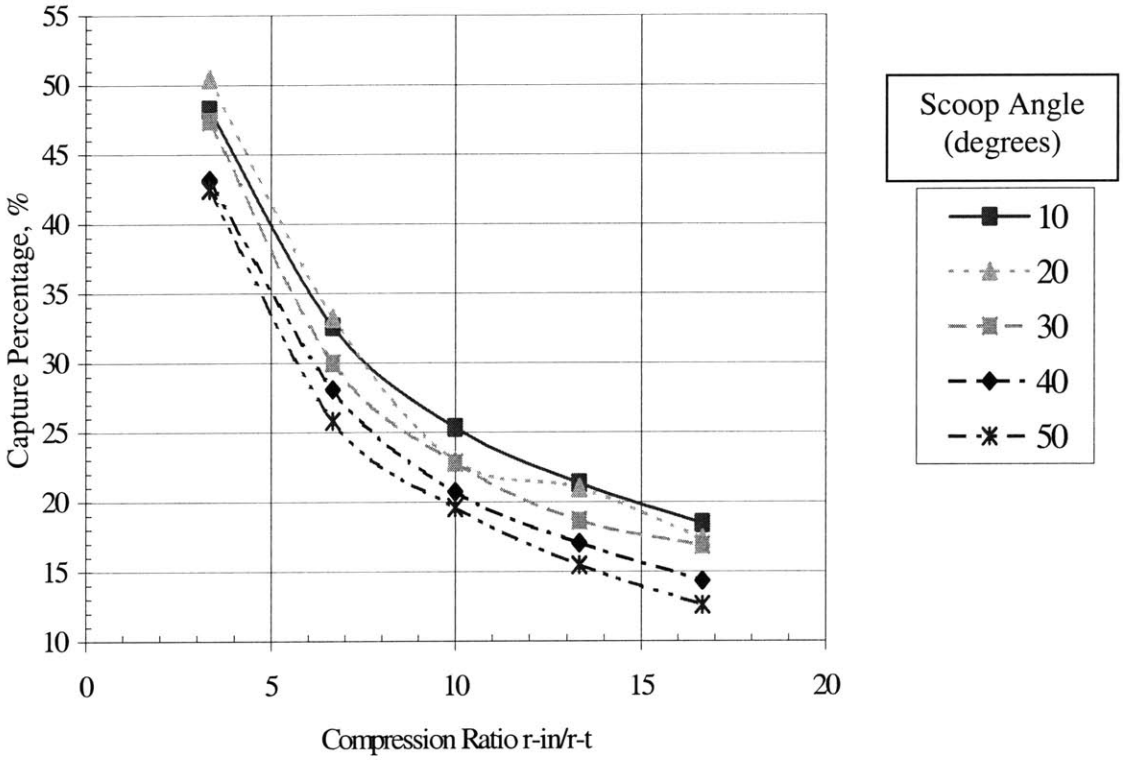

Fig. 4.26, Capture percentage versus compression ratio

In Figure 4.26 the trend looks much better; the plots almost lie on top each other, suggesting that compression ratio is the main independent variable in the determination of capture percentage. This should give some pause if we consider that a real scoop would have to compress the gas to the size of the engine, which could be as small as 10 cm in diameter for a compact magnetoplasmadynamic thruster. This result would say that most of the particles would be rejected, leaving very little gas for the engine. There is some hope, though, in that the density near the throat is getting higher, and eventually the assumptions of the model will break down,

such as low-density wall interactions. Similarly, the drag coefficient is plotted versus compression ratio in Figure 4.27.

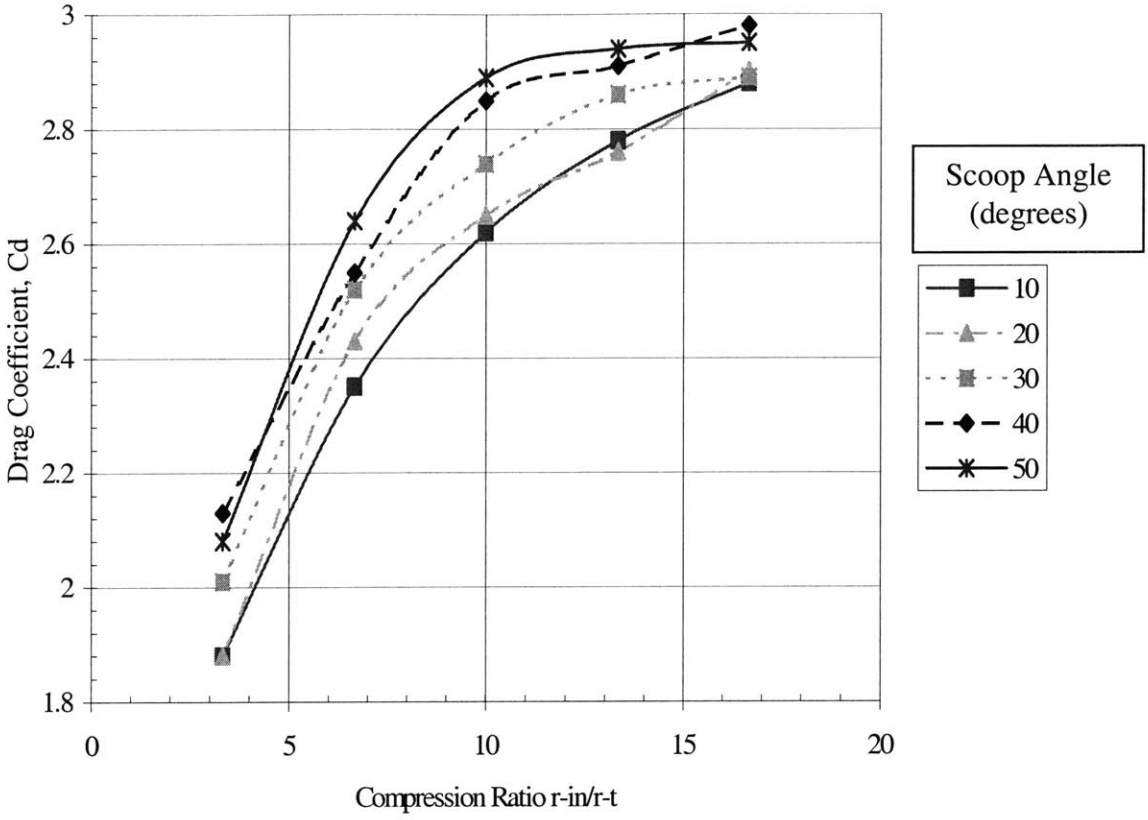

Fig. 4.27, Drag coefficient versus compression ratio

For C_d, the trend is less clear, but also shows a good relationship with compression ratio. One can fit a power law to the capture percentage versus compression ratio with the constants being weak functions of scoop angle,

$$\% = C(\alpha) \cdot \left(\frac{r_{in}}{r_t} \right)^{D(\alpha)} \qquad \dot{m} = \% \rho A_{in} u_{in} \tag{41}$$

For the accuracy of this model, a more general relationship is perhaps more justified. The drag coefficient was difficult to fit to power laws, low-order polynomials, exponentials, logarithmic, and simple trigonometric functions. Nevertheless, general power laws (R^2 values greater than 0.9) are shown in Figure 4.28.

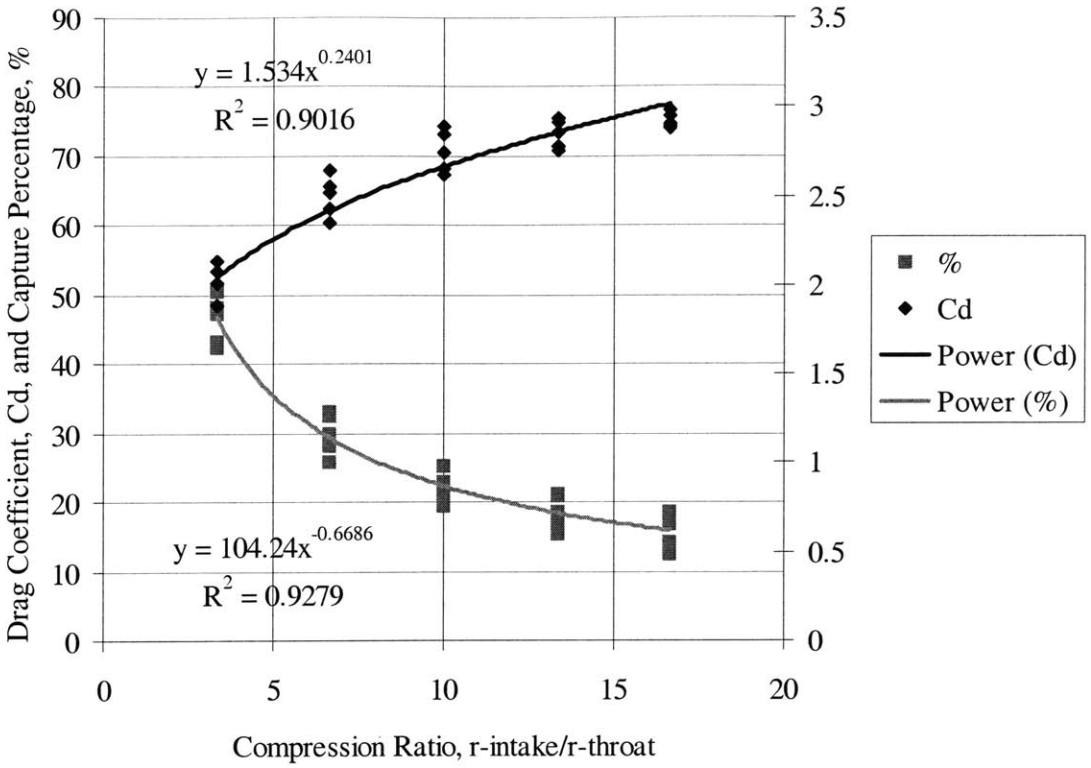

Fig. 4.28, Power law fits for drag coefficient, C_d, and capture percentage, %

These results suggest that smaller scoops will have better capture and drag characteristics. There is plenty of uncertainty in this argument due to the break-down of the model's assumptions near the throat. One could propose that at some critical compression ratio, low-density behavior no longer applies. This point would effectively cap the drag coefficient and set the lower limit for particle loss percentage. In order to keep the drag down, low-altitude scoops would be better. Since the size of the scoop can be reduced by setting the target scooping altitude lower without loss in performance, this is not a problem. The limiting process is the heat transfer increases that will go hand in hand with higher density flow.

In order to check if compression ratio is really the key parameter to vary, using the constants defined above, we can predict the percent capture for different mouth sizes. These values should experimentally match with the curve fits above. A check case was run with a

throat size (A-B) of 3 meters and a scoop radius of 25 meters, and a scoop angle of 30 degrees. With the same computation space (except for the mouth size), a value of 25.57% is obtained numerically. This fits well with the curve fit value of 25.9% at the same compression ratio and scoop angle. If the scoop angle is ignored, and the curve fit across all scoop angles is used, a predicted value of 25.25% is obtained, still a good approximation.

These parametric relations are useful in the second order design of a reusable orbital transfer vehicle. They give a good estimate of the drag and mass flow, allowing the scoop to be sized. They give an idea of how much is to be gained by making the scoop a longer and narrower as opposed to short and stout. The most important result is that the drag coefficient will be greater than 2, possibly even 3. The percentage capture is less important since it depends highly on the flow conditions near the throat, which tend to violate the assumptions of the code. Therefore, the model tells a scoop designer to expect a large amount of particle loss, >50%, but should not be used much beyond that.

The hot wall results are validated somewhat by allowing for some accommodation at the wall, i.e. energy transfer to the wall. When this is included, denser oblique shocks form and more particles are captured. For this model, the coefficient of accommodation, α, is implemented by setting the wall temperature and the α. The emerging velocity from a surface is then:

$$v_r^2 = v_i^2(1-\alpha) + \alpha v_s^2 \qquad v_s^2 = \frac{4kT_s}{m_p} \tag{42}$$

,where v_r is the emergent velocity, v_i is the incident velocity, v_s is the thermal velocity associated with the wall temperature, k is Boltzman's constant and m_p is the mass of the emerging particle[32]. An example of this calculation is shown below for a 15-meter radius, 30-degree angle scoop, and $\alpha = 0.8$, a good estimate for most materials[33]:

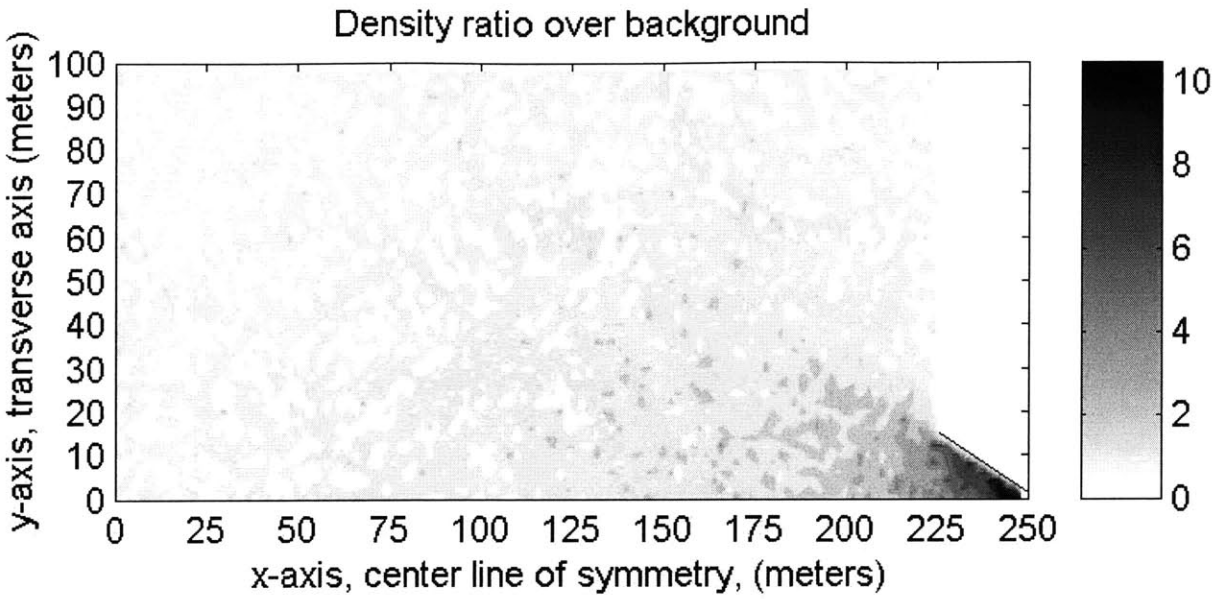

Fig. 4.29, Density map for T = 300 K scoop

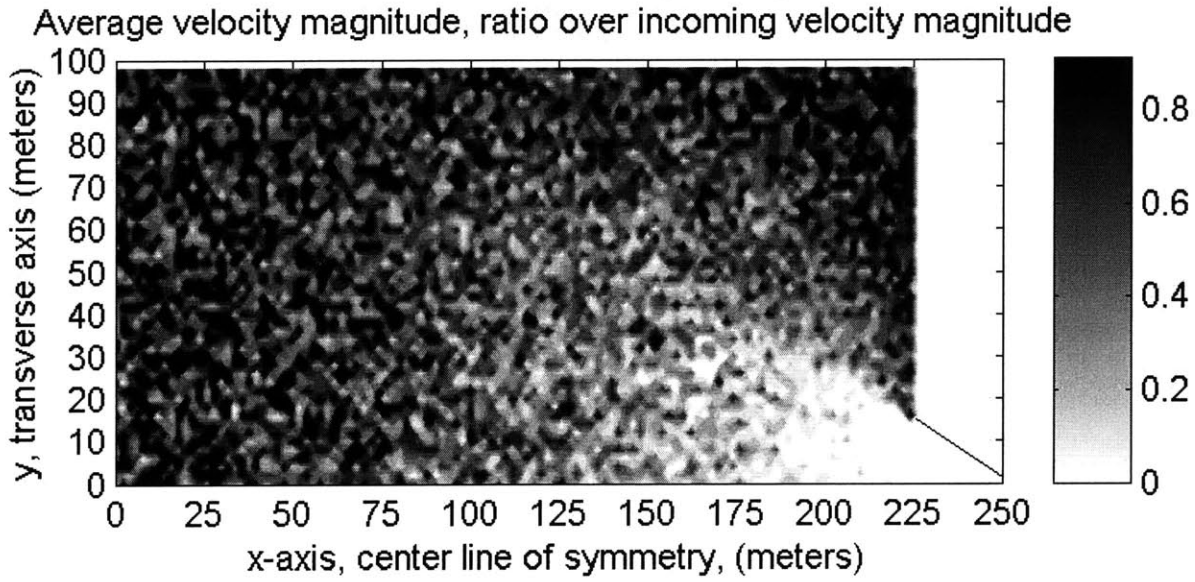

Fig. 4.30, Velocity magnitude contour map for T = 300 K scoop

The ratio of density over ambient density in the shock has increased from 3-4 to 10. The plot above shows eight cycles. More cycles are needed for a cold scoop wall in order to reach a steady-state number of particles in the system. The number of particles versus time is shown below:

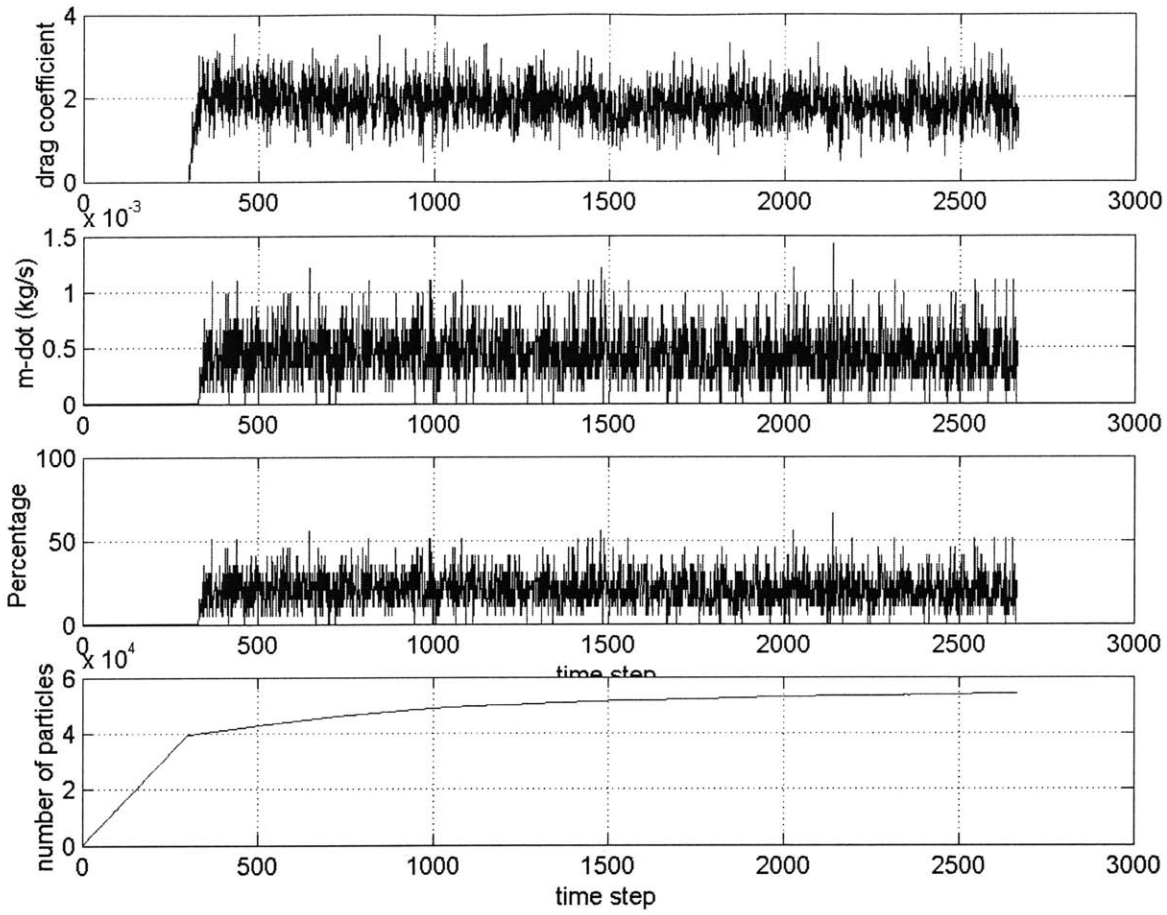

Fig. 4.31, Time history of computation of T=300 K scoop

As seen above, the drag, mass flow, and capture percentage are shown to stabilize after a few cycles, despite the lack of steady-state conditions. The drag coefficient in this case is 1.8, compared to 2.74 in the 'hot wall' case. This is a large decrease in drag coefficient. The capture percentage is 19.7%, a difference of only 3.1% less capture.

As α is increased to one and the wall is kept cold, the particles lose most of their energy to the wall and build up very dense shocks. To accomplish a higher order calculation, the wall temperature profile and material specific α would have to be specified. This data, however, shows that 'hot wall' calculations serve well as a conservative estimate of the drag coefficient without going to higher order estimations. The percentage capture should also improve with

increasing α, despite the opposite trend as described in the above result. The result for capture is well within the error bars for this study, however. One can think about the particles that meet the wall with $\alpha = 1$. They hit the wall and are thermalized at the wall temperature, which will probably be low (~300K). As the gas builds up, the hypersonic relations will apply and capture will tend to 100%, so the hot wall again is a conservative estimate for the purposes of conceptual design.

There are, of course, other possible uses of this simulation code. The model could easily be adapted to quickly solve for drag and the flowfield around satellites and spacecraft. More accurate treatments of surface interactions could be implemented and multiple particle types could be introduced. The DSMC-PIC approach is quite versatile; it can be made as complex as needed. For this study, the code effectively showed the large-scale structure of the flow field and generated engineering relations useful for design. The following chapter uses these results and develops a near-term realistic orbital transfer concept based on atmospheric ingestion.

Chapter 5

Orbital Transfer Vehicle Design Studies

5.1 Introduction

If the AAOTV where to be built using currently available technology, the performance will be somewhat less than the ideal models presented in Chapter 3. This chapter looks at just how much of a difference this is. The remainder of the chapter details some of the main remaining technical issues and outlines potential future studies related to this concept.

5.2 Near-term reusable conventional payload system

The cycle time for the ideal reusable system was around 100 days. This number grows considerably when the following factors are included: limitations of current battery specific energy density, high drag scoops, and limited capture percentage from low-density effects. This model uses the best battery technology developed today, sodium sulphur batteries. These store energy at a density of 200 W-hr/kg. These batteries still do not have the needed discharge capability of MW, which would have to be achieved. From the above numerical studies, the drag coefficient will be greater than 2. For this study, let's set it at 2 by setting the compression ratio low (obtained via a small scoop at low scooping altitudes). This drag coefficient is much greater than the ideal system value of 0.5.

Other changes include the reduction of masses. The numbers grow so bad for the 4,000 kg satellites in the ideal system, that this near-study looks at much smaller, but modernly sized satellites of 1,500 kg. The previous orbit raising model is modified by introducing the capture percentage, %:

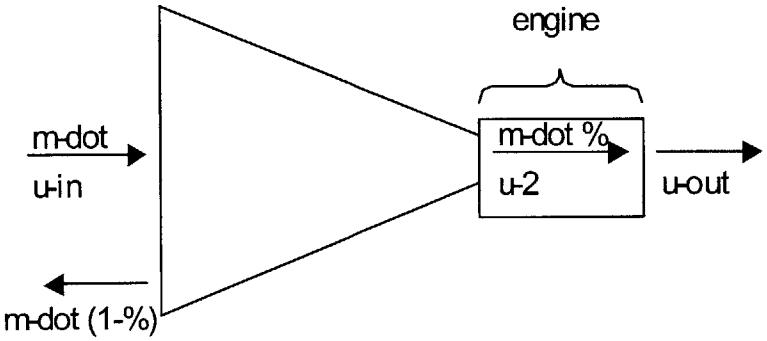

Fig. 5.1, Orbit raising model for percentage capture

where u_2 is the velocity entering the engine mouth. Drag refers the drag on the scoop, and doesn't include any drag due to the engine, which is neglected.

Thrust minus drag is given by:

$$T - D = \dot{m}\%(u_{out} - u_{in}) - \frac{1}{2}\dot{m}u_{in}C_d \tag{43}$$

The power added to the beam is:

$$P = \frac{\dot{m}}{2\eta}\%(u_{out}^2 - u_2^2) \tag{44}$$

If we now allow the velocity entering the engine, u_2, to vary linearly with the intake velocity, u_{in}, we can write the exit velocity in terms of the power added to the beam.

$$u_2 = \beta u_{in} \qquad u_{out} = \sqrt{\frac{2\eta P}{\%\dot{m}} + \beta^2 u_{in}^2} \tag{45}$$

By substituting (45) into (43), obtain the net force on the AAOTV:

$$T - D = \dot{m}\%\left(\sqrt{\frac{2\eta P}{\%\dot{m}} + \beta^2 u_{in}^2} - u_{in}\right) - \frac{1}{2}\dot{m}u_{in}C_d \tag{46}$$

The constant of proportionality, β, can be obtained via the numerical modeling of the previous chapter. The net force isn't very sensitive to this parameter in the orbit-raising model. The numerical scoop modeling showed that the value of β is much less than 1. For this 'realistic' study, the percentage capture was taken to be 40%, near the high end of what the numerical simulation showed was possible.

5.3 Scoop design and sizing

The scoop is assumed to be a lightweight inflatable structure with a mass on the order of 100's of kilograms. This mass can be estimated by using modern thin film materials, the baseline is aluminum-coated Kapton. A metal coating is necessary to resist the corrosive effects of atomic oxygen[34]. This material can be made to a thickness of 7.6 micrometers with a low areal density, ρ_a. Aluminum at this thickness would give a ρ_a of 0.023 kg/m^2. Since Kapton is a good deal lighter than aluminum, we can estimate ρ_a as half of this, 0.012 kg/m^2. Assume a cone-type scoop geometry:

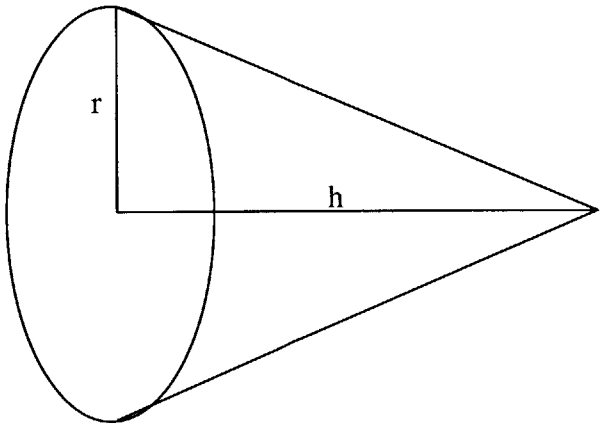

Fig. 5.2 Scoop sizing geometry

The surface area of the curved surface is:

$$SA = \pi r\sqrt{r^2 + h^2} \tag{47}$$

Then define a ratio between r and h, and rewrite (47):

$$h = \mathrm{X}r \qquad SA = \pi r^2 \sqrt{1+\mathrm{X}^2} \tag{48}$$

The mass of the scoop can then be estimated by:

$$mass = \left(\rho_a + \rho_{structures}\right)\pi r^2 \sqrt{1+\mathrm{X}^2} + m_{pressurant\ system} \tag{49}$$

Drag forces produce compressive stresses in the scoop. In order to resist these loads, inflatable-tube struts are proposed to take these loads and provide a rigid framework over the scoop will be stretched. Long axial struts take the main compressive loads, while hoop-shaped tubes take hoop stresses and provide transverse support, as shown in Figure. 5.3.

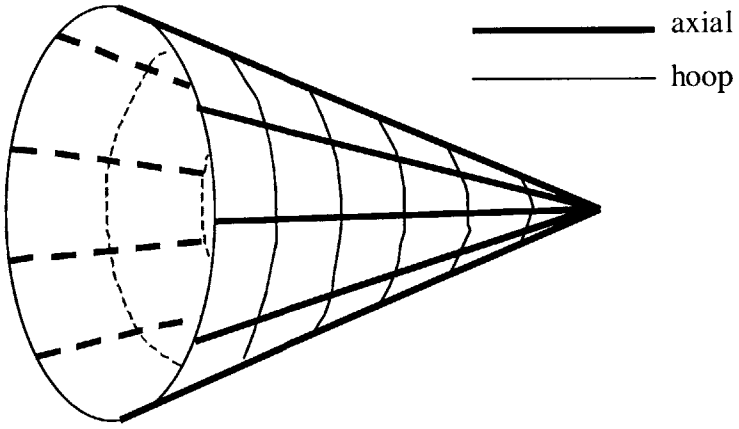

Fig. 5.3, Scoop structural support

The pressurized gas inside the axial struts will support the axial forces, and the strut wall material acts as a pressure vessel to contain the gas. This scheme requires relatively low-pressure gas. Pressure in the struts is simply:

$$P = \frac{F}{A_{strut}} \tag{50}$$

The worst-case force will be near the scoop throat, where the drag on the scoop equals the max force on the pressurant gas. The area of the axial struts can be divided equally among n struts. By defining a drag law, the required pressure can be written as:

$$D = \frac{1}{2}\rho u_{in}^2 A C_d \qquad P = \frac{\frac{1}{2}\rho u_{in}^2 \pi r_{scoop}^2 C_d}{n\pi \frac{d^2}{4}} \tag{51}$$

,where d is the diameter of a strut and r is the scoop radius. For n = 8, C_d = 3, ρ = 3e-10 kg/m^3, u_{i_n}= 11,000 m/s, d = 10 cm, the pressure is 1.7 kPa (~0.25 psi). The maximum plane stresses in the strut wall can then be calculated.

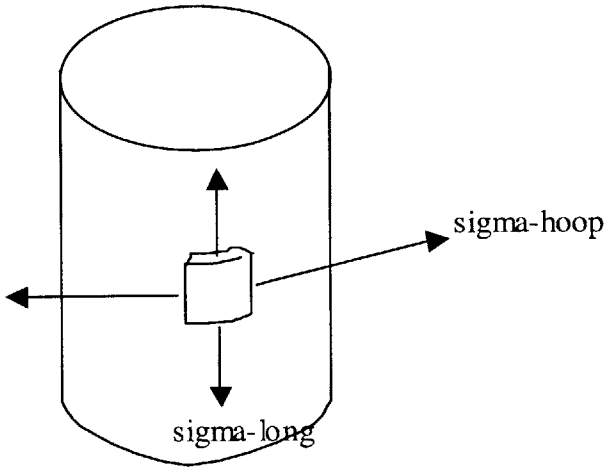

Fig. 5.4, Strut wall element stresses

The longitudinal and hoop stress in the walls is given by pressure vessel equations:

$$\sigma_{hoop} = \frac{pr}{t} \qquad \sigma_{long} = \frac{pr}{2t} \tag{52}$$

The shear stress equals zero, and the σ_{hoop} for a p = 6.9 kPa (1 psi), d = 0.1 m, t = 7.6 μm equals 45 MPa, which is similar to allowable stresses for other plastics. Steels, for example, have σ_y = 200 MPa.

These numbers show that inflatable struts should provide enough support for the scoop. An estimate of the pressurant gas mass is needed to complete the computation of the scoop's mass. This is done by assuming a pressure, a suitable gas, and a volume to fill. For pressure,

assume 6.9 kPa (1 psi), a nice factor over the minimum calculated above. Any heavy gas that will avoid leakage problems should be fine, assume air for this calculation. The volume is done by assuming a geometry and adding up the contributions of each strut. The volume is given by the sum of the axial and hoop struts (where the hoop struts are assumed to the be the largest size, with the same area as the axial struts, and with the same cross-section).

$$V = n\pi\left(\frac{d}{2}\right)^2 \sqrt{1+X^2}r^2 + n(2\pi r)\pi\left(\frac{d}{2}\right)^2 \tag{53}$$

The gas is estimated then by assuming an equation of state:

$$\rho_{gas} = \frac{p}{RT} \qquad m = \rho_{gas} V \tag{54}$$

For air at T = 300 K, R = 287 [J/kg·K], X = 3, r = 25 meters, n = 8, the mass equals about 11 kilograms. There will also be tankage, regulators, and back-up gas. To complete our estimation, set the density of the structures in the scoop wall (the tubes and rip-stop structures) equal to the areal density of the Kapton material, ρ_a of 0.024 kg/m^2. This is the equivalent of assuming the scoop is solid aluminum. The mass by equation (49) is 150 kg.

These estimates justify the claim that a workable scoop can be made on the order of 100's of kilograms, in this case less than 200 kg. The above estimates could be used to scale scoop sizes to other designs. The radius of 25 meters corresponds to the baseline scoop size for a 100 kW reusable AAOTV.

5.4 Scoop controllability and attitude control system sizing

There is some concern that a large deployable scoop structure will give the AAOTV bad stability characteristics. Of interest then, is the sizing of an adequate attitude control system, to

make sure it is not a limiting design factor (i.e. that it doesn't drive the total system mass).

There are two main disturbances of interest, (1) gravity gradient and (2) atmospheric drag.

The gravity gradient disturbance torque is given by:

$$T_g = \frac{3}{2}\frac{\mu}{R^3}|I_z - I_x| \tag{55}$$

where R is the orbit radius, μ is the Earth's gravitational constant and I_z and I_x are the moments of inertia with respect to nadir and the smaller of the two transverse moments of inertia. With estimates of the moments of inertia difference as 300,000 kg·m^2 for the 100 kW system, and worst-case altitude of 200 km, the disturbance torque is 0.6 N·m. This torque turns out to be many orders of magnitude less important than the aerodynamic torque, as is shown next.

The aerodynamic torque is important since the scoop is flying through the atmosphere in an unstable manner. If some angle is introduced between the cone centerline and flight path by random processes or intentionally for thrust vectoring purposes, the vehicle will experience a destabilizing torque. One can think of the worst-case scenario as the scoop maneuvering 180 degrees, the scoop moving from behind the bus to a position in front of the bus where it can function as a scoop. The aerodynamic torque here can be modeled as the triangular cross-sectional area of the scoop producing a drag offset from the vehicle center of mass. As in Figure 5.2, let h be the height of the cone and r is the intake radius. Drag is the standard relation used thus far:

$$
\begin{aligned}
&height, h = \mathrm{X}r \\
&area, A = r \cdot \mathrm{X}r = \mathrm{X}r^2 \\
&drag, D = \frac{1}{2}\rho u_{in}{}^2 AC_d \\
&torque, T_a = \frac{1}{3}h \cdot D = \frac{1}{3}\mathrm{X}r \cdot \frac{1}{2}\rho u_{in}{}^2 \mathrm{X}r^2 C_d = \frac{1}{6}\rho u_{in}{}^2 \mathrm{X}^2 r^3 C_d
\end{aligned}
\tag{56}
$$

At our nominal scoop altitude of 200 km, ρ = 3e-10 kg/m^3, and we may take variables similar to the scoop sizing example above. Let X = 3, r = 25 meters, C_d = 2.5 (Ref. 3), u_{in} = 11,000 m/s. This yields a worst-case aerodynamic torque for the 100 kW system, T = 2,552 N·m.

This level of moment suggests the use of control moment gyros, (CMG's) or attitude control thrusters. Thrusters would work, but they require propellant. CMGs do not require propellant for cyclic loads and can handle the high torques required. The CMG could be unsaturated via magnetic torque rods or aerodynamic means, thereby eliminating propellant with lightweight systems. While this torque level is very high, normal operation would not require such a huge torque. Large maneuvers like this could be performed near the apogee of the mission orbits, where the atmosphere density is much less. Normal operation would require just the damping out of deviations from the flight path attitude and possibly holding an offset to allow for off-axis thrusting. If this load is determined to be too large, the engine itself could be gimbaled mechanically or possibly electrically. In any case, the weight for CMGs that can support the torque level of 2,500 Nm for 1 second is given as only 160 kg (Ref. 3). This serves to illustrate that the weight of the CMGs is low in comparison to the assumed bus weight in the mission studies (>1000 kg). It is not a negligible factor, but as with the scoop mass, it is not a driving factor.

5.5 Reverse thrust

Another complication is the reverse thrust needed to return the AAOTV to LEO at the end of a mission. This reverse thrust could be achieved in a number of ways. The first would be to simply let the high drag of the scoop do the work with no thrusting. This results in lengthening the return trip by about 140 days for the 100 kW system, as detailed in Table 5.1. The second option would be to mount the thrusters at angles to the flight path such that reverse thrust is achieved without excessive impingement on the scoop, as shown below in Figure 5.2. The thrusting would be less efficient due to cosine losses, and the gas feed system would have to be capable of routing the incoming gas to these 'side' engines. Another option is to have the thruster set up so that it could thrust upstream into the scoop, as shown in Figure 5.2. The scoop would be sized so that the plume would not impinge upon the wall. The effectiveness of the scoop during this type of operation is unclear, but it might be okay if the exhaust plume doesn't expand very much. The exhaust plume is moving much faster than the incoming flow, so it may clear the scoop before it disrupts the flow structure in the scoop. Eventually, the exhaust would interact with incoming gas, and this type of system might suffer from greatly reduced capture characteristics.

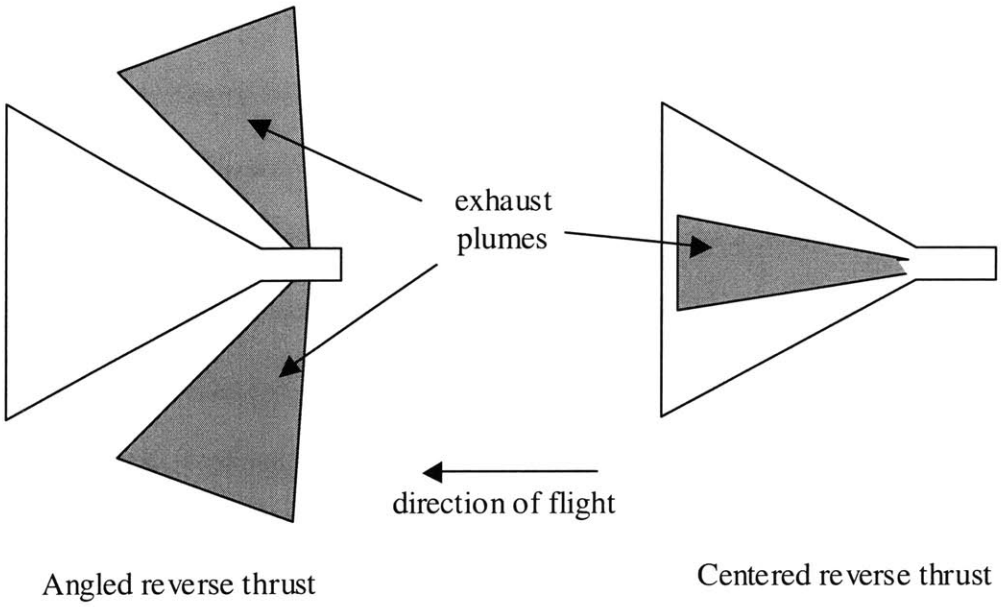

Fig. 5.5, Reverse thrust options for a reusable AAOTV

The centered reverse thrust scheme is compared with the plain drag scheme below for two systems, (1) a 100kW nuclear powered system based on the SP-100 and (2) a 300kW nuclear powered system using masses scaled directly from the SP-100. The results are shown in Table 5.1.

5.6 Results

Table 5.1, Realistic, near-term reusable AAOTV mission performance

	100 kW		300 kW	
	10 MW max discharge		23 MW max discharge	
	scoops, Cd = 2, size not important:			
	24 meter radius scoop		40 meter radius scoop	
	target altitude-200km			
	Rev. Thust	Drag	Rev. Thust	Drag
Power (kW)	100	100	300	300
Inverse Specific Power (kg/kW)	20	20	20	20
Power mass (kg)	2000	2000	6000	6000
Battery mass (kg)	2778	2778	2778	2778
Bus mass (kg)	1000	1000	1000	1000
Payload mass (kg)	1500	1500	1500	1500
Delta-V (m/s)	1600	1600	1600	1600
Isp (seconds)	298	298	298	298
Fuel mass (kg)	1094	1094	1094	1094
Total payload mass (kg)	2594	2594	2594	2594
Launched mass (kg)	8372	8372	12372	12372
Days to GEO	113	113	78	78
Return mass (kg)	5778	5778	9778	9778
Days to LEO	39	177	31	138
Cycle time (days)	152	290	109	216
Missions per year	**2.40**	**1.26**	**3.35**	**1.69**

For the above data, the bus mass includes the scoop mass, all the avionics, attitude control system docking interfaces, etc. The 100 kW system was optimized (gave the best performance) for 2e9 J of energy storage, while the 300 kW system used 4e9 J. The drag coefficient drives the transfer time, not the scoop size as long as the scoop is sized optimally for the target altitude as was shown in Chapter 3. I don't propose that 200 km altitude is the 'right' altitude for these missions, but that a scoop operating at $C_d = 2$ with good capture percentage is the 'right' choice. This scoop may then operate at a lower altitude, but it won't change the answers here.

The main result is that the transfer for a 100 kW baseline system has increased to 152 days from about 100 days. This brings our 'missions per year' below 3. This certainly doesn't kill the system, but it is not as attractive as the 'ideal' case. The high power systems yield a significant missions-per-year improvement, but still not spectacular. Also, the pure drag systems take a long time to return to LEO and consequently have long cycle times. A pure drag system could only perform a few missions each year at most.

One can project the trend of better performance with increased power levels. This was done for a 1 MW power supply at 15 kg/kW, a battery weight 3 times lighter than current tech, 600 W-hr/kg and 10e9 J of energy storage. The engines in this case would drive at maximum powers of 100 MW. Here, a 50 meter radius scoop at $C_d = 2$ and 40% capture could cycle 1,500 kg to GEO in 81 days. This is 4.5 missions per year. For much heavier satellites, the performance is still high; a Thuraya-sized satellite of 5,000 kg to GTO takes only 90 days to cycle. The performance doesn't fall off quickly because the AAOTV mass is much larger than the payloads for these cases.

5.7 Technical issues and potential future work

The flow physics very close to the engine mouth is still unexplored. The dense gas near the throat was not modeled as part of this work and may hold surprises. This flow is necessary in order to design the gas feed system for an engine and especially important for developing a reverse thrust mode. Potentially, hypersonic shocks could be used to slow and compress the incoming gas to a point where it could be routed into piping or directly into an engine. This problem could be tackled via numerical and experimental methods such as blow-down tunnels.

Engine development is another main issue. The engine would have to be able to support

high power levels repeatedly for durations of 2-10 minutes, with a cool-off time as short as 80 minutes. An MPD, magnetoplasmadynamic, engine has potential due to its high power density but suffers problems of heat dissipation. There may be better-suited systems, such as magnetic mirrors with electromagnetic wave heating. Development of such engines is progressing at NASA despite the current lack of suitable MW class power supplies.

Battery technology must improve in the power discharge rates and masses over the current capabilities. Lightweight batteries would make this concept much more attractive. Installed terrestrial superconducting magnetic energy systems, SMES[29], can support the need discharge and storage levels, but are very heavy.

An effective business plan for an AAOTV most likely requires a mission life of many years in order to amortize the cost of the AAOTV. The longevity of such a high-power system and thin-film structure raises serious questions. The battery system will undergo many cycles and the engine will go through many thermal cycles. The thin film scoop will be susceptible to micrometeoroid impacts and tearing. The micrometeoroid damage could be possibly handled by 'rip stop' type construction with a net of strong fibers fused to the material in order to localize damage. In general, these are technical issues that can probably be overcome, and their study would be applicable to high-energy space systems and thin film structures in general.

The scalability of the AAOTV concept is limited upwards by available power systems. This concept already calls for the largest power system yet developed for space. The concept could be scaled down for LEO satellites, and quick calculations show that it has promise. The atmospheric ingestion technique could let small satellites counter-act drag forces and maneuver in LEO, possibly without lots of energy storage, and even maintain non-Keplarian orbits.

Chapter 6

Summary

6.1 Chapter summaries

The motivation for this work has been to ultimately make it cheaper to do business in space. Specifically, the current methods of chemical spacecraft propulsion on orbit are inefficient and could be improved. The AAOTV will use the thin gas present in LEO as propellant for its primary propulsion systems. The idea is to eliminate mass from on-board propellant requirements and reap the associated cost savings. A proposed mission would look at moving satellites from LEO to GTO, ultimately reducing the cost of placing a satellite in GEO.

An orbit-raising model for a LEO-GEO mission was constructed and used to explore the feasibility and performance of the system. The model is useful in finding the optimal scoop size to complete a given mission in the shortest time. The model was also useful in finding optimal operating conditions, such as the level of energy storage, duration of engine burns, and design perigee altitudes. A simplified, 'ideal' AAOTV was then compared against current methods of GEO insertion and as well as improved systems that are being developed today. A reusable AAOTV was found to be very promising, with large increases in payload capability to GEO or reduced launch costs for a given payload. The attractiveness of the 'ideal' system provided the impetus for further work into the specifics of the scoop physics and some more detailed design

studies.

There are numerous ideas for a suitable scoop for the system, such as electromagnetic fields and ionizing laser systems. Of all the ideas, though, a conical inflatable thin-film structure seemed the most realistic in terms of simplicity and technical difficulty. As the incoming gas enters the scoop, it will encounter very weak, 'fuzzy', shocks that compress the incoming flow into the engine mouth. The big questions with this method, however, are what will the flow really look like and how will the drag scale?

A numerical study was conducted to try to answer these questions. A Direct Simulation Monte Carlo (DSMC) code models the incoming gas as superparticles and accounts for low-density gas surface interactions and collisions between incoming and reflected particles. A parametric study found that the drag coefficient of the scoop increased as the compression ratio of the scoop increased, roughly to the ¼ power. The calculated drag coefficients were much higher than those assumed for the 'ideal' study (2's and 3's instead of 0.5). Another troublesome realization is a low 'capture percentage', which means the mass flow is considerably less than was assumed for the ideal studies. One major limitation found was the violation of the model's assumptions near the engine intake for high compression ratios. The dense flow in this region would be expected to behave more as a continuum flow due to the large decrease in mean free path. Also, energy transfer at the wall was assumed to be zero. If the wall cools the incoming flow, dense shocks are found to form. The drag for these cases is lower. The drag for the no energy transfer case thus forms a 'worst-case' scenario as far as scoop performance is concerned. This gives a good design point for designing a near-term AAOTV. The effect of this high drag is to slow down the AAOTV, which lengthens the amount of time required to transfer a satellite to GTO.

In order to see just how much these high drag, low-capture scoops affect performance, a more 'realistic' conceptual design is presented. In this near-term version, the masses of the payloads are taken to be 1,500 kg at GEO instead of 4,000 kg. Current battery technology, nuclear reactor masses, and a relatively heavy structure are assumed. The scoop mass and attitude control system mass is also calculated and included. In addition, the complications with reverse thrust to lower the apogee of the vehicle is explored and found to be vital in producing reasonable mission cycle times. The bottom line is that the high drag scoop drives the ideal mission cycle time up from about 100 days to about 150 days. As a worst-case scenario with regards to drag coefficient and capture percentage, this isn't too bad, since it already corresponds to a couple of missions per year.

6.2 Conclusion

The numbers for the system look very promising. They include: (1) the tripling of GEO capabilities of existing launch vehicles, (2) reduction of launch vehicle payload requirements and associated costs of bigger vehicle, and (3) orbital transfer capability without refueling costs. A near-term, reusable AAOTV using 100 kW power supplies could operate over 2 missions per year, each mission saving $50M to $100M dollars in launch costs. The price for this cost savings is the increased transfer time required to get to GEO over chemical propulsion methods. Recently, this has become more acceptable, with some satellites taking ~6 months to use a mix of chemical and electrical propulsion to reach GEO. There will always be some pause given to ideas requiring nuclear power, but space nuclear reactors will be necessary for the future of space development. They will be with us eventually, like it or not; it is just too attractive for many missions.

The real caveat of this concept is the risk vs. payoff trade. The technical concepts are basically sound and problems could be tackled with development money. The system will also have a substantial operating cost due to the long-term nature of the vehicle. Despite its lack of refueling, it would still require human oversight. The main problem is that the risk and development cost will be so high that they potentially outweigh the considerable benefits if this system.

The benefits of this system are so promising that continued work on the concept is warranted. Development programs into high-energy thrusters, battery systems, nuclear reactors, and thin film structures all have application beyond this concept. If this concept were pursued seriously, all of these areas would benefit. In the worst-case scenario, you still have a boon of technology that you can use elsewhere in space activities.

Alternately, the development of advanced space component systems such as reactors and engines will make this concept more and more achievable as time passes. The real question is, will the economics support this type of concept if the cost of space launch is reduced substantially in the coming years? That is, if launch costs are reduced from today's low-end price of $5,000 per pound to what NASA envisions, $100 per pound, then this concept wouldn't be very viable. I believe NASA's goals will be achieved eventually (>20 years from now?), but until then, the prohibitive cost of space launch should drive the development of technologies such as the AAOTV.

Appendix

This is the Matlab Code for the parametric study. The verification, flat plate, and cold wall studies are variations of this core code. The m-file was compiled into a stand-alone C-code graphics enabled executable. The compilation speeds up the code by about a factor of 2.

Matlab m-file

```
function scoop
% Thomas J. McGuire
% Scoop low-density flow model
% Compilable version with no real-time display (for speed)
% October 25, 2000

%variable list and initation algorithm

format short g

prompt  = {'Enter angle in degrees:','Enter radius in meters:'};
title   = 'Input for scoop dynamics simulator';
lines = 1;
def     = {'45','10'};
answer  = inputdlg(prompt,title,lines,def)

ang = str2double(answer(1));
 %angle of scoop wall to incoming flow
radius = str2double(answer(2));  %radius of intake

[newfile,newpath] = uiputfile('*.*','Save file name');
fid = fopen(newfile,'w');

NA=0;          %current number of particles in system
N=1000000;     %Maximum number of particles allowed
vin=8000;      %atmospheric velocity in meters per second
cycles=3;      %number of cycles to execute, hopeful reaching steady state
R = 0.9e-10;   %average size of particles in atmosphere
rho = 3e-10;   %atmospheric density in kg/m^3
MM = 2.326e-26;      %molecular mass in kg per particle
rhon = rho/MM;       %particle number density

%note: tsteps*Nin should be much less N, max particles allowed
```

```
%define x-y coords of boundaries of scoop
xa=250;         %a is bottom of mouth of scoop
ya=0;
xb=xa;          %b is top of mouth of scoop
yb=1.5;
xc=xa-(radius-1)/tan(ang*pi/180);     %c is lip of scoop
yc=radius;
xd=xc;          %d if space edge near lip
yd=100;
xe=0;           %e if front top of computation space
ye=yd;

Nx=125;         %number of cells in the x-direction
Ny=50;          %number of cells in the y-direction
TT = 7;         %average number of particles per cell

mBC = (yb-yc)/(xb-xc);  %slope of wall

% define computational space discretization
ttotal= xa/vin;

dt = yb/2/vin
duration = ceil(ttotal/dt*cycles);        %number of time steps to execute

Nin = floor(TT*yb/2*Nx*Ny/xa);     %particles in is specified by cell size.
rhof = rhon*ye*vin*dt/Nin;   %proportionality constant for mass of particles

disp('cell x-dimension')
dx=xa/Nx;       %x spacing of field grid in meters
disp('cell y-dimension')
dy=ye/Ny;       %y spacing of field grid in meters

F=zeros(N,1,7);          %initialize particle informatrix
GO=zeros(Nx,Ny,6);  %initialize old cell informatrix
GN=zeros(Nx,Ny,6);  %initialize new cell informatrix
K = zeros(duration,7);           %initialize output matrix

%begin stepping loop
for iii=1:duration
  tic
        %error check for particle overload
    if NA + Nin > N
      iii=duration;
      Nin=0;
      disp('Particle Overload Error')
      NA
```

```
  end
%introduction code
Nleft = Nin; %number of particles left to introduce
i=1; %particle counter
while Nleft > 0
  if F(i,1,1)== 0 %check for empty slot
    F(i,1,1) = 1; %change status of particle
    F(i,1,4) = rand*vin*dt+0.0001; %give a random new x-position
    F(i,1,5) = ye*rand;       %give particle a random new position
    F(i,1,3) = F(i,1,5);      %set new ypos= old y pos
    F(i,1,2) = 0.0001;        %set nex xpos = old x pos
    F(i,1,6) = vin;    %give axial velocity
    F(i,1,7) = 0;      %give initial y-velocity
    Nleft = Nleft - 1;
    NA = NA + 1;
  end
  i=i+1;
end

%step particles
GN(:,:,1:5) = zeros(Nx,Ny,5);              %refresh new cell matrix
MS = 0;      %reset solid reflection tally
MVX = 0;     %reset x-momentum tally, drag
ML = 0;      %reset mass lost tally
MC = 0;      %reset mass captured tally
MVC = 0;     %reset x-momentum captured tally
MVO = 0;     %reset x-momentum lost tally
coll = 0;    %reset total collision tally

Nleft = NA;
i=1;
while Nleft > 0
 if F(i,1,1) == 1;      %check to see if particle is present
  Nleft = Nleft - 1;  %decrement particles left

  F(i,1,2) = F(i,1,4); %x1 transfer new x pos into old x pos
  F(i,1,3) = F(i,1,5); %y1 transfer new y pos into old y pos
  F(i,1,4) = F(i,1,4) + F(i,1,6)*dt;  %x2 step x-coord
  F(i,1,5) = F(i,1,5) + F(i,1,7)*dt;  %y2 step y-coord

  %check for collisions
  xx = ceil(F(i,1,2)/dx);            %cell x-position of particle
  yy = ceil(F(i,1,3)/dy);            %cell y-position of particle
  vx = GO(xx,yy,4);                  %cell x-velocity of particle
  vy = GO(xx,yy,5);                  %cell y-velocity of particle
  rel = ((vx-F(i,1,6))^2 + (vy-F(i,1,7))^2)^0.5;      %cell magnitude of velocity
```

```
if rand <(4*pi*R*R*dt*rel*GO(xx,yy,1)*rhof/dx/dy)    %random collision process

  theta = rand*2*pi;        %calculate new trajectory
  F(i,1,6) = vin*cos(theta);        %new x-velocity
  F(i,1,7) = vin*sin(theta);        %new y-velocity
  F(i,1,4) = F(i,1,4) + F(i,1,6)*dt;        %x2 step x-coord
    F(i,1,5) = F(i,1,5) + F(i,1,7)*dt;        %y2 step y-coord
  GN(xx,yy,6) = GN(xx,yy,6)+1;%step collision tally
  coll = coll + 1;          %step total collisions tally
end

    %check for intersections
    % beginning steps
  m = F(i,1,4) - F(i,1,2);  %define slope of particle trajectory

  if abs(m) < 0.0001        %check for zero slopes
    m = 0.0001;             %if it is too small, set to standard error
  end
  %B-C scoop intake
  m12 = (F(i,1,5)-F(i,1,3))/m;  %slope of particle path
  x=yb-F(i,1,3)+F(i,1,2)*m12-xb*mBC;
  x=x/(m12-mBC);  %find intersection x coord
  if ((x>F(i,1,2)) == (x<F(i,1,4)) & (x>xb) == (x<xc))   %test for intersection
    B = atan(mBC) - pi/2;       %find old velocity direction
    B = B + pi*(rand-0.5);      %generate new velocity direction
    %VV=(F(i,1,6)^2 + F(i,1,7)^2)^0.5;  %magnitude of incident velocity
    MVX = MVX + (vin*cos(B) - F(i,1,6));      %step x-momentum to wall tally
    F(i,1,6) = vin*cos(B);      %generate new x-velocity
    F(i,1,7) = vin*sin(B)  ;    %generate new y-velocity
    y = m12*(x-F(i,1,2)) + F(i,1,3);      %y intersection point
    tp = (((x-F(i,1,2))^2 + (y-F(i,1,3))^2)^0.5)/vin;          %time travelled to
intersection &point
    tt = dt-tp;     %time left to travel;
    F(i,1,2) = x;   %define old x-position
    F(i,1,3) = y;   %define old y-position
    F(i,1,4) = F(i,1,6)*tt + F(i,1,2);  %define new x-position
    F(i,1,5) = F(i,1,7)*tt + F(i,1,3);  %define new y-position
    MS = MS + 1;
  end

  %O-A  center line
  m = F(i,1,4) - F(i,1,2);  %define slope of particle trajectory

  if abs(m) < 0.0001        %check for zero slopes
    m = 0.0001;             %if it is too small, set to standard error
  end
```

```
m12 = (F(i,1,5)-F(i,1,3))/m;      %slope of particle path
x=-F(i,1,3)/(m12+.001) + F(i,1,2);
if ((F(i,1,5)<0) & (x<xa) & (x>0))
  F(i,1,3) = -F(i,1,3);     %flip about center line
  F(i,1,5) = -F(i,1,5);     %flip about center line
  F(i,1,7) = -F(i,1,7);     %flip about center line
end

%A-B  intake port
if F(i,1,4) > xa
  MC = MC + 1;          %step captured mass counter
  MVC = MVC + F(i,1,6);       %step captured momentum counter
  F(i,1,1) = 0;    %exit particle from system
  NA = NA - 1;  %adjust total particle count
  end

%C-D  lip loss boundary
m = F(i,1,4) - F(i,1,2);   %define slope of particle trajectory

if abs(m) < 0.0001        %check for zero slopes
  m = 0.0001;             %if it is too small, set to standard error
end
m12 = (F(i,1,5)-F(i,1,3))/m;      %slope of particle path
mCD = 100000;  %slope of boundary, very large number
x = (yc-F(i,1,3)+F(i,1,2)*m12 - xc*mCD)/(m12-mCD);
y = m12*(x-F(i,1,2)) + F(i,1,3);
if (((x>F(i,1,2))==(x<F(i,1,4))) & ((y<yc)==(y>yd)))
  ML = ML + 1;%step lost mass tally
  MVO = MVO + F(i,1,6);       %step lost x-momentum tally
  F(i,1,1)=0;      %exit particle from system
  NA = NA - 1;  %adjust total particle count
end

%D-E top boundary
mDE = 0;
x= (yd - F(i,1,3) + F(i,1,2)*m12)/(m12+0.001);
if  (x>F(i,1,2) == x<F(i,1,4)) & (F(i,1,5)>ye)
  ML = ML + 1;          %increment particle lost tally
  MVO = MVO + F(i,1,6);       %increment x-momentum lost tally
  F(i,1,1) = 0;             %exit particle from system
  NA = NA - 1;              %reduce total number tally
end

%E-O intake boundary
%mEO = 100000;         %slope of intake boundary (approaching infinity)
%x= (ye - F(i,1,3) + F(i,1,2)*m12- xc*mEO)/(m12-mEO);     %intersection point
```

```
    %if (x>F(i,1,2)==x<F(i,1,4))
    if F(i,1,4)<0
      ML = ML +1; %step particle lost tally
      MVO = MVO + F(i,1,6);      %tally x-momentum lost tally
      F(i,1,1) = 0;    %exit particle from system
      NA = NA -1; %decrement total number of particles in system
    end

      %tally field quantities
  if F(i,1,1) == 1
    NNx = ceil(F(i,1,4)/dx);          %find particle x position
      NNy = ceil(F(i,1,5)/dy);        %find particle y position
    GN(NNx,NNy,1)= GN(NNx,NNy,1) +1; %step cell value
    GN(NNx,NNy,2)= GN(NNx,NNy,2) + F(i,1,6); %step sum x-velocity
    GN(NNx,NNy,3)= GN(NNx,NNy,3) + F(i,1,7); %step sum y-velocity
            end
end
i=i+1;

end %close the particle walk-through loop


%average cell quantities
for i=1:Nx
  for ii=1:Ny
    if GN(i,ii,1)==0
      GN(i,ii,4)=0;
      GN(i,ii,5)=0;
    else
      GN(i,ii,4) = GN(i,ii,2)/GN(i,ii,1); %avg. x velocities
      GN(i,ii,5) = GN(i,ii,3)/GN(i,ii,1); %avg. y velocities
    end
  end
end

GO = GN;   %transfer new values into the old values

%display table of values in MATLAB window
  disp(['Thomas J. McGuire'])
  disp(['Scoop low-density flow model'])
  disp(['date  radius  angle'])
            disp([date num2str(radius) num2str(ang)])
            disp('      In:     Cap:    Loss:    Total:    Collisions:')
            disp([Nin MC ML NA coll]) %display #in #out and total # in system
  disp('      Step:  Total Steps: Time for step in seconds')
  ttt = toc;
```

```
    disp([iii duration ttt])
    disp('density')
    disp(rho)
    disp('m-dot/l, ideal    Actual   percentage captured')
    mdot = Nin*yc/ye*rhof*MM/dt;
    mdot2 = MM*rhof*MC/dt;
    percent = (mdot2+.0000000001)/(mdot)*100;
    disp([mdot mdot2 percent])

    disp('Step:  Cd      Mom-Drag(N)      Cd     Impact-Drag(N)')
    drag = rhof*MM/dt*(Nin*vin-MVC-MVO);      %calculate drag on scoop via momentum
flux
    drag2 = -MVX*rhof*MM/dt;
    Cd1 = 2 * drag / (rho * vin * vin * yc);   %calculate drag coefficient
    Cd2 = 2 * drag2 / (rho * vin * vin * yc); %calculate drag coefficient
    disp([Cd1 drag Cd2 drag2])

    disp('Square scoop Characteristics')
    disp('   Edge (m)   Area (m2)    m-dot     drag')
    mdot3 = percent*rho*vin*4*yc*yc/100; %square scoop mdot
    drag3 = 2*rho*vin*vin*yc*yc*Cd2;      %square scoop drag
    disp([2*yc 4*yc*yc mdot3 drag3])

    %Write to output vector
    K(iii,1:7) = [iii NA coll Cd2 drag3 mdot3 percent];

 end

 subplot(3,1,1);
       [c,h]=contourf(GO(:,:,1)',20);
              %caxis([0 (10*NA/(Nx*Ny))])       %set max color to about ten times average
density
              set(h,'edgecolor','none');
       ylabel('y-axis, transverse axis')
       axis([1 Nx+1 1 Ny+1])
       set(gca,'XTick',1:Nx/10:Nx+1)
       set(gca,'XTickLabel',0:xa/10:xa)
       set(gca,'YTick',1:Ny/10:Ny+1)
    set(gca,'YTickLabel',0:ye/10:ye)
    grid on
    hold on
       w = [xc (xb+xc)/2 xb];
       q = mBC*(w-xb) + yb;
       w = (Nx)/xb*w + 1;
       q = (Ny)/ye*q + 1;
       plot(w,q,'k');
```

```
            hold off

subplot(3,1,2);
      [c,h]=contour(GO(:,:,1)',5);
  hold on
  quiver(GO(:,:,4)',GO(:,:,5)')
      ylabel('y-axis, transverse axis')
      axis([1 Nx+1 1 Ny+1])
      set(gca,'XTick',1:Nx/10:Nx+1)
      set(gca,'XTickLabel',0:xa/10:xa)
      set(gca,'YTick',1:Ny/10:Ny+1)
  set(gca,'YTickLabel',0:ye/10:ye)

  w = [xc (xb+xc)/2 xb];
      q = mBC*(w-xb) + yb;
      w = (Nx)/xb*w +1;
      q = (Ny)/ye*q +1;
      plot(w,q,'k');
      hold off



 subplot(3,1,3);
      [c,h]=contour(GO(:,:,6)',10);
  hold on
      xlabel('x-axis, center line of symmetry')
      ylabel('y, transverse axis to incoming flow')
      axis([1 Nx+1 1 Ny+1])
      set(gca,'XTick',1:Nx/10:Nx+1)
      set(gca,'XTickLabel',0:xa/10:xa)
      set(gca,'YTick',1:Ny/10:Ny+1)
  set(gca,'YTickLabel',0:ye/10:ye)
  grid on
  w = [xc (xb+xc)/2 xb];
      q = mBC*(w-xb) + yb;
      w = (Nx)/xb*w + 1;
      q = (Ny)/ye*q + 1;
      plot(w,q,'k');
      hold off

%average all important quantities over last cycle to get steady values
avgmdot = 0;  %initialize all average quantites
avgCd = 0;
avgdrag3 = 0;
avgpercent = 0;
POE = floor(duration/cycles);  %number of steps in a cycle
```

```
for i = 0:(POE-1)
  avgmdot = avgmdot + K(duration-i,6);
  avgCd = avgCd + K(duration-i,4);
  avgdrag3 = avgdrag3 + K(duration-i,5);
  avgpercent = avgpercent + K(duration-i,7);
end
  avgmdot = avgmdot/POE;
  avgCd = avgCd/POE;
  avgdrag3 = avgdrag3/POE;
  avgpercent = avgpercent/POE;

disp('One-cycle Average Square scoop Characteristics')
disp('  Edge (m)   Area (m2)   m-dot   drag    Cd    %captured')
disp([2*yc 4*yc*yc avgmdot avgdrag3 avgCd avgpercent])

 %print run data to file
 fprintf(fid,'%s with Angle %f and Radius = %f\n',newfile,ang,radius);
 fprintf(fid,'Thomas J. McGuire   Scoop low-density flow model\n');
 fprintf(fid,'%s\n',date);
 fprintf(fid,'Particles in = %f  Total Particles = %f\n',Nin,NA);
 fprintf(fid,'\n');
 fprintf(fid,'One-cycle Average Square scoop Characteristics\n');
 fprintf(fid,'Edge length = %f meters\n',2*yc);
 fprintf(fid,'Area = %f square meters\n',4*yc*yc);
 fprintf(fid,'Mass flow = %f kg/sec\n',avgmdot);
 fprintf(fid,'Drag = %f Newtons\n',avgdrag3);
 fprintf(fid,'Cd = %f \n',avgCd);
 fprintf(fid,'Percentage Captured = %f %\n',avgpercent);

figure
subplot(3,1,1);
plot(K(:,1),K(:,5))
hold on
        ylabel('drag (N)')
    grid on
hold off

subplot(3,1,2);
plot(K(:,1),K(:,6))
hold on
        ylabel('m-dot (kg/s)')
    grid on
    hold off

subplot(3,1,3);
plot(K(:,1),K(:,7))
```

```
hold on
        xlabel('time step')
        ylabel('Percentage ')
    grid on
hold off


%display relative density contour plot
figure

    JIVE = GO(:,:,1).*(rhof/dx/dy/rhon);  %ratio of local density to ambient space density
    JIVE = JIVE'; % take transverse
    qwe = [0.1 0.5 0.75 1 1.5 2 2.5 3 4 5 6 7 8 9 10]; %define contour levels
    [c,h]=contour(JIVE,qwe);
    clabel(c,h)
        ylabel('y-axis, transverse axis')
        axis([1 Nx+1 1 Ny+1])
        set(gca,'XTick',1:Nx/10:Nx+1)
        set(gca,'XTickLabel',0:xa/10:xa)
        set(gca,'YTick',1:Ny/10:Ny+1)
    set(gca,'YTickLabel',0:ye/10:ye)
    grid on
    hold on
        w = [xc (xb+xc)/2 xb];
        q = mBC*(w-xb) + yb;
        w = (Nx)/xb*w + 1;
        q = (Ny)/ye*q + 1;
        plot(w,q,'k');
        hold off

    fclose(fid);
    msgbox('C"est fini, mon ami.');
```

Matlab Code for cold wall study, scoop131coldwall.m

Matlab code for flatplate code

References

Chapter 1: Introduction

1. Caceres, Marco Antonio, "Launch Vehicles Outlook and Specifications, Industry Faces Launcher Excess," Aviation Week and Space Technology, January 17, 2000, pg. 135-149.

2. Caceres, Marco Antonio, "Spacecraft Outlook and Specifications, Financing Woes Soften Satellite Market," Aviation Week and Space Technology, January 17, 2000, pg. 151-164.

3. Wiley J. Larson and James R. Wertz, ed. Space Mission Analysis and Design, Second Edition, Microcosm and Kluwer Academic Publishers, 1991.

4. Martinez-Sanchez, Manuel, 16.522 Space Propulsion Class Notes, 2000.

5. "MR-501B Electrothermal Hydrazine Thruster, specification sheet," http://www.rocket.com/pdfs/MR-501B6.pdf Primex Technologies, 1999.

6. "MR-510 Arcjet Thruster & Cable Assembly, specification sheet," http://www.rocket.com/pdfs/MR-510AJ.pdf Primex Technologies, 1999.

7. "Arcjet Technology Provides Revolutionary Propulsion Breakthrough," http://nctn.hq.nasa.gov/innovation/Innovation22/ArcJet.html NASA web, 1994.

8. "Arcjet Thruster Technology," http://ranier.hq.nasa.gov/scrs_page/historic/arcjet.htm NASA web, 1992.

9. "Busek Hall Thrusters," http://www.busek.com/bht.htm The Busek Company, 2000.

10. "NSTAR Ion Engine," http://www.hughespace.com/factsheets/xips/nstar/ionengine.htm The Boeing Company, 2000.

11. "Xenon Ion Propulsion," http://www.hughespace.com/factsheets/xips/xips.htm The Boeing Company, 2000.

12. "Boeing 702," http://www.hughespace.com/factsheets/702/702.htm The Boeing Company, 2000.

13. Fowler, Harmon, "Low Thrust in the Real World," Hughes Space & Communications, 16.S26 'Modern Space Science and Engineering' Class Lecture at Massachusetts Institute of Technology, February 16, 2000.

14. Bussard, R.W., "Galactic Matter and Interstellar Flight," Astronautica Acta, 6, pg. 179-194, 1960.

15. Andrews, D.G., "Interstellar Ramjet-30 Years of Engineering Analyses," 40th Congress of

the International Astronautical Federation, IAA-89-666, Malaga, Spain, October 7-13, 1989.

16. Martin, Anthony R., "Magnetic Intake Limitations on Interstellar Ramjets," Astronautica Acta, Volume 18, No. 1, pg. 1-10, 1973.

17. Matloff, Gregory, L. and Fennelly, Alphonsus J., "Interstellar Applications and Limitations of Several Electrostatic/Electromagnetic Ion Collection Techniques," Journal of the British Interplanetary Society, Volume 30, No. 6, pg. 213-222, June 1977.

18. Berger, Brian, "Propulsion Changes Delay Encounter 2001 Mission," Space News, November 3, 2000, pg. 3.

19. R.M. Zubrin and D.G. Andrews, "Magnetic Sails and Interplanetary Travel," AIAA/ASME/SAE/ASEE 25th Joint Propulsion Conference, AIAA 89-2441, Monterey, CA, 1989.

20. "SPI Power Cable Fact Sheet," http://www.eren.doc.gov/superconductivity/power2.html.

21. Winglee, Robert et al, "Mini-Magnetospheric Plasma Propulsion (M2P2): High Speed Propulsion Sailing the Solar Wind," Space Technology and Applications International Forum-2000.

Chapter 2: Mission Studies

22. McKissock, Barbara I., "High Capacity Battery Cell Flight Qualified," http://www.lerc.nasa.gov/WWW/RT1996/5000/5440m.htm NASA web site, 1997.

23. Wilson, Richard M., "Li-Ion Batteries," http://www.lerc.nasa.gov/WWW/RT1996/5000/5420w.htm NASA web site, 1997.

24. "Experimental Sodium-Sulfur power storage battery equipment enters operation," http://www.energia.co.jp/energiae/tech/topics1998/nas.html The Chugoku Electric Power Company Inc. web site.

25. Tanokura, Yasou, "NEC Proton Polymer Battery Offers Capacitor Properties," http://www.nikkeibp.asiabiztech.com/nea/200008/cmpo_108677.html Nikkei Electronics Asia, August 2000 Issue.

26. Solar Orbit Transfer Vehicle," http://www.boeing.com/defense-space/space/propul/SOTV.html The Boeing Company Home Page, 2000.

27. Steven J. Isakowitz, International Reference Guide to Space Launch Systems, American Institute of Aeronautics and Astronautics, 1995.

Chapter 3: Scoop Options

28. Buford Ray Conley, "Utilization of Ambient Gas as a Propellant for Low Earth Orbit Electric Propulsion," Master's thesis, Massachusetts Institute of Technology, 1995.

29. Magnetic Energy Storage Efforts in the United States, http://itri.byola.edu/scpa/02_08.htm

30. Kentaro Takahashi, Harunori Nagata, and Isao Kudo, "Simulation for Deployment of an Inflatable Disk in Orbit," Journal of Spacecraft and Rockets, Vol. 37, No. 5, Engineering Notes, 2000.

Chapter 4: Scoop Modeling

31. Johnson, Francis S., ed. Satellite Environment Handbook, pages 18,19,22,40-41, Stanford University Press, Stanford, CA 1961.

32. Hastings, Daniel and Garrett, Henry, Spacecraft Environment Interactions, pages 7,25-27,49-53, Cambridge University Press, New York, NY, 1996.

33. Patterson, Gordon N., Molecular Flow of Gases, John Wiley & Sons, Inc., New York, 1956.

34. Leger, L.J., Visentine, J.T., and Schliesing, J.A., "A Consideration of Atomic Oxygen Interactions with Space Station," AIAA 23rd Aerospace Sciences Meeting, AIAA 85-0476, Reno, Nevada, 1985.

35. Anderson, Jr.,John D., Modern Compressible Flow, McGraw Hill, Inc., 1990.

36. Bird, G.A., Molecular Gas Dynamics, Oxford University Press, London, 1976.

37. Al'pert, Ya. L. The Near-Earth and Interplanetary Plasma, Vol. 2, Cambridge University Press, 1983.

38. CHEMystery : Atomic Structure and Bonding, Element 7 – Nitrogen, http://library.thinkquest.org/3659/pertable/7f.html